Research Paper

THEMED ISSUE: Anatomy of Rifting: Tectonics and Magmatism in Continental Rifts, Oceanic Spreading Centers, and Transforms

GEOSPHERE

GEOSPHERE; v. 12, no. 6

doi:10.1130/GES01375.1

14 figures; 5 tables; 3 supplemental files

CORRESPONDENCE: james.muirhead@fulbrightmail.org

CITATION: Muirhead, J.D., Kattenhorn, S.A., Lee, H., Mana, S., Turrin, B.D., Fischer, T.P., Kianji, G., Dindi, E., and Stamps, D.S., 2016, Evolution of upper crustal faulting assisted by magmatic volatile release during early-stage continental rift development in the East African Rift: Geosphere, v. 12, no. 6, p. 1670–1700, doi:10.1130/GES01375.1.

Received 3 June 2016
Revision received 21 August 2016
Accepted 7 October 2016
Published online 25 October 2016

Evolution of upper crustal faulting assisted by magmatic volatile release during early-stage continental rift development in the East African Rift

J.D. Muirhead[1,*], S.A. Kattenhorn[2], H. Lee[3], S. Mana[4], B.D. Turrin[5], T.P. Fischer[3], G. Kianji[6], E. Dindi[6], and D.S. Stamps[7]

[1]Department of Geological Sciences, University of Idaho, 875 Perimeter Drive, Moscow, Idaho 83844, USA
[2]Department of Geological Sciences, University of Alaska Anchorage, 3211 Providence Drive, CPSB 101, Anchorage, Alaska 99508, USA
[3]Department of Earth and Planetary Sciences, University of New Mexico, Northrop Hall, 221 Yale Boulevard NE, Albuquerque, New Mexico 87131, USA
[4]Department of Geological Sciences, Salem State University, 352 Lafayette Street, Salem, Massachusetts 01970, USA
[5]Department of Earth and Planetary Sciences, Rutgers University, Wright Laboratories, Busch Campus, 610 Taylor Road, Piscataway, New Jersey 08854, USA
[6]Department of Geology, Chiromo Campus, University of Nairobi, P.O. Box 30197-00100, Nairobi, Kenya
[7]Department of Geosciences, Virginia Tech, 4044 Derring Hall, 1405 Perry Street, Blacksburg, Virginia 24061, USA

ABSTRACT

During the development of continental rifts, strain accommodation shifts from border faults to intra-rift faults. This transition represents a critical process in the evolution of rift basins in the East African Rift, resulting in the focusing of strain and, ultimately, continental breakup. An analysis of fault and fluid systems in the younger than 7 Ma Natron and Magadi basins (Kenya-Tanzania border) reveals the transition as a complex interaction between plate flexure, magma emplacement, and magmatic volatile release. Rift basin development was investigated by analyzing fault systems, lava chronology, and geochemistry of spring systems. Results show that extensional strain in the 3 Ma Natron basin is primarily accommodated along the border fault, whereas results from the 7 Ma Magadi basin reveal a transition to intra-rift fault–dominated strain accommodation. The focusing of strain into a system of intra-rift faults in Magadi also occurred without oblique-style rifting, as is observed in Ethiopia, and border fault hanging-wall flexure can account for only a minor portion of faulting along the central rift axis (~12% or less). Instead, areas of high upper crustal strain coincide with the presence of hydrothermal springs that exhibit carbon isotopes and N_2-He-Ar abundances indicating mixing between mantle-derived (magmatic) fluids and air saturated water.

By comparing the distribution of fault-related strain and zones of magmatic fluid release in the 3 Ma Natron and 7 Ma Magadi basins, we present a conceptual model for the evolution of early-stage rifting. In the first 3 m.y., border faults accommodate the majority of regional extension (1.24–1.78 mm yr^{-1} in Natron at a slip rate ranging 1.93–3.56 mm yr^{-1}), with a significant portion of intra-rift faulting (38%–96%) driven by flexure of the border fault hanging wall. Fluids released from magma bodies ascend along the border fault and then outward into nearby faults forming in the flexing hanging wall. By 7 m.y., there is a reduction in the amount of extension accommodated along the border fault (0.40–0.66 mm yr^{-1} in Magadi at a slip rate ranging from 0.62 to 1.32 mm yr^{-1}), and regional extension is primarily accommodated in the intra-rift fault population (1.34–1.60 mm yr^{-1}), with an accompanying transition of magmatic volatile release into the rift center. The focusing of magma toward the rift center and concomitant release of magmatic fluids into the flexing hanging wall provides a previously unrecognized mechanism that may help to weaken crust and assist the transition to intra-rift dominated strain accommodation. We conclude that the flow of magmatic fluids within fault systems plays an important role in weakening lithosphere and focusing upper crustal strain in early-stage continental rift basins prior to the establishment of magmatic segments.

INTRODUCTION

The initiation of continental rifting is fundamental to plate tectonic theory, yet the combination and relative importance of processes driving the initial breakup of continental lithosphere remain largely enigmatic. The tectonic forces driving rift initiation (e.g., gravitational potential energy, basal shear from mantle convection; Coblentz and Sandiford, 1994; Bird et al., 2008; Stamps et al., 2015) are theoretically too small to rupture thick lithosphere, particularly in the absence of tractions provided by boundary forces acting on the sides of lithospheric plates (e.g., slab pull; Buck, 2004; Stamps et al., 2014). However, some continental rift zones are also sites of asthenospheric and lithospheric heating (e.g., Kenya Rift; Rooney et al., 2012) that may predate rifting (Courtillot et al., 1999; Campbell, 2005), with subsequent tectonic thinning commonly accompanied by decompression melting and the rise of volatiles and magma through the lithosphere (McKenzie and Bickle, 1988; White and McKenzie, 1989; Geissler et al., 2005; Lee et al., 2016). Therefore, intrusion of magma and volatile release are thought to play a major role in the conti-

*Now at Department of Earth Sciences, Syracuse University, 204 Heroy Geology Laboratory, Syracuse, New York 13244, USA.

nental rifting process (Buck, 2004; Reyners et al., 2007; Lindenfeld et al., 2012; Rowland and Simmons, 2012; Ebinger et al., 2013).

The buoyancy of magma enables dike intrusions at continental rift settings to ascend from melt generation zones in the mantle toward the surface (Buck, 2004). Dike opening accommodates extensional strain, while the transfer of heat from intrusions weakens the crust locally (e.g., Buck, 2004; Calais et al., 2008; Bialas et al., 2010; Daniels et al., 2014). The rise of magmatic volatiles from mantle depths may also assist rifting. These fluids are hypothesized to mechanically weaken lithosphere through increases in pore-fluid pressure (Sibson, 2000; Reyners et al., 2007) and hydration mineral reactions (Moore and Rymer, 2007). Earthquake swarms signaling brittle failure in the lower crust and upper mantle have been detected beneath cratonic lithosphere in the East African Rift (EAR), and interpreted as the rise of fluids through the plate (Lindenfeld et al., 2012; Albaric et al., 2014; Lee et al., 2016). Soil CO_2 flux and carbon isotope data collected in a companion study (Lee et al., 2016) from the Natron basin, Tanzania, and Magadi basin, Kenya, support these interpretations, revealing that mantle-derived CO_2 ascends to the surface along deeply penetrating faults in parts of the EAR.

The early-stage (the first 10 m.y.) development of continental rift basins is recorded in extensional fault systems observed at the surface. For many continental rifts, active deformation is concentrated in graben or asymmetric half-graben depressions with accompanying synrift sedimentation and volcanic resurfacing (Baker and Mitchell, 1976; Baker, 1986; Rosendahl, 1987; Scholz et al., 1990; Gawthorpe and Leeder, 2000; Ebinger and Scholz, 2012). Sedimentary cover often conceals fault scarps, resulting in uncertainty regarding the geometry and kinematics of fault populations, as well as calculations of bulk strain and time-averaged extension rates. Although these difficulties arise in many parts of the EAR, faults are well exposed in some basins in Ethiopia and the Kenya Rift (Fig. 1B; Le Turdu et al., 1999; Gupta and Scholz, 2000; Manighetti et al., 2001; Vetel et al., 2005; Agostini et al., 2011a). Well-exposed fault systems in the Kenya Rift include the Kino Sogo fault belt of the Turkana basin (Vetel et al., 2005), the Maji-Moto fault system of the Baringo basin (Le Turdu et al.,

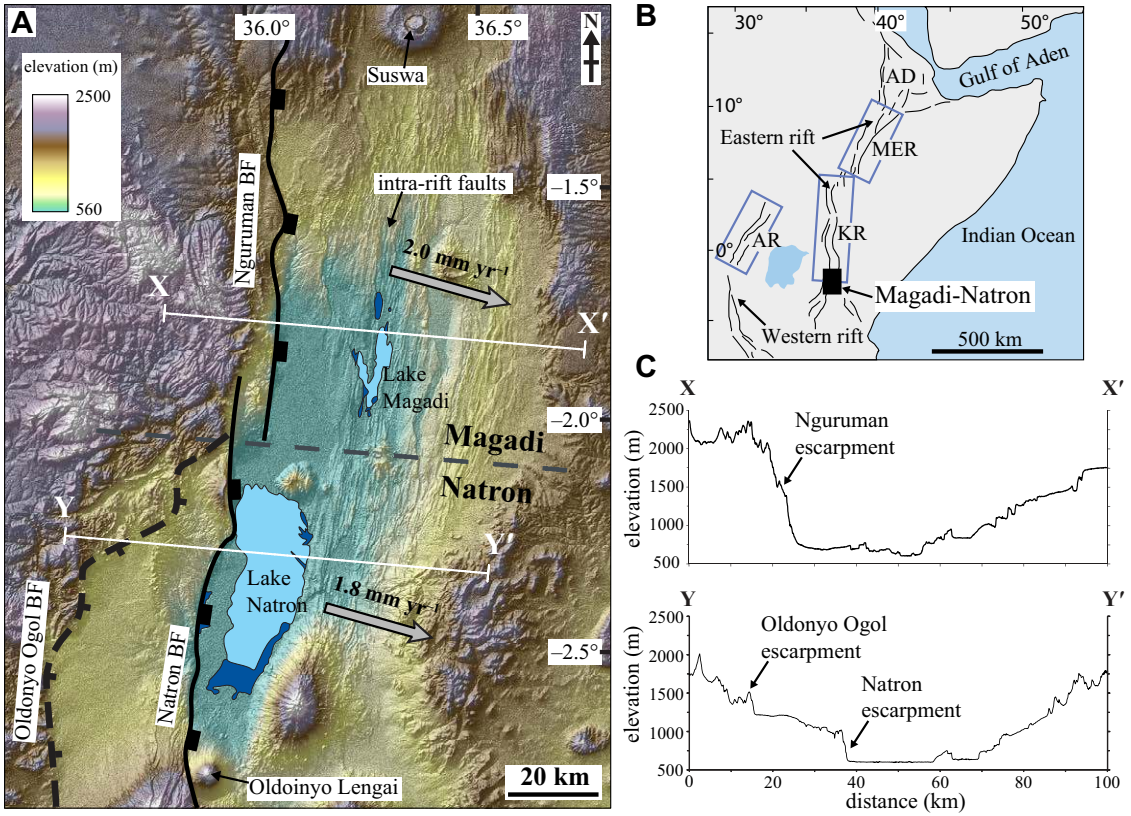

Figure 1. (A) Simplified map of the Magadi and Natron basins on a 30-m-resolution Shuttle Radar Topography Mission digital elevation model. Active volcanoes (Suswa and Oldoinyo Lengai) at the northern and southern terminus of the basins are annotated. Bold black lines indicate active border faults (BF). Dashed black line shows the now extinct Oldonyo Ogol fault, an early border fault of the Natron basin (Foster et al., 1997). Dashed gray line shows the inferred boundary between the Magadi and Natron basins based on the northern termination of the Oldonyo Ogol fault and southern termination of the Nguruman border fault of the Magadi basin. Dark blue areas show the distribution of permanent spring waters in the rift basin lakes, whereas light blue areas indicate ephemeral lake waters. Extension rates and directions in the center of each basin (gray arrows) were calculated from the kinematic model of Saria et al. (2014) (see Supplemental Materials, Section S3 [footnote 1]). Profiles X-X′ in Magadi and Y-Y′ in Natron are shown in C. (B) Map of the northeastern part of the African continent, showing the distribution of major fault structures (black lines) in the Western and Eastern rifts of the East African Rift. Solid black box shows the location of the Magadi and Natron basins in A. Also annotated are the general locations of the Afar Depression (AD), Main Ethiopian Rift (MER), Kenya Rift (KR) and Albertine Rift (AR). (C) Elevation profiles (10× vertical exaggeration) through the Magadi (X-X′) and Natron (Y-Y′) basins.

1999; Le Gall et al., 2000), and faults of the Magadi basin (Baker, 1958, 1963; Baker and Mitchell, 1976; Le Gall et al., 2008). A common feature of these fault systems is that they formed in young volcanic units (ca. 3 Ma or younger) with limited sedimentary cover (Baker and Wohlenberg, 1971; Vetel et al., 2005). Despite covering earlier-formed faults, widespread lavas also provide constraints on the accumulated fault strain since the time of their emplacement (Baker and Mitchell, 1976; Baker et al., 1988; Vetel et al., 2005; Le Gall et al., 2008). Therefore, these locations have served as focus sites for studies addressing the growth and kinematics of fault systems in the Kenya Rift of the EAR (Le Turdu et al., 1999; Morley, 1999; Le Gall et al., 2000, 2008; Vetel et al., 2005).

By comparing fault systems in basins of different ages across the Eastern rift of the EAR (Fig. 1B), we can infer how upper crustal strain is distributed within rifts as they evolve through time (Hayward and Ebinger, 1996; Ebinger, 2005; Corti, 2009; Agostini et al., 2011a). Similarly, geophysical and geochemical studies along the Eastern rift provide insights into how magma and volatile systems assist rift basin development (Birt et al., 1997; Ebinger and Casey, 2001; Pik et al., 2006; Albaric et al., 2014; Halldórsson et al., 2014; Keir et al., 2015). This study uses fault population data and lava chronology in well-exposed fault systems to investigate the evolution of fault-related strain, specifically during early-stage rifting (the first 10 m.y.). To achieve this we target two rift basins, the 3 Ma Natron (Foster et al., 1997) and 7 Ma Magadi basins (Crossley, 1979) (Fig. 1), which are in relatively early developmental stages. These data are examined alongside recently acquired spring geochemistry to investigate the role of magmatic volatile release in rift basin evolution. We show that areas of high fault strain coincide with zones of magmatic volatile release, revealing for the first time a strong link between the evolution of upper crustal strain and release of fluids from deep magma bodies in the EAR.

RIFT BASIN DEVELOPMENT IN THE EASTERN RIFT OF THE EAR

The EAR forms a >3000-km-long zone of individual rift basins, which are typically ~100 km long and tens of kilometers wide (Fig. 1B). It is the type example of active continental breakup occurring through extensional faulting, magmatism, and ductile thinning of lithosphere. Rifting in the central parts of the EAR occurs at the eastern and western edges of the Tanzanian craton, dividing the system into distinct Eastern and Western rifts (Rosendahl, 1987).

Faulting in the Eastern rift initiated ca. 25 Ma in north Kenya and Ethiopia (Ebinger et al., 2000). Geological and geophysical investigations of rift basins of different ages in the Eastern rift have highlighted major shifts in fault and magma systems during basin development (Hayward and Ebinger, 1996; Ebinger and Casey, 2001; Ebinger, 2005; Corti, 2009; McCartney and Scholz, 2016) (Fig. 2). In early-stage basins (younger than 10 m.y.), strain is focused along rift-bounding faults (termed border faults), which are often hundreds of kilometers long and can accrue >1000 m of throw. Flexure of the downthrown border fault hanging wall produces extensional strains (Vening Meinesz, 1950; Lavier et al., 2000; Cowie et al., 2005), which can manifest as smaller intra-rift faults that are typically tens of kilometers long with tens to hundreds of meters of throw (McClay and Ellis, 1987; Imber et al., 2003; Ebinger, 2005; Corti, 2009). Over the course of rift evolution in the EAR, the locus of strain has migrated away from border faults into these developing intra-rift fault systems (Hayward and Ebinger, 1996; Wolfenden et al., 2004; Corti, 2009). For evolved basins in the Eastern rift (older than 10 m.y.), strain migrated into en echelon magmatic segments in the center of the rift, with dimensions approximately 60 km by 20 km (Ebinger and Casey, 2001; Keranen et al., 2004; Maguire et al., 2006). Deformation in these magmatic segments manifests at the surface as slip along intra-rift faults (Rowland et al., 2007; Corti, 2009). At deeper levels of the crust (~5–20 km), strain is primarily accommodated through swarms of rift-parallel dikes (Ebinger and Casey, 2001; Rooney et al., 2005; Keir et al., 2006; Wright et al., 2012).

The transition from border fault to intra-rift fault-dominated strain accommodation is a critical process to focus strain as continental rifts evolve toward proto–spreading ridges (Corti, 2009). However, the timing and magmatic-tectonic processes controlling this transition are debated. Evidence of extensive diking below magmatic segments from shear-wave splitting and seismic tomography highlights an active magmatic influence on rift basin development (Keranen et al., 2004; Keir et al., 2005, 2011; Kendall et al., 2005; Bastow et al., 2010). The transition to intra-rift faulting in these segments is also accompanied by extensive volcanism in the rift center, often manifesting as rift-parallel chains of scoria cones and eruptive fissures (Rooney et al., 2011, 2014; Keir et al., 2015; Muirhead et al., 2015; Mazzarini et al., 2016). Recent fault-slip events on intra-rift faults in the Afar depression and the Natron basin coincide with the emplacement of rift-parallel dikes, suggesting that favorable stress conditions for intra-rift faulting are achieved during diking events (Rubin and Pollard, 1988; Wright et al., 2006; Rowland et al., 2007; Baer et al., 2008; Calais et al., 2008; Belachew et al., 2013).

Others suggest that the initiation of intra-rift faulting is a product of oblique continental rifting, and occurs independent of magmatic processes below the rift center (e.g., Corti, 2008). For example, in the Main Ethiopian Rift, the earlier formed (before 2 Ma) large border faults trend oblique to the regional extension direction (as much as 45°; Keir et al., 2015), whereas younger intra-rift faults (ca. 2 Ma to present) trend normal to the regional extension (Bonini et al., 1997; Agostini et al., 2011a). Oblique continental rifting in the Main Ethiopian Rift was previously attributed to changes in the relative motions between the Somalian and Nubian plates, where an initial Miocene–Pliocene phase of approximately northwest-southeast extension was followed by approximately east-west extension during the Quaternary (e.g., Bonini et al.,1997; Boccaletti et al., 1998; Wolfenden et al., 2004). The resulting change in plate kinematics produced sinistral motions on the earlier formed northeast-southwest–trending border faults, and drove the formation of north-south–trending intra-rift faults (Bonini et al., 1997; Corti et al., 2003). Alternatively, oblique rifting in the Main Ethiopian Rift may not require changes in far-field plate motions, but reactivation of preexisting lithospheric weaknesses trending oblique to the regional extension direction (Corti, 2008; Agostini et al., 2009, 2011b). Analog

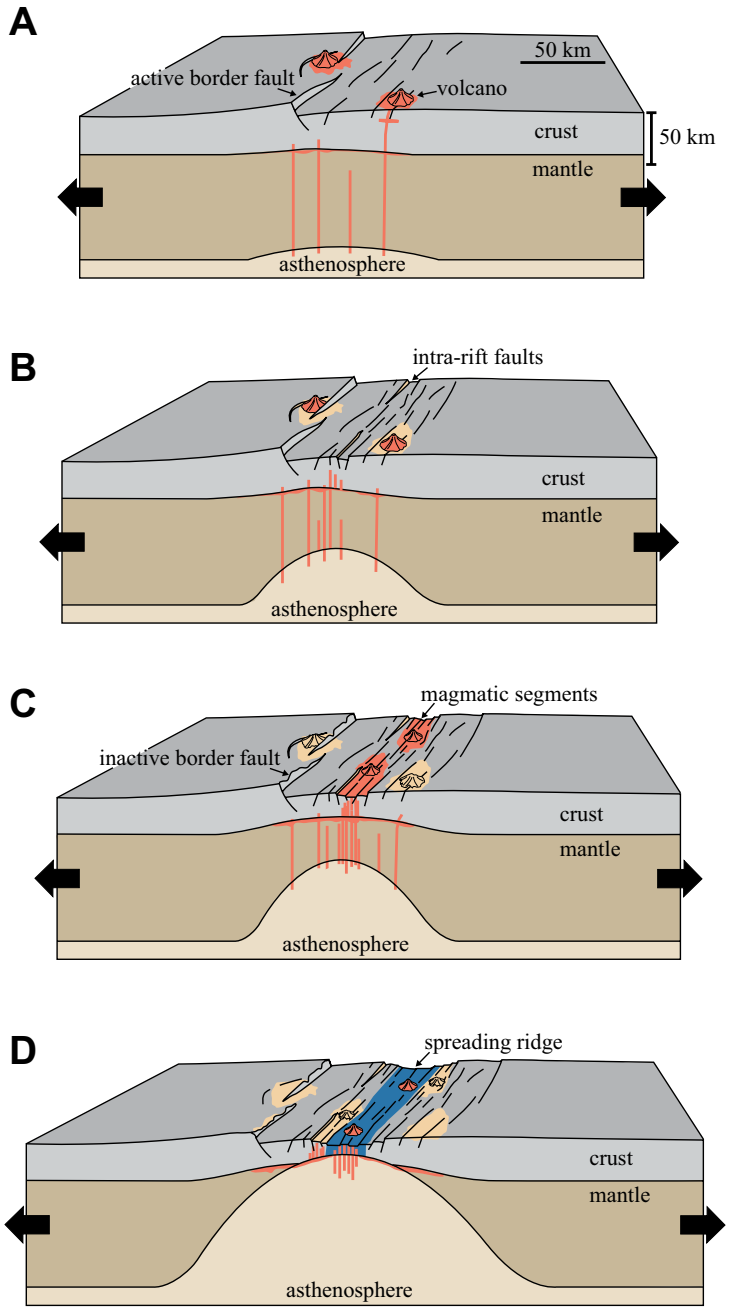

Figure 2. Current conceptual model for the development of rift basins in the Eastern rift, modified from Ebinger (2005) and Corti (2009). (A) Within 5 m.y. of the onset of rifting, the lithosphere thins through brittle (faulting) and ductile deformation. Brittle strain focuses on border faults, which may initiate on preexisting shear zones (McConnell, 1972; Daly et al., 1989). Slip along the border fault causes the crust to flex, forming a linear basin. Strain in the lower crust is accommodated though ductile thinning. Asthenosphere (i.e., viscously deforming, nonlithosphere mantle) begins to rise in response to thinning lithosphere, causing heat transfer and decompression melting to produce magmas that intrude lithosphere as dikes (red) or accrete along the crust-mantle boundary. Fluids released from magmas may alter and even melt rocks near the base of the crust. Magmatism that reaches the surface primarily forms volcanoes along the rift margins. (B) Approximately 5–10 m.y. after rift initiation, brittle strain begins to focus on smaller intra-rift faults in the rift center, driven either by magmatism (Keir et al., 2006) or oblique rifting (Corti, 2008), with a contribution from plate flexure (Lavier et al., 2000). Ongoing lithospheric thinning leads to further upwelling of asthenosphere and generation of greater melt volumes (which may or may not erupt at the surface). Faulting in the upper crust is thus accompanied by dike intrusions fed from these melt sources, which heat and weaken lithosphere. Strain in the lower crust is accommodated through magmatic intrusion and ductile thinning. (C) Continued magmatism along the rift axis results in the development of narrow zones of intense magmatism in the rift center, called magmatic segments, after ~10–15 m.y. Dike intrusions and related faulting within these segments accommodate the majority of strain in the upper crust, rendering border faults inactive. Strain in the lower crust is accommodated through magmatism and ductile thinning. (D) Nascent spreading ridges, much like those seen in the Afar Depression (e.g., Asal Rift; Stein et al., 1991; Ebinger and Casey, 2001), are initiated. Magma injection along the rift axis creates new oceanic lithosphere (dark blue) as continental crust is replaced by a thin, mafic igneous material.

investigations of rift-oblique extension under this model show that the earliest stages of basin development are still characterized by oblique slip on border faults, and then followed by a second stage of dip-slip motion within intra-rift faults, that group into discrete populations arranged en echelon in the rift center (Clifton et al., 2000; Clifton and Schlische, 2001; Corti, 2008; Agostini et al., 2011b). These experimental results are consistent with fault patterns in the Wonji fault belt of the Main Ethiopian Rift (Mohr, 1967; Gibson, 1969; Chorowicz et al., 1994; Bonini et al., 1997; Boccaletti et al., 1998; Agostini et al., 2011a, 2011b; Corti et al., 2013). The experiments suggest that the transition to intra-rift faulting may be driven by an upwelling mantle that (1) imposes upward-bending forces on the lithosphere that restrict slip on border faults, and (2) drives outward flow of an overlying (thinning) lower crust, leading to shear stresses acting on the base of the brittle crust below the rift center (Corti, 2008; Agostini et al., 2009). In the context of these models, the development of intra-rift fault systems may predate magmatism, and uprising of warm mantle and enhanced melt production occurred in areas of focused lithospheric thinning below intra-rift fault systems (Corti, 2008, 2009) to produce the magmatic segments imaged geophysically below the rift (Keranen et al., 2004; Mackenzie et al., 2005; Cornwell et al., 2006; Daly et al., 2008).

The studies described here highlight a fundamental question related to the magmatic-tectonic processes controlling continental rifting. Does rift basin architecture evolve in response to changes in plate kinematics and oblique rifting, or is it controlled by deeper processes, such as decompression melting and enhanced magma production (and related volatile release) below the rift? Early-stage rifts actively transitioning from border fault to intra-rift fault–domi-

nated strain accommodation represent prime targets to investigate processes controlling rift basin evolution. For example, if magmatism drives strain localization in evolving basins, then changes in fault system dynamics should be accompanied by changes in underlying magma systems and/or zones of magmatic volatile release. The 3 Ma Natron and 7 Ma Magadi basins are currently in their earliest stages of rifting, and provide an ideal location to test and advance existing models of continental rift initiation and evolution.

METHODS

Field and remote-sensing analyses were used to investigate faults in the Magadi and Natron basins. Fault traces were mapped from 0.5-m-resolution aerial photographs (provided by the Polar Geospatial Center, University of Minnesota, St. Paul). Individual segments were identified by the presence of visible fault tips. Following the method of Vetel et al. (2005), segments were interpreted to form part of a longer, segmented fault if they (1) exhibited relay zones with small offsets relative to the segment length, (2) had similar dip directions, and (3) displayed regular and systematic changes in throw patterns between segments, indicating that segments are geometrically and kinematically coherent (Peacock and Sanderson, 1991; Walsh and Watterson, 1991; Cartwright et al., 1995; Bohnenstiehl and Kleinrock, 1999; Walsh et al., 2003). Fault throws were measured from 30 m SRTM (Shuttle Radar Topography Mission) data, which have an estimated vertical error of 7.6 m (95% confidence) in the study area (Rodríguez et al., 2005). These remote-sensing analyses were verified with three field investigations in the Magadi and Natron basins from 2012 to 2014 (Fig. 3). Throws, and occasionally lengths, were measured on border fault and intra-rift fault segments in the field using a Trimble global positioning system (GPS) (GeoExplorer 6000 Series; GeoXT Handheld). Collected GPS data had a mean vertical error of 3.0 m (95% confidence) (Fig. 4). Faults were also examined for evidence of recent rupturing, such as fresh scarp surfaces or open fissures (Figs. 3A–3D). Throws were converted to displacements and heaves by assuming an optimal 60° dip for normal faults (Fig. 5). These data relate to fault displacements in only the most recently emplaced volcanics (e.g., Magadi Trachyte, Gelai lavas, Singaraini basalt; Baker and Mitchell, 1976; Mana et al., 2015), and do not reflect possible displacements that predate the emplacement of these units. Each basin has been affected by widespread volcanic resurfacing, where voluminous outpourings of lava erased the surface expression of earlier faulting (e.g., the 295 km^3 Magadi Trachyte; Baker and Mitchell, 1976; Guth, 2015). The strain analyses performed in this study, and described in the following, relate to horizontal extensional strains since the emplacement of the lava units in which faults are contained. Maximum displacements (D_{max}) refer only to displacements accrued on surficial fault scarps, and do not reflect possible fault displacements that occurred prior to emplacement of the faulted lavas. Maximum ages represent the maximum age of only the surficial fault scarp, and not necessarily the fault plane at depth.

Strain Calculations

Fault-scaling relations in the Magadi and Natron basins were investigated to calculate horizontal normal strain. First, to estimate individual fault displacements within the large fault population (>1000 faults), fault displacement-length ratios were constrained in the Magadi-Natron region. The conventional relationship between maximum displacement, D_{max}, and fault length, L, for continental faults is defined as:

$$D_{max} = \gamma L^n, \quad (1)$$

where γ is the scaling factor or displacement-length coefficient, and n is a power-law exponent that defines the rate of displacement accumulation with increasing fault length (Scholz and Cowie, 1990; Cowie et al., 1993; Dawers et al., 1993; Cartwright et al., 1995; Schultz et al., 2006). Although the value of n for individual fault data sets has been shown to be as high as 2 in some cases (Walsh and Watterson, 1988; Marrett and Allmendinger, 1991; Gillespie et al., 1992), linear elastic fracture mechanics models predict n = 1 (Cowie and Scholz, 1992; Bonnet et al., 2001), which is consistent with the full range of global displacement-length data sets (Cowie and Scholz, 1992; Gudmundsson, 1992; Dawers et al., 1993; Cowie et al., 1993, 1994; Carbotte and MacDonald, 1994; Dawers and Anders, 1995; Cartwright et al., 1995; Schlische et al., 1996; Bohnenstiehl and Kleinrock, 1999, 2000; Schultz et al., 2006, 2010). Therefore, studies quantifying extensional strains in fault populations often assume a linear relationship between fault displacement and length (e.g., Cowie et al., 1993; Carbotte and MacDonald, 1994; Schultz et al., 2010; Nahm and Schultz, 2011). The displacement-length coefficient, however, varies between fault populations depending on the tectonic setting and mechanical properties of the host rock (Cowie and Scholz, 1992; Bohnenstiehl and Kleinrock, 2000), and therefore must be determined by analyzing displacement-length ratios for each system of interest. On Earth, values of γ typically range from 10^{-1} to 10^{-3} (Schultz et al., 2010). Constraining this relationship within a given fault population (see following), and assuming a characteristic fault dip at depth, allows an estimate of D_{max} on any fault within a population from only measurements of L (Cowie et al., 1993, 1994; Carbotte and MacDonald, 1994; Nahm and Schultz, 2011).

Although D_{max} can be inferred from fault length data, estimates of crustal strain are based on average, rather than maximum, displacements along faults. The displacement profile along the trace of an individual fault tends to be bell shaped or elliptical (Dawers et al., 1993; Cartwright et al., 1995; Gupta and Scholz, 2000; Kattenhorn and Pollard, 2001), where the displacement remains relatively constant over at least the central third of the fault before reducing to zero at the fault tips (Walsh and Watterson, 1988; Cowie et al., 1993; Willemse et al., 1996; Peacock, 2002). Therefore, to estimate the average displacement along a given fault, the maximum displacement must be corrected by a value, κ, depending on the shape of the displacement distribution along the fault trace. Fault formation under the assumption of linear elastic fracture mechanics behavior (Pollard and Fletcher, 2005) is expected to produce an ideal elliptical displacement profile that would result in a κ of 0.7854 (Schultz et al., 2010).

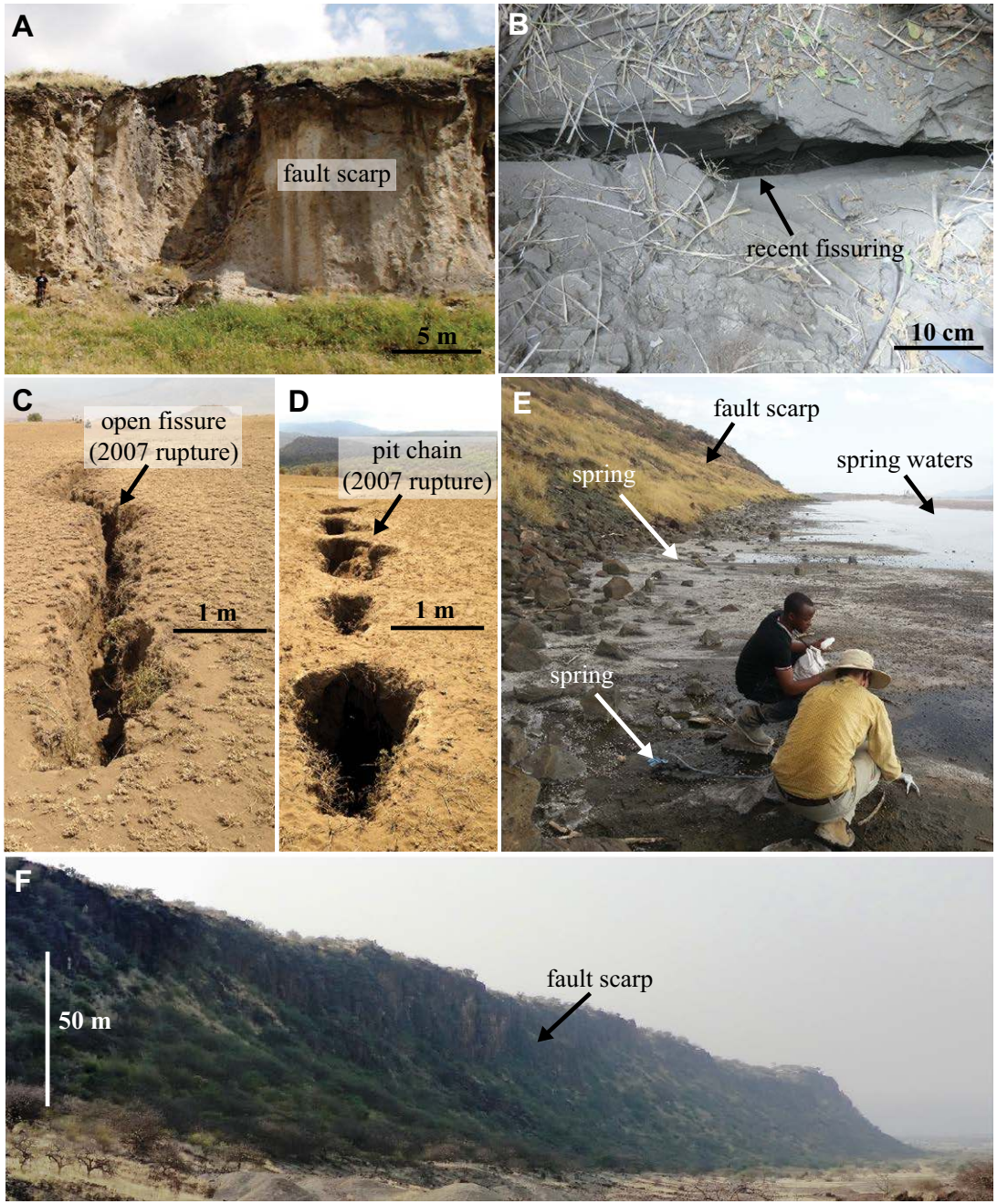

Figure 3. Field images from the Natron and Magadi basins. (A) Small border fault segment (<30 m high) in the Natron basin displacing a 200 ± 5 ka tuff and Pleistocene debris avalanche deposits sourced from Oldoinyo Lengai volcano (Sherrod et al., 2013) (photo location: 2.6122°S, 35.8661°E). (B) Recent dilational fissure along the trace of a subsidiary fault segment of the Natron border fault (photo location: 2.6801°S, 35.8821°E). (C) Open fissure related to recent activity along an intra-rift fault in the Natron basin during the 2007 dike-related rifting event (photo location: 2.7272°S, 36.0696°E). (D) Aligned pit chains related to the 2007 earthquake rupture (photo location: 2.7277°S, 36.0693°E). (E) Fault-parallel springs expelling from the base of an intra-rift fault in the Magadi basin (photo location: 1.8599°S, 36.3064°E). (F) Intra-rift fault scarp (77 m high) dissecting ca. 0.9 Ma Magadi Trachyte lavas in the Magadi basin (photo location: 1.82061°S, 36.2044°E).

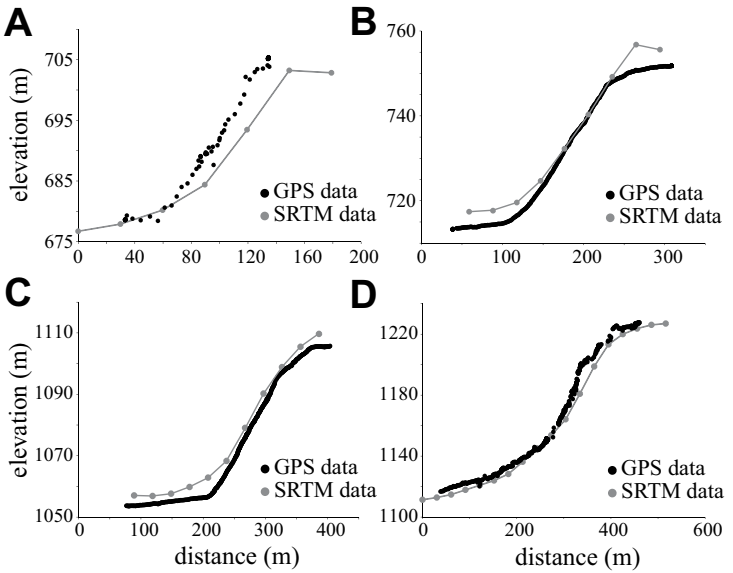

Figure 4. Examples of fault profiles in the Natron and Magadi basins measured using a Trimble global positioning system (GPS) instrument. Shuttle Radar Topography Mission (SRTM) data presented for comparison. (A) Scarp location is 1.8258°S, 36.2083°E. (B) Scarp location is 1.8603°S, 36.2159°E. (C) Scarp location is 1.8388°S, 36.5011°E. (D) Scarp location is 1.50138°S, 36.4965°E.

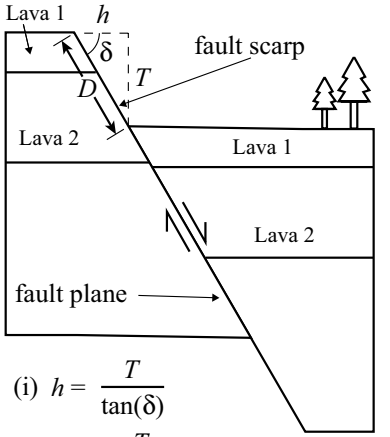

Figure 5. Simplified cross-sectional depiction of a normal fault (orthogonal to fault strike). Fault heave (*h*), throw (*T*), and dip (δ) are annotated. By assuming a fault dip (optimally 60° for normal faults), throw can be converted to both (i) heave and (ii) displacement (*D*). The youngest displaced lava, situated at the top of the fault scarp (lava 1), provides a maximum age for the fault, which is used to understand changes in time (Δ*t*). The age of the fault can be compared against the cumulative heave and displacement to calculate the time-averaged extension rate (iii) and slip rate (iv), respectively.

(i) $h = \frac{T}{\tan(\delta)}$

(ii) $D = \frac{T}{\sin(\delta)}$

(iii) extension rate $= \frac{\Delta h}{\Delta t}$

(iv) slip rate $= \frac{\Delta D}{\Delta t}$

The brittle horizontal normal strain (ε_n) represented by a normal fault population (number of faults = N) may be estimated by summing the extensional strain accommodated along all faults, and is given by a modified version of the Kostrov summation (Kostrov, 1974; Scholz and Cowie, 1990; Nahm and Schultz, 2011):

$$\varepsilon_n = \frac{\sin\delta\cos\delta}{V}\sum_{(i=1)}^{N} D_i L_i H_i, \quad (2)$$

where δ is the fault dip (assumed to be optimally 60° for normal faults), *V* is the volume of the faulted region, *L* is the fault length, *H* is the fault depth extent, and *D* is the average displacement ($\kappa \times D_{max}$). Studies investigating fault population strain on Earth's surface (Gupta and Scholz, 2000) and seafloor (Cowie et al., 1993), and other planetary bodies (e.g., Mars; Nahm and Schultz, 2011), make the simplifying assumption that *H* = *L*. The assumptions made by these studies therefore require a downward-propagating fault model, which is consistent with observations from many studies at magmatic rift settings (e.g., Ethiopia and Iceland; Gudmundsson and Bäckström, 1991; Forslund and Gudmundsson, 1992; Gudmundsson, 1992; Acocella et al., 2003, 2008; Trippanera et al., 2015). For example, field observations in Tertiary fault systems in Iceland show that the greatest frequency of faults occurs in the upper few kilometers of the crust, suggesting that these faults nucleated at relatively shallow depths (~1 km) and propagated downward (Forslund and Gudmundsson, 1992; Gudmundsson, 1992). Downward fault propagation in magmatic rifts may also be promoted where fault activation is assisted in part by crustal flexural (e.g., bending of the border fault hanging wall or the flexural margins of subsiding crust; Vening Meinesz, 1950; Lavier et al., 2000; Acocella et al., 2008; Corti et al., 2015), as flexure produces the highest extensional stresses at the near surface (Turcotte and Schubert, 1982).

Once *L*, and hence *H*, is equal to the depth of the brittle crust, faults can only grow by increasing *L* while *H* remains constant (Cowie et al., 1993). As a result, horizontal extensional strains may be estimated from two separate equations for small (*L* < brittle crust thickness) and large (*L* > brittle crust thickness) faults from the method of Cowie et al. (1993). For small faults, the brittle horizontal normal strain can be calculated using:

$$\varepsilon_n = \frac{\sin\delta\cos\delta}{V}\sum_{(i=1)}^{N} \gamma\kappa(L_i^3), \quad (3)$$

whereas the brittle horizontal normal strain for large faults may be calculated from the equation:

$$\varepsilon_n = \frac{\cos\delta}{A}\sum_{(i=1)}^{N} \gamma\kappa(L_i^2), \quad (4)$$

where *A* is the area of the faulted region.

The equations and scaling relations described here were used to estimate horizontal normal strain within fault populations of the Magadi and Natron basins. Brittle crust thickness estimates are from Albaric et al. (2009) for central Magadi and the north Natron–south Magadi border (11 and 19 km, respectively).

Measuring Fault Lengths, Throws, and Slip Rates from Remote Sensing and Field Data

Broad-scale analyses of fault populations from remote-sensing data are prone to both natural and detection biases (Soliva and Schultz, 2008; Schultz et al., 2010). Natural biases are a consequence of processes such as erosion and basin infilling, whereas detection biases relate to the resolution of the data acquisition method (e.g., aerial or satellite photos, SRTM data). These factors lead to truncation biases, which underestimate the size and number of smaller faults in a given population (Schultz et al., 2010), and cannot resolve the contributions of small tension fractures. The resolution of aerial photos used to measure fault lengths in this study is 0.5 m/pixel; given the estimated throw-to-length ratio in this study of 0.005 (Fig. 6E) and an average ~20° slope measured for degraded scarps throughout the field (Fig. 4), these images should resolve the hanging-wall and footwall cutoffs of faults with lengths >36 m. However, faults with small throws (e.g., <5 m) are also prone to natural bias because they are easily eroded and buried by sediments. For example, faults with lengths <250 m could not be identified using aerial photography in the Magadi and Natron basins, and only 7 faults were identified with lengths between 250 and 500 m (i.e., faults with estimated throws <~2.5 m). As a result, it is conservatively assumed in this study that faults with throws <5 m are frequently below the detection limit of the aerial photos due to natural biases, resulting in a fault length truncation bias of 1000 m (Fig. 6C). This truncation bias is consistent with that applied by Soliva and Schultz (2008) for faults in the Afar region of the EAR.

Fault throws could not be measured from aerial photographs; therefore, throw data were remotely acquired from the 30 m SRTM data set. The accuracy of the throw data depends on the estimated vertical precision of this data set for the African continent (7.6 m to 95% confidence; Rodríguez et al., 2005). Based on the precision of the SRTM, it is inferred that throws <10 m cannot be confidently measured (i.e., across faults <~2000 m in length), however, throws of these smaller can be confidently estimated by assuming a linear relationship between fault length and throw (Schlische et al., 1996). Maximum throws were estimated using SRTM data for 40 intra-rift faults in the Natron and Magadi basins by systematically measuring throw along the lengths of

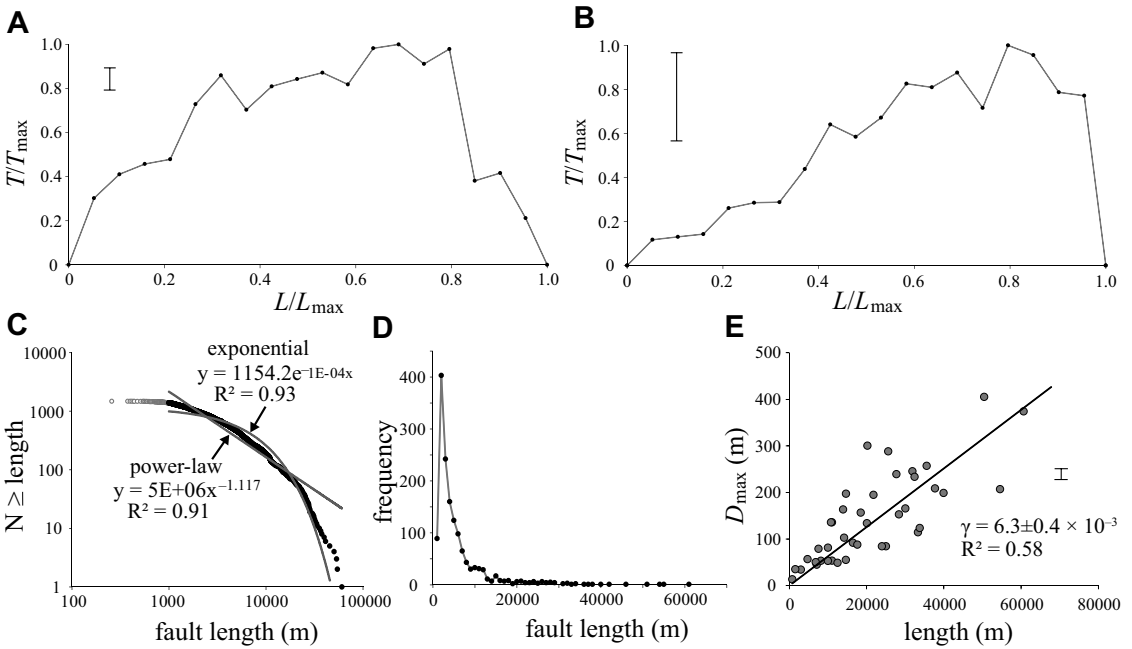

Figure 6. Summary plots of remotely acquired fault data. (A) Example of a throw profile across a fault in the Magadi basin. All length (*L*) and throw (*T*) data are normalized by the maximum length (L_{max}) and maximum throw (T_{max}) values, respectively. Error bar (top left) is to 95% confidence. Fault location is shown in Figure 7A. (B) Example of an asymmetric throw profile across a fault in the Magadi basin. All length and throw data are normalized as in A. Error bar (top left) is to 95% confidence. Fault location is shown in Figure 7A. (C) Cumulative frequency plot of fault lengths for all intra-rift faults in the Natron and Magadi basins. Gray points represent faults with lengths below the truncation bias limit, whereas black points show fault lengths greater than the truncation bias. Gray lines show exponential (curved line) and power-law (straight line) fits for the data. Comparable R-squared values suggest that length distributions cannot be confidently defined by either negative power-law or negative exponential functions. (D) Incremental length-frequency distribution of all intra-rift faults in the Natron and Magadi basins. (E) Scatter plot of maximum displacement (D_{max}) versus length for faults in the Natron and Magadi basins (assumed 60° dip). Slope of the best-fit line (black line) represents the displacement-length coefficient (γ). Bar on the right of the graph shows the estimated error of measured fault displacements (95% confidence), whereas length errors are less than the size of the points. Error for the displacement-length coefficient is based on best fit lines where all displacements are given minimum and maximum values to 95% confidence, based on the vertical error of the Shuttle Radar Topography Mission data set.

SUPPLEMENTAL MATERIAL FOR

Evolution of upper crustal faulting assisted by magmatic volatile release during early-stage continental rift development in the East African Rift

J. D. Muirhead[1,2], S. A. Kattenhorn[1,3], H. Lee[4], S. Mana[5,6], B. D. Turrin[6], T. P. Fischer[4], G. Kianji[7], E. Dindi[7], D. S. Stamps[8]

[1]Department of Geological Sciences, University of Idaho, Moscow, Idaho 83844, USA.

[2]Department of Earth Sciences, Syracuse University, Syracuse, New York 13244, USA

[3]Department of Geological Sciences, University of Alaska Anchorage, Anchorage, Alaska 99508, USA

[4]Department of Earth and Planetary Sciences, University of New Mexico, Albuquerque, New Mexico 87131, USA.

[5]Department of Geological Sciences, Salem State University, Salem, Massachusetts 01970, USA

[6]Department of Earth and Planetary Sciences, Rutgers University, Piscataway, New Jersey 08854, USA.

[7]Department of Geology, Chiromo Campus, University of Nairobi, P.O. Box 30197-00100, Nairobi, Kenya.

[8]Department of Geosciences, Virginia Tech, 4044 Derring Hall, Blacksburg, Virginia 24061, USA.

SUMMARY OF CONTENT

[1]Supplemental Materials. Description of supplemental geological map for the region (Figure S1), as well as methods for calculating flexural strain in a fault hanging wall, estimating the basin-scale extension rate in study region, spring sampling and analysis, and $^{40}Ar/^{39}Ar$ dating of volcanics. Please visit http://dx.doi.org/10.1130/GES01375.S1 or the full-text article on www.gsapubs.org to view the Supplemental Materials.

faults (e.g., Figs. 6A, 6B). Comparison of fault throws measured in the SRTM with those measured using a Trimble GPS in the field shows good agreement (Fig. 4). To avoid biases related to erosion and burial by sediments, throws were remotely measured only on well-exposed faults with relatively steep scarps (typically 15°–30° dips on the SRTM) that were not surrounded or covered by extensive rift sediments. However, the precision of throw profile analyses will also be affected by sediments that collect against the fault scarp on the downthrown hanging wall (Cartwright et al., 1995). Although the sedimentary cover is expected to be only a few meters thick in arid, extensional basins (e.g., Volcanic Tablelands and Canyonlands, USA; Dawers and Anders, 1995; Moore and Schultz, 1999), the measured throws likely represent minimum values. To avoid detection biases related to the resolution of the SRTM, faults with throws <10 m were not included in comparative throw-length analyses (e.g., Figs. 6A, 6B, 6E). However, the throws of smaller faults were inferred assuming a linear relationship between fault length and throw (e.g., Cowie et al., 1993; Schultz et al., 2010; Nahm and Schultz, 2011), and then used in the horizontal extensional strain calculations. Throw values were also converted to displacement and heave by assuming an optimal 60° dip for normal faults (Fig. 5). Together, fault lengths and throws along 40 intra-rift faults give a best-fit displacement-length coefficient (i.e., γ in Equation 1) of $6.3 \pm 0.4 \times 10^{-3}$ (Fig. 6E), which is in good agreement with faults dissecting Quaternary lavas in rift zones elsewhere, such as Iceland (Gudmundsson, 1992; Angelier et al., 1997), the Kino Sogo fault belt of the Turkana basin, Kenya (Vetel et al., 2005), and the East Pacific Rise (Cowie et al., 1993, 1994; Carbotte and MacDonald, 1994).

Volcanic rocks at the tops of scarps were sampled for ^{40}Ar-^{39}Ar age analyses (Table 1; see Supplemental Materials, Section S5[1]), providing constraints on the ages of major lava units and maximum ages of the measured faults. By comparing faulted lava ages with fault throw values, and converting throw to both displacement and heave, these data can be used to estimate maximum slip rates and extension rates, respectively. As shown in Figure 5, slip rates refer to changes in displacement over time, whereas extension rates relate to changes in heave over time.

TABLE 1. $^{40}Ar/^{39}Ar$ AGES FOR FAULTED VOLCANIC ROCKS IN THE MAGADI AND NATRON BASINS

Sample no.	Long (°E)	Lat (°S)	Fault throw (m)	Throw error (95%)	Geological unit	$^{40}Ar/^{39}Ar$ age (Ma)	Error 1σ	Minimum time-averaged slip rate (mm yr^{-1})*	Error 95%^
1	36.1585	2.4107	59.1	7.3	Gelai lavas	1.158	0.017	0.059	0.005
2	35.8637	2.6083	125.1	10.2	Sekenge Crater[b]	1.248	0.006	0.116	0.008
3	35.8672	2.6155	125.1	10.2	Nephelinite[c]	4.057	0.006	N/A[a]	N/A[a]
4	36.1476	2.7295	59.6	1.9	Gelai lavas	1.053	0.004	0.065	0.002
5	36.1693	2.6946	68.1	2.6	Gelai lavas	1.19	0.007	0.066	0.002
6	36.184	2.6401	57	5.7	Gelai lavas	1.167	0.003	0.056	0.005
7	35.8334	2.5506	151.8	3.4	Sambu basalts	1.968	0.02	0.089	0
8	36.2288	2.4864	75.7	10.2	Gelai lavas	0.961	0.02	0.091	0.008
9	35.8744	2.5902	N/A[f]	N/A[f]	Tuff[d]	0.095	0.004	N/A	N/A
10	35.8676	2.5933	90.8	4.3	Natron lavas[e]	1.16	0.027	0.09	0
11	35.8787	2.7814	N/A[f]	N/A[f]	Tuff[d]	0.226	0.006	N/A	N/A
12	35.8818	2.6795	28.1	1.9	Tuff[d]	0.2	0.005	0.162	0.002
13	36.2184	1.8617	154.3	5.9	Magadi trachyte	1.367	0.034	0.13	0.001
14	36.2014	1.8266	76.7	2.3	Magadi trachyte	0.946	0.005	0.094	0.002
15	36.502	1.8382	118.1	10.8	Singaraini basalt	1.96	0.09	0.07	0
16	36.3634	1.6091	11.8	2.9	Magadi trachyte	1.152	0.013	0.012	0.003
17	36.2834	1.9815	73.2	7.2	Magadi trachyte	1.15	0.014	0.073	0.005
18	36.4967	1.5013	52.9	2.3	Limiru trachyte	2.048	0.021	0.03	0.001
19	36.3693	1.8108	N/A	N/A	Dike intrusion	1.098	0.02	N/A	N/A

Note: Map of sample locations provided in Figure 7. Also included are the minimum time-averaged slip rates of faults based on acquired dates.
*Slip rates assume a 60° dip on all faults at depth.
^Slip rate errors consider both the errors in age and throw presented.
[a]Lavas outcrop below sample no. 2. Most recent slip rate is based on sample no. 2.
[b]Sampled a basaltic boulder with a breadcrust appearance, suggesting it may be a primary component of the deposit.
[c]Lavas likely sourced from Mosonik volcano.
[d]Inferred to be from Oldoinyo Lengai based on proximity, but could also be sourced from the Natron-Engaruka field.
[e]Basalt occurs as part of Natron escarpment sequence. The source is unknown.
[f]Draping over subsidiary scarps with no observable offset.

RESULTS: FAULT CHARACTERISTICS, LAVA CHRONOLOGY, AND SPRING GEOCHEMISTRY OF THE NATRON AND MAGADI BASINS

General Observations

The 3 Ma Natron basin (Foster et al., 1997) is bounded by an ~600-m-high border fault escarpment (Natron border fault) along its western margin. Rift-normal topographic profiles north of Gelai volcano in the Natron basin (Fig. 1D) show the lowest elevations (595 m) in the lake-filled basin adjacent to the currently active Natron border fault, where a number of hydrothermal springs expel water into the lake at the base of the border fault scarp. In addition to the main escarpment (bold black line in Fig. 1A), the Natron basin comprises a number of smaller, subsidiary segments with throws of as much as 200 m. Incised gullies and ravines within the footwall of the border fault also expose subsidiary faults with measured throws of as much as 91 m (e.g., sample 10, Table 1). Locally, the border fault exhibits recent fissures displacing Holocene alluvium (Sherrod et al., 2013) (Fig. 3B) and at least one relatively young fault segment (Fig. 3A) offsets tuff (maximum age of 200 ± 5 ka; Table 1) and debris avalanche deposits sourced from Oldoinyo Lengai (Kervyn et al., 2008; Sherrod et al., 2013). This fault exhibits as much as 28.1 ± 1.9 m of throw, implying recent and probably ongoing border fault activity (0.16 mm yr^{-1} since the late Pleistocene on this subsidiary segment). Tuff deposits with $^{40}Ar/^{39}Ar$ ages ranging from 91 ± 4 to 230 ± 6 ka are observed draping some subsidiary border fault segments with no accompanying fault displacements; this suggests that not all the observed (subsidiary) fault segments along the border fault have produced surface ruptures since ca. 230 ka.

For this study the intra-rift faults of the Natron basin dissecting Gelai volcano lavas were measured and sampled in the field in the southernmost ~40 km of the basin. Logistical restrictions prevented access to intra-rift faults in Magadi Trachyte lavas between Lenderut volcano and the northern slopes of Gelai (Fig. 7A; see also Supplemental Fig. S1[2]). Faults analyzed in the field on

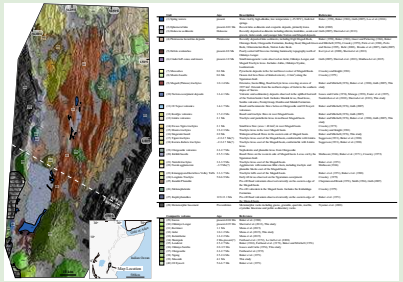

[2]Supplemental Figure S1. Geological map of the Magadi-Natron region. Please visit http://dx.doi.org/10.1130/GES01375.S2 or the full-text article on www.gsapubs.org to view the Supplemental Figure.

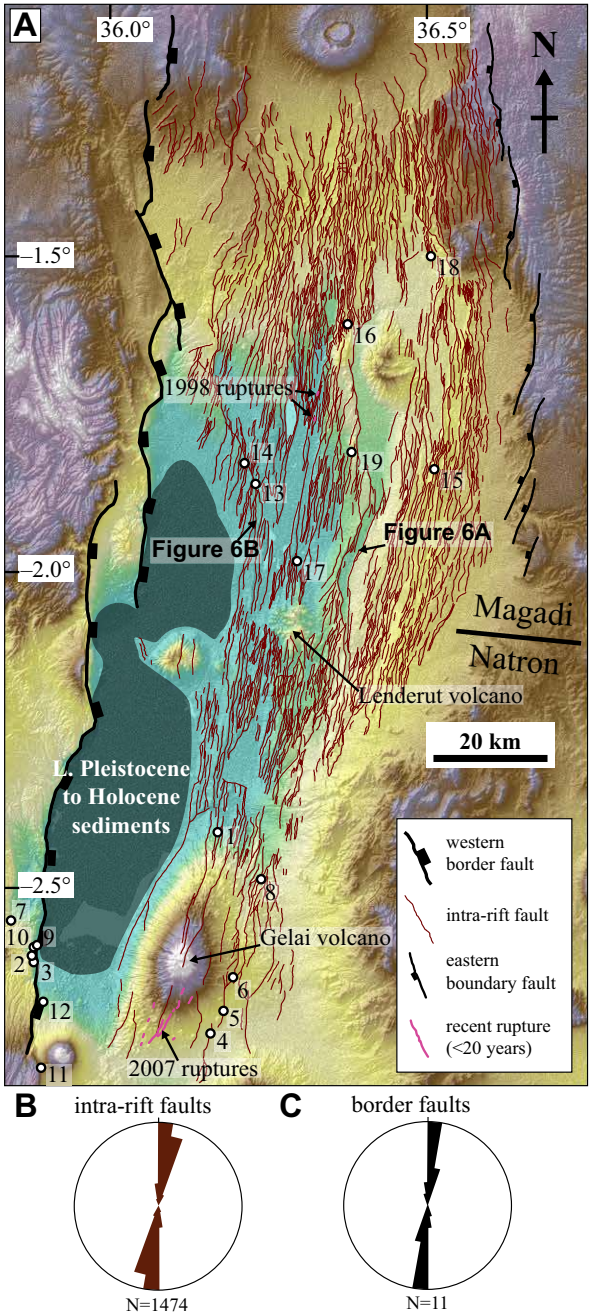

Figure 7. (A) Distribution of fault traces in the Natron-Magadi region as mapped from 0.5-m-resolution aerial photographs. Thick black lines are rift margin border faults; thin black lines are opposing rift margin boundary faults; thin red lines are intra-rift faults. The western border faults are the major fault structures (throws >1000 m; Baker et al., 1971; Ebinger et al., 1997; Birt et al., 1997) defining the original half-graben basin structure. The eastern boundary fault is an old fault escarpment (2.3–3.3 Ma Ngong-Turoka fault; Baker and Mitchell, 1976) that defines the eastern margin of the basin, but with significantly less throw (~200–500 m) than the border faults. Only the main escarpments along the rift-bounding faults are shown; however, additional minor subsidiary fault segments are also present. Numbers refer to sample locations for $^{40}Ar/^{39}Ar$ dating of faulted volcanics (see Table 1). Recent ruptures from Wauthier (2011) and Ibs-von Seht et al. (2001) were also identified and mapped in the field. The locations of the fault throw profiles shown in Figures 6A and 6B are annotated. Late (L.) Pleistocene to Holocene lake sediments (dark shading) likely conceal some faults in the region, particularly below present-day Lake Natron (see Fig. 1). (B) Length-weighted rose diagram of the strikes of all intrafault traces in the Natron-Magadi region. (C) Length-weighted rose diagram of the strikes of border and boundary fault escarpments in the Natron-Magadi region.

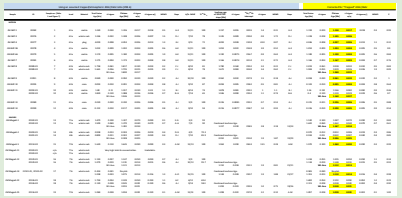

[3]Supplemental Table S1. Incremental-heating $^{40}Ar/^{39}Ar$ data for newly analyzed volcanic rocks in the Natron and Magadi basins. Ages reported in bold and highlighted in yellow are considered most reliable, and take into account the isochron determined $^{40}Ar/^{36}Ar$ ratio for the "trapped" component. Please visit http://dx.doi.org/10.1130/GES01375.S3 or the full-text article on www.gsapubs.org to view the Supplemental Table.

and around Gelai volcano exhibit typical throws of between 50 and 100 m. Age dating of faulted lavas around Gelai reveals that these faults have been active since ca. 1.2 Ma (Table 1), and ongoing intra-rift fault activity in the Natron basin is suggested by persistent shallow (<10 km) tectonic earthquakes below Gelai, with magnitudes ranging from 1.0 to 4.5 (Lee et al., 2016), as well as a 2007 dike-induced surface rupture (Baer et al., 2008; Calais et al., 2008). This surface rupture produced a small dilational fault scarp (as much as 65 cm throw; Wauthier, 2011; Fig. 3C), which could still be observed ~7 yr later as a series of aligned pit chains (to 5 m long and 2 m wide; Fig. 3D). Throws documented by Wauthier (2011) were rapidly removed by erosion of the original small scarp in loose surface materials.

The 7 Ma Magadi basin (Crossley, 1979) comprises an ~1600-m-high border fault escarpment (the Nguruman fault). During field work, there was no identified evidence of recent rupturing, such as recently opened fissures or fault displacements on younger than 250 ka volcanics or sediments, in contrast to the Natron border fault (Figs. 3A, 3B). Based on field observations, discussions with the local residents, and existing hydrothermal spring maps (e.g., Baker, 1958; Eugster, 1970), no springs are present along the Nguruman border fault escarpment of the Magadi basin. Late Pleistocene lake deposits (e.g., Oloronga Beds; Baker, 1958; Behr and Rohricht, 2000) within ~20 km of the Nguruman escarpment suggest that a paleolake was once situated along the western side of the Magadi basin, forming a northern extension of present-day Lake Natron (Crossley, 1979; see Supplemental Fig. S1 [footnote 2]).

Rift-normal elevation profiles show that the deepest part of the Magadi basin occurs away from the border fault in the rift center (603 m elevation compared to 680 m at the base of the Nguruman escarpment), where faults pervasively dissect 1.37–0.95 Ma trachyte lavas (Fig. 1C). Recent east-southeast–west-northwest extension is indicated by rift-parallel, dilational joint sets in late Pleistocene and Holocene lake sediments in the intra-rift graben and around Lake Magadi (Atmaoui and Hollnack, 2003; Muirhead, 2016). This assertion is further supported by a surface rupturing event during a period of enhanced seismicity in 1998. Focal mechanisms from this event reflect normal faulting in response to a west-northwest–east-southeast–directed extensional stress field, which at the surface produced a small, north-northeast–south-southwest–trending dilational fault scarp (~10 cm throw; Ibs-von Seht et al., 2001; Atmaoui and Hollnack, 2003) (Fig. 7). Within the intra-rift fault system, numerous springs feed water into perennial Lake Magadi. Much like Lake Natron, this shallow lake (only a few meters deep) has little surface drainage input and a high evaporation rate, yet survives due to the influx of CO_2-rich, saline fluids from below (Eugster, 1970; Roberts et al., 1993; Lee et al., 2016). The combination of CO_2-rich spring waters, alkali-rich volcanics, saline fluids, and arid conditions create unique environmental conditions necessary to produce economically viable trona and nahcolite deposits in these lakes (Eugster, 1970; Jones et al., 1977; Monnin and Schott, 1984; Jagniecki et al., 2015; see also Supplemental Fig. S1 [footnote 2]).

Geochronology of Volcanic Units and Fault Slip Rates

The timing of fault activity was investigated using new $^{40}Ar/^{39}Ar$ dating of volcanic units (Table 1; Supplemental Table S1[3]) and by reviewing geological maps and previously published K-Ar and $^{40}Ar/^{39}Ar$ ages (see Supplemental Fig. S1 [footnote 2]). Volcanic rocks dissected by 17 faults were sampled for $^{40}Ar/^{39}Ar$ age analyses in the Magadi and Natron basin, including 13 intra-rift faults (6 from Magadi and 7 from Natron) and 4 fault segments that collectively form part of the Natron border fault escarpment. Sampled rocks include basalt, trachyte, and nephelinite lavas, as well as volcanic tuff. All samples were collected along the footwall cutoffs at the tops of fault scarps and away from fault tips to avoid the reduced fault throw in those regions. Determined ages range from 4.05 to 0.10 Ma.

These data provide new constraints on the timing of volcanic events that were previously dated using K-Ar techniques (Isaacs and Curtis, 1974; Baker and Mitchell, 1976; Crossley, 1979; Baker et al., 1988; Foster et al., 1997). In the Natron basin, nephelinite (sample 3, Fig. 7A; Table 1) sampled on the Natron border fault and the eastern flank of Mosonik volcano (Supplemental Fig. S1 [see footnote 2]) gives an age of 4.06 Ma, suggesting this volcano began erupting ~0.5 m.y. earlier than previously estimated (Dawson, 1992; Foster et al., 1997). Basalts from Oldonyo Sambu volcano (Supplemental Fig. S1 [see footnote 2]), sampled at the top of the footwall of the Sangan fault segment of the Natron border fault (sample 7), give an age of 1.97 Ma. Although this date is consistent with previous K-Ar studies, which range from 3.5 to 1.8 Ma (Isaacs and Curtis, 1974), the date of 1.8 Ma was originally considered anomalous, with the authors favoring an age of 3.5–3.1 Ma for the volcano. This new $^{40}Ar/^{39}Ar$ age, however, suggests that Oldonyo Sambu was active until ca. 1.97 Ma. Sekenge crater rim pyroclastic deposits were also sampled (Neukirchen et al., 2010; Sherrod et al., 2013; sample 2, Fig. 7A). These deposits are displaced by a subsidiary fault segment in the footwall of the Natron border fault escarpment. They contain rare basaltic breadcrust bombs (as much as 30 cm diameter), which give a maximum age of 1.25 Ma. Tuff in close proximity to Oldoinyo Lengai (samples 9, 11, and 12) range in age from 0.23 to 0.10 Ma. Some of these deposits are offset by small segments of the Natron border fault in the hanging wall of the main escarpment. Although these deposits cannot be correlated to Oldoinyo Lengai with complete certainty, the dates are within the range of published ages for the volcano (minimum age of 350 ka to present; Sherrod et al., 2013). Faulted lavas in the intra-rift portion of the Natron valley were derived from Gelai volcano. The new ages presented here demonstrate a longer duration of activity for Gelai (minimum of 230 k.y.), with ages in the range of 1.19–0.96 Ma (samples 1, 4, 5, 6, and 8), compared to 1.19–1.11 Ma reported in Mana et al. (2015).

In the Magadi basin, age data suggest that the Singaraini basalt was emplaced by 1.96 Ma (sample 15; Fig. 7A; Table 1), rather than the 2.31 Ma originally proposed by Baker and Mitchell (1976) based on K-Ar dating. This study also provides the first published $^{40}Ar/^{39}Ar$ ages for Magadi Trachyte lavas (samples 13, 14, 16, 17), a recent and widespread lava unit observed along the center of the Natron and Magadi basins. The new ages of 1.37–0.95 Ma are

within previously documented K-Ar ages ranging from 1.4 to 0.8 Ma (Baker and Mitchell, 1976; Baker et al., 1988). However, only the youngest lavas were sampled, exposed at the tops of fault scarps; therefore, these data only reflect the ages of lavas emplaced during the later stages of the Magadi Trachyte volcanic event. A new date of 2.05 Ma for Limiru trachyte (sample 18) is consistent with the 2.01–1.88 Ma age of Baker and Mitchell (1976).

Age dating of faulted lavas at the tops of fault scarps provides the maximum ages of sampled faults. When combined with measurements of fault throw, the dates also constrain time-averaged minimum slip rates (Fig. 5). Minimum slip rates (Table 1) for intra-rift faults in the Natron basin range from 0.06 to 0.09 mm yr^{-1}. Subsidiary border fault segments in Natron exhibit higher minimum slip rates, ranging from 0.09 to 0.16 mm yr^{-1}. Time-averaged minimum slip rates estimated for sampled intra-rift faults of the Magadi basin range from 0.01 to 0.13 mm yr^{-1}, but are generally higher than slip rates in equivalent-age lavas in the Natron basin. However, these data (Table 1) do not include the largest fault throws (as much as 362 m) measured from SRTM data in Magadi Trachyte lavas, which would suggest that intra-rift faults have maximum slip rates ranging 0.30–0.45 mm yr^{-1} in the 0.95–1.37 Ma Magadi Trachyte.

Fault Statistics of Intra-Rift Fault Populations

We identified 1474 intra-rift faults in the Natron and Magadi basins. The mean trend of intra-rift faults (008°) roughly parallels the border fault system (006° mean trend) (Figs. 7B, 7C). Intra-rift fault lengths range over 3 orders of magnitude, from 0.26 to 60.7 km (Figs. 6C, 6D). Fault throws were measured along 40 well-exposed intra-rift faults. Throw profiles are typically elliptical or bell-shaped and consistent with unrestricted fault growth, where fault tips grow unimpeded during each slip event (Cowie and Scholz, 1992; Cartwright et al., 1995; Nicol et al., 1996) (Fig. 6A). Throw profiles along some faults in the Natron and Magadi basins also exhibit varying degrees of asymmetry (Kattenhorn et al., 2013) (Fig. 6B). Asymmetric throw profiles are indicative of restricted fault growth, where propagation at one end of the fault is stymied by a mechanical barrier (Nicol et al., 1996; Manighetti et al., 2001). Maximum throws are as high as 362 m within the Magadi Trachyte in the Magadi basin (Fig. 6E). The displacement-length coefficient of $6.3 \pm 0.4 \times 10^{-3}$ is low compared to normal fault populations in softer (typically sedimentary) rocks (e.g., 10^{-1} to 10^{-2}; Schultz et al., 2006), but is comparable to faults dissecting Quaternary lavas in rift zones elsewhere (Cowie et al., 1993, 1994; Carbotte and MacDonald, 1994; Angelier et al., 1997; Vetel et al., 2005).

Fault-Related Extensional Strain

Faults were subdivided into populations based on the ages of the volcanic units they dissect (Table 2; Supplemental Fig. S1 [see footnote 2]). Ages were determined from the new and existing $^{40}Ar/^{39}Ar$ analyses. In instances where no $^{40}Ar/^{39}Ar$ dates were available, existing K-Ar ages were applied. Total fault-related strain was then calculated within each lava unit.

Extension Rates in Lava Groups

We identify 14 major volcanic units in this study in order to subdivide the fault population. These units give maximum ages for the faults dissecting them, given that the time interval between lava eruption and subsequent faulting cannot be determined. The ages of faults can then be translated into a time-averaged extension rate since the eruption of each respective unit based on the calculated horizontal extensional strain within the fault population (Fig. 5; Table 2).

Extensional strain was calculated in each of the fault populations using the method described in this study. The time-averaged extension rate was then estimated by dividing total extension by the age of the lava unit (Table 2). The mean time-averaged extension rates are as high as 0.93 ± 0.28 mm yr^{-1} (unit 3; Table 2) for intra-rift fault populations in the 7 Ma Magadi basin. Estimated extension rates are lower in intra-rift fault populations in the 3 Ma Natron basin (as much as 0.47 ± 0.14 mm yr^{-1}), consistent with the generally lower slip rates along intra-rift faults in the Natron basin compared to the Magadi basin. These extension rates are within the modeled rates (i.e., less than) of 1.8 and 2.0 mm yr^{-1} for the Natron and Magadi basins, respectively (Saria et al., 2014; see Supplemental Materials, Section S3 [footnote 1]). The highest extension rates occur in the center of each intra-rift fault population, decreasing to 0.20–0.30 mm yr^{-1} in the eastern ~20 km of the intra-rift fault population in the Singaraini basalt and Limiru trachyte lavas. In each basin, extension rates are lowest around the extinct Olorgesailie, Eyaseti, Lenderut, and Shompole volcanoes (<0.03 mm yr^{-1}). Away from these volcanoes, extension rates are lowest (< 0.1 mm yr^{-1}) in the western 10–20 km of the intra-rift fault populations. For example, late Pleistocene lake sediments in southwest Magadi basin are relatively unfaulted, suggesting little to no recent fault activity. In the Natron basin, however, Holocene sediments from ephemeral Lake Natron possibly mask the surface expression of recent faults and thus prohibit a detailed analysis of strain on the western side of the Natron basin (discussed further in the following section). Recently observed seismicity implies active normal faulting below the lake (Lee et al., 2016). However, displacements on these faults are too low to produce scarps high enough to rise above the shallow Lake Natron waters (a few meters deep).

Extension Rates across the Magadi and Natron Basins

To understand how strain is distributed within intra-rift faults across-axis fault-related extensional strain was analyzed along two rift-normal transects through the Magadi and Natron basins (Fig. 8). Rift-normal extensional strain was calculated in 15 rectangular areas, 4 km wide by 15 km long, with long axes trending parallel to rift faults. Results of these analyses, presented in Figures 8B and 8D, show how intra-rift fault-strain is distributed across each basin. Similar to results shown in Table 2, analyzed faults in the Magadi basin accommodate more extensional strain (as much as 6.8%) than those in Natron (as much as 4.0%). Within the center of the Magadi basin, total extension exceeds 3% in 10 of the 15 analyzed areas (Fig. 8B). In contrast, only 2 of the 15 analyzed areas in Natron exhibit extension in excess of 3% (Fig. 8D).

TABLE 2. SUMMARY OF THE GENERAL DISTRIBUTION OF FAULT STRAIN CALCULATED IN DESIGNATED LAVA UNITS IN THE MAGADI AND NATRON BASINS

	Unit no.	Unit name	Area (km^2)	Length (km)	Mean width (km)	Strain	Extension (km)	Age of faulted lavas (Ma)	Extension rate ($mm\ yr^{-1}$)
Magadi	1	Mao	162	15.2	10.6	0.0534 ± 0.0003	0.057 ± 0.004	0.60	**0.095 ± 0.006**
	2	West Magadi	816	63.8	12.8	0.0123 ± 0.0008	0.158 ± 0.010	1.70–2.30	**0.082 ± 0.017**
	3	Magadi Trachyte	2542	95.8	26.5	0.0405 ± 0.0026	1.075 ± 0.068	0.95–1.37	**0.932 ± 0.277**
	4	Limiru	566	34.9	16.2	0.0349 ± 0.0022	0.566 ± 0.036	1.80–2.00	**0.300 ± 0.035**
	5	Ol Tepesi	313	28.3	11.0	0.0189 ± 0.0012	0.208 ± 0.013	1.40–1.65	**0.138 ± 0.020**
	6	Ol Eyaseti	88	11	8.0	0.0122 ± 0.0008	0.097 ± 0.006	5.60–5.90	**0.017 ± 0.002**
	7	Olorgesailie	186	21.2	8.8	0.0065 ± 0.0004	0.057 ± 0.004	2.20–2.70	**0.024 ± 0.004**
	8	Singaraini	672	54.7	12.3	0.0322 ± 0.0020	0.396 ± 0.025	2.31–2.33	**0.202 ± 0.013**
	9	Lenderut	38	6.8	5.5	0.0034 ± 0.0002	0.019 ± 0.001	2.50–2.70	**0.007 ± 0.001**
Natron	10	Shompole	131	13.5	9.7	0.0007 ± 0.00004	0.007 ± 0.0004	2.00	**0.003 ± 0.0002**
	11	Magadi Trachyte	636	35.7	17.8	0.0306 ± 0.0019	0.545 ± 0.035	0.95–1.37	**0.473 ± 0.140**
	12	Lenderut	45	7.3	6.1	0.0074 ± 0.0005	0.046 ± 0.003	2.50–2.70	**0.018 ± 0.002**
	13	Singaraini	362	38.7	9.4	0.0260 ± 0.0016	0.243 ± 0.015	1.96	**0.124 ± 0.008**
	14	Gelai	1194	50	23.9	0.0099 ± 0.0006	0.235 ± 0.015	0.95–1.137	**0.222 ± 0.014**

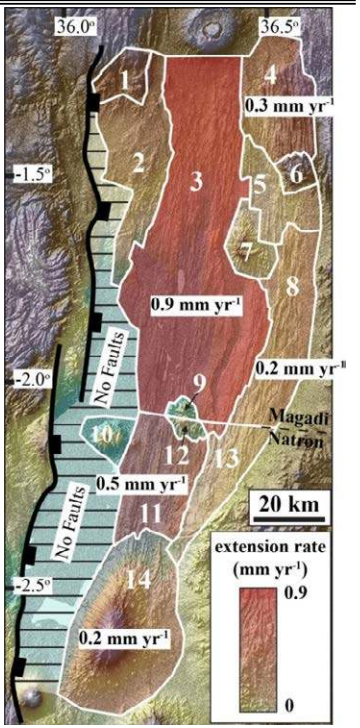

Note: The areal distributions of the lava units are from the geological map provided in Supplementary Figure S1 [see footnote 2]. Length values correspond to the length of the unit in a north-south direction, whereas mean width is in an east-west direction. Map shows the distribution of each lava group (1–14). Extension rates represent the mean extension rate based on the mean width, total strain, and age of each unit. Errors are based on the range of ages of faulted lavas and the vertical uncertainty of the SRTM (Shuttle Radar Topography Mission) data. Brittle crustal thicknesses used for strain calculations (from Albaric et al., 2009) are 11 km for areas 1–8, and 19 km for areas 9–14. Areas not included (southwest Magadi, Lake Natron) contain no faults visible in the aerial photos. Each unit is shaded (red) based on relative extension rate (inset map). Also annotated are the extension rates in lava units with rates ≥0.2 mm yr^{-1}.

Time-averaged extension rates were estimated by dividing the total extension by the age of the lavas displaced by faults (Fig. 8). By summing values across each transect from west to east in Figures 8C and 8E, the total time-averaged extension rates in the intra-rift populations were calculated. Results show that intra-rift faults in the 7 Ma Magadi basin accommodate more extension (1.63 ± 0.10 mm yr^{-1}) than those in the younger, 3 Ma Natron basin (0.50 ± 0.03 mm yr^{-1}). The remaining extension for each basin is likely focused along border faults.

It is notable that some intra-rift faults in transect Y-Y′ across the Natron basin may be concealed by Holocene lake deposits within ~16 km of the Natron border fault (Fig. 8A). These complications provide additional uncertainties in the presented extension rate estimates. Given that intra-rift faults in Magadi clearly accommodate more strain than those in Natron (Fig. 8B and D), extension rates within 16 km of the Nguruman border fault can perhaps provide an upper limit for intra-rift faults buried by Lake Natron sediments. Analyses show that well-exposed faults in Pleistocene lake sediments and Magadi Trachyte within 16 km of the Nguruman border fault in the Magadi basin (transect X-X′; Fig. 8) accommodate 0.36 ± 0.01 mm yr^{-1}. Assuming that this is an upper limit for faults below Lake Natron, it is estimated that intra-rift faults in the Natron basin accommodate between 0.47 and 0.90 mm yr^{-1} of extension.

Estimating Flexure of the Border Fault Hanging Wall

Slip along a planar normal fault in the upper crust can be modeled by assuming that two vertical line loads are applied in equal and opposite directions to an elastic plate either side of the fault plane (i.e., where $x = 0$ in Fig. 9) (Vening Meinesz, 1950; Turcotte and Schubert, 1982; Stein et al., 1988; Bott, 1996).

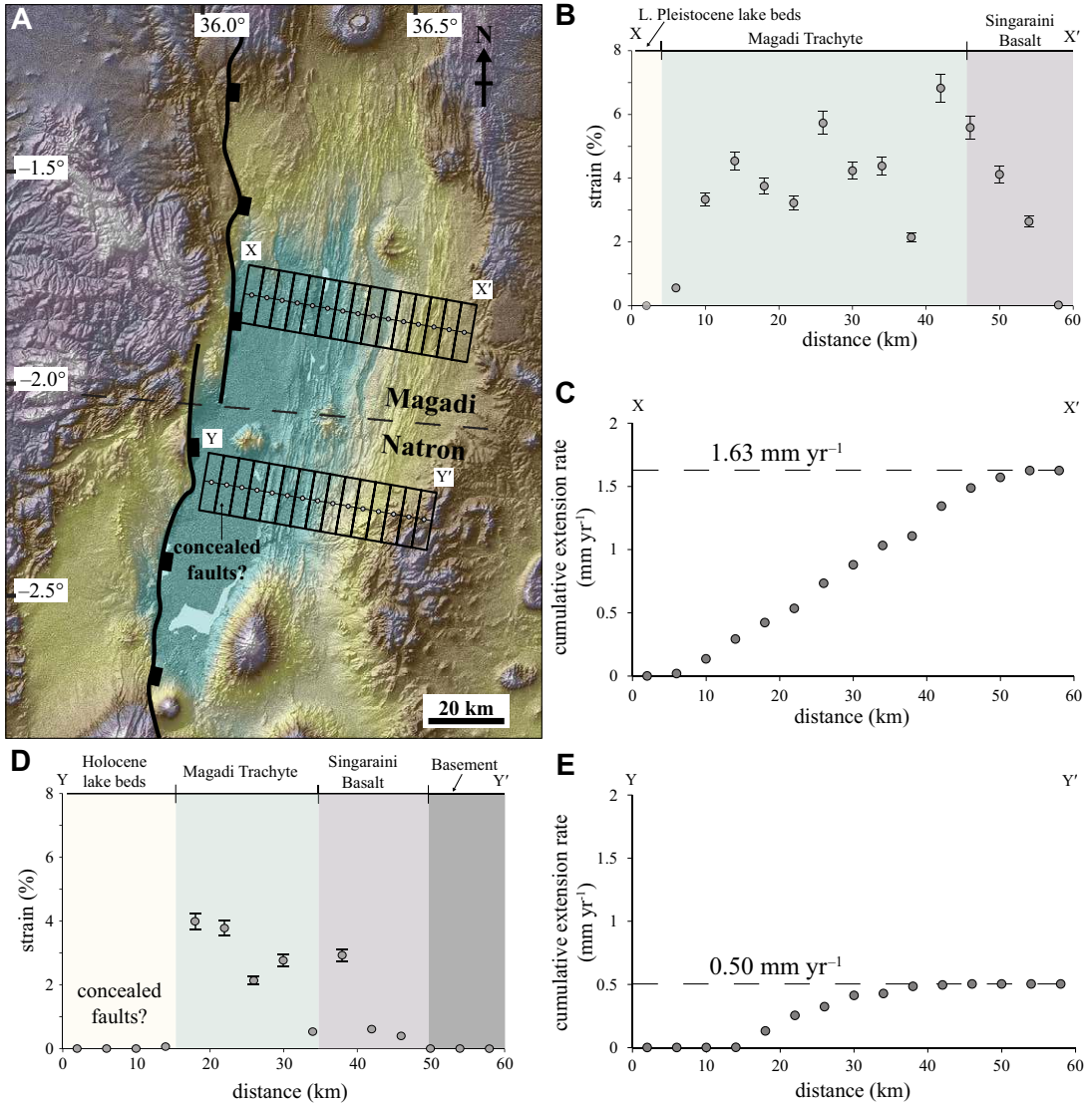

Figure 8. Rift-normal distribution of intra-rift fault-related strain across two 60-km-long transects in the Magadi and Natron basins. (A) Annotated Shuttle Radar Topography Mission (SRTM) image showing the location of each transect and the polygons in which strain was calculated. Gray filled circles in the center of each box correspond to the locations of data points in B–E. (B) Strain calculated in each polygon along profile X-X′ in the Magadi basin. Confidence intervals consider the vertical precision of the SRTM to 95% certainty. Points without confidence intervals have uncertainties below the resolution of the data point. Faults dissect 0.3 Ma lacustrine sediments (Behr and Rohricht, 2000), 1.15 Ma Magadi Trachyte lavas (mean age of sampled lavas), and 1.96 Ma Singaraini basalt lavas (Table 2). Colors refer to the geological units dissected by the faults. The ages of these units are used to estimate extension rates in C. L.—late. (C) Cumulative extension rate in the intra-rift fault population of the Magadi basin. Extension rates in each polygon are summed from west to east, resulting in a total time-averaged extension rate of 1.63 ± 0.10 mm yr^{-1}. (D) Strain calculated in each polygon along profile Y-Y′ in the Natron basin. Ephemeral lake waters and Lake Natron sediments (Holocene age) may mask faults within ~16 km of the border fault. No rift faults are identified in the basement. (E) Cumulative extension rate in the intra-rift fault population of the Natron basin. Extension rates in each polygon are summed from west to east, resulting in a total time-averaged extension rate of 0.50 ± 0.03 mm yr^{-1}.

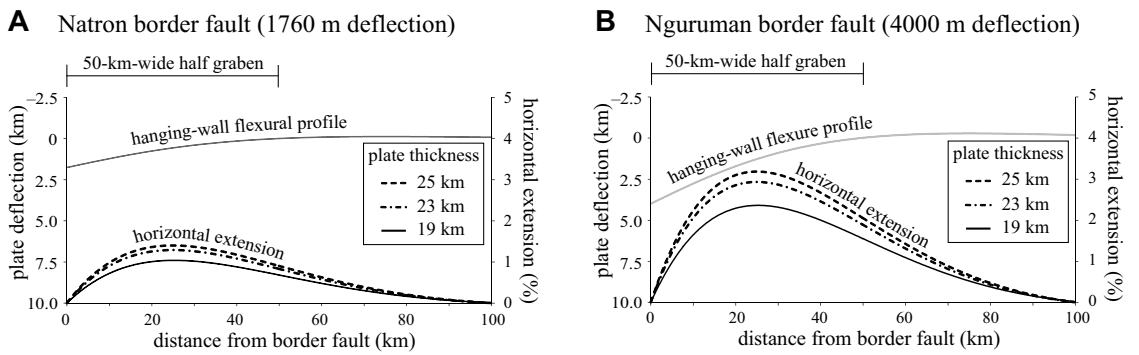

C Summary

	1.2 Ma Natron border fault			7 Ma Nguruman border fault		
plate thickness (m)	25000	23000	19000	25000	23000	19000
mean extension (%)	1.1	1.0	0.8	2.4	2.2	1.8
total horizontal extension (m)	546	502	405	1240	1142	921
time-averaged extension rate (mm yr^{-1})	0.45	0.42	0.34	0.18	0.16	0.13

Figure 9. Results of modeled broken plate deflections from border faulting and the development of 50-km-wide half-graben basins. Both the flexural profile and horizontal extensional strain were estimated using the methods of Turcotte and Schubert (1982) and Billings and Kattenhorn (2005), and are described further in the Supplementary Materials [see footnote 1]. (A) Expected flexural profile for a 1.76-km-deep by 50-km-wide half-graben basin in Natron. Maximum deflection (1.76 km) occurs at the left of the graph (distance = 0 km) and approaches zero at 50 km. Also plotted is the horizontal extension that would result across the basin from the deflection of a 19-, 23-, and 25-km-thick plate. (B) Expected flexural profile for a 4-km-deep by 50-km-wide half-graben basin in Magadi. Maximum deflection (4 km) occurs at the left of the graph (distance = 0 km) and approaches zero at 50 km. Also plotted is the horizontal extension that would result across the basin from the deflection of a 19-, 23-, and 25-km-thick plate. (C) Summary of data from the models presented in A and B. Mean extension (%) and total horizontal extension considers the average of all the extensional strain over the 50-km-wide basin. The time-averaged extension is estimated by dividing the total extension by the age of the half-graben basin, based on the age of the border faults (Crossley, 1979; Foster et al., 1997).

The footwall and hanging wall of the fault locally respond to this load by bending, with the subsequent deflection profile (i.e., hanging-wall flexural profiles in Fig. 9) dependent on the rigidity of the plate. Fault slip can thus generate extensional bending stresses that manifest at the near-surface in the flexing hanging wall and, in part, can drive the initiation of intra-rift faults (McClay and Ellis, 1987; Lavier et al., 2000; Imber et al., 2003; Ebinger, 2005).

Estimating extensional bending stresses from border fault activity in each basin first requires constraints on subsurface border fault throws that are provided by both gravity and seismic velocity data in the region (Birt et al., 1997; Ebinger et al., 1997). These studies give estimates of rift basin sediment fill of 3.6 km for Magadi and 1.6 km for Natron. Above the ground surface, the Nguruman and Natron escarpments exhibit throws of ~1.4 km and ~0.6 km, respectively. Summing values of subaerial and subsurface throws for each basin equates to total border fault throws of 2.2 km for Natron, and 5.0 km for Magadi. Assuming a ratio of upthrow to downthrow on the fault of 0.2 (e.g., Stein and Barrientos, 1985; refer also to Supplemental Materials, Section S2 [footnote 1]), the maximum downward deflection of the hanging wall (i.e., deflection at $x = 0$ in Fig. 9) is estimated to be 4 km for Magadi and 1.76 km for Natron. These values are within constraints provided by basins depths (Birt et al., 1997; Ebinger et al., 1997), which require minimum hanging-wall deflections of 3.6 km and 1.6 km in Magadi and Natron, respectively.

Based on hanging-wall deflections for each basin and a basin width of 50 km (Foster et al., 1997; Ebinger, 2005), the flexural profile and subsequent horizontal extensional strain can be approximated using the methods of Turcotte and Schubert (1982) and Billings and Kattenhorn (2005) (Fig. 9; refer to Supplemental Materials, Section S2 [footnote 2]). Using effective elastic thicknesses ranging 19–25 km for rift basins in north Tanzania, based on Ebinger et al. (1997), it is estimated that border fault flexure has produced ~0.8%–1.1% and 1.8%–2.4% of extension in the Natron and Magadi basins, respectively. By making the simplifying assumption that strain was accumulated at a constant rate from border fault activation to the present day, time-averaged extension rates related to hanging-wall flexure range 0.34–0.45 mm yr^{-1} for Natron and 0.13–0.18 mm yr^{-1} for Magadi. These results have implications for how much regional extension is accommodated via intra-rift faulting in each basin (see DISCUSSION).

Distribution of Springs and Their Geochemistry

Hydrothermal springs are observed at the bases of some fault scarps in the study region, and are often aligned in fault-parallel clusters (Figs. 3E and 10A). In Magadi, springs occur in an ~11-km-wide zone (rift-normal measurement) in the center of the basin, whereas springs in the Natron basin are present along an ~23-km-wide zone extending normal to the rift from the border fault eastward across the hanging wall to an antithetic fault bounding the eastern side of Lake Natron. No springs are documented or observed along the Nguruman border fault of the Magadi basin, nor are any springs present in the center of the intra-rift fault population in Natron.

Spring-water samples were collected in the field using Giggenbach bottles, and dissolved gases were analyzed at the Volatiles Laboratory and

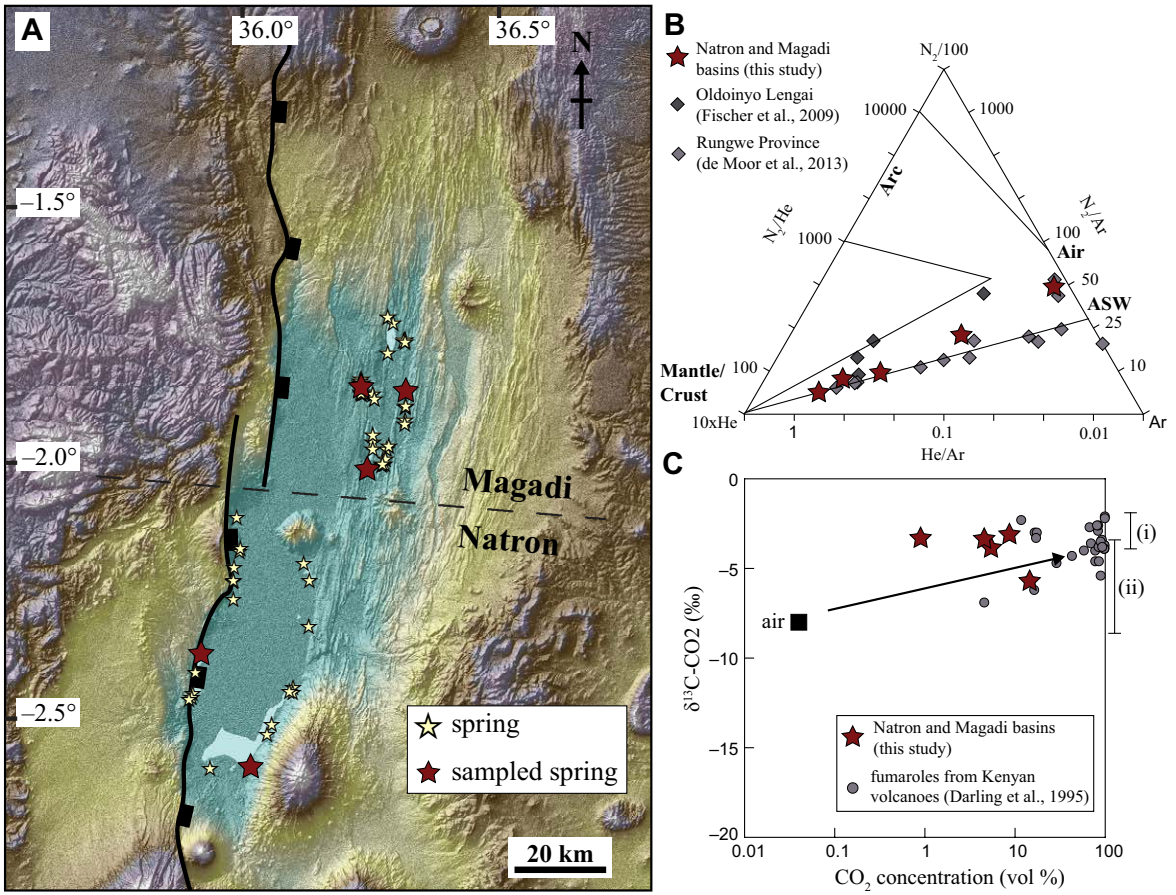

Figure 10. (A) Annotated digital elevation map of the Natron and Magadi basins, showing the distribution of springs (yellow stars) mapped in this study and from Baker (1958) and Eugster (1970). Springs sampled for geochemical analyses are indicated by red stars (see Table 3). Black lines are border faults. (B) Ternary plot of N_2-He-Ar abundances in the sampled springs (red stars) compared to samples from Rungwe Province (light gray diamonds) and Oldoinyo Lengai (dark gray diamonds). Samples from this study plot on a mixing line between air-saturated water (ASW) and a mantle end member. (C) Carbon isotope compositions and concentrations of spring samples in this study (red stars) compared to gases from fumaroles at Kenyan volcanoes (gray circles) from Darling et al. (1995). The $\delta^{13}C$-CO_2 values are presented as per mil (‰) against a standard Peedee belemnite limestone. Also shown are the ranges of isotope values for (i) Oldoinyo Lengai fumaroles and (ii) mantle carbon, from Fischer et al. (2009) and Sano and Marty (1995), respectively. Black arrow represents a typical mixing line between mantle carbon and air observed for magmatic volatiles (e.g., Parks et al., 2013; Lee et al., 2016).

Center for Stable Isotopes, University of New Mexico (Albuquerque) (methods described in Supplemental Materials, Section S4 [see footnote 1]). Sampled springs exhibit high pH (8.9–10.3) and warm temperatures, from 35.0 to 50.7 °C (Table 3). The N_2-He-Ar systematics of spring samples were compared with fluids and gases from springs, gas vents, and fumaroles from the Rungwe Province (southern Tanzania) and Oldoinyo Lengai volcano of the EAR (Fischer et al., 2009; de Moor et al., 2013) (Fig. 10B). On an N_2-He-Ar ternary diagram (Fig. 10B), fluids derived from the mantle should plot near the He apex, consistent with He/Ar and N_2/Ar ratios of the upper mantle, which are shown to be ~1 and 80, respectively (Burnard et al., 1997; Marty and Zimmermann, 1999). In contrast, both air and air-saturated water have N_2/Ar ratios of 84 and ~40 (varies slightly depending on temperature), respectively, and low proportions of He relative to Ar (<0.01) (de Moor et al., 2013). Consistent with magmatic gases and fluids from the Rungwe Province and Oldoinyo Lengai volcano, spring samples from the Natron and Magadi basins plot on a mixing line between air-saturated water and a mantle and/or crust end member (Fig. 10B). Values of $\delta^{13}C$ (–3.1‰ to –5.7‰; Table 3) from CO_2 gases dissolved in spring samples overlap previous values from Kenya Rift volcanoes (–1.7‰ to –6.9‰), which were interpreted as derived from the upper mantle (Darling et al., 1995) (Fig. 10C). These data are also consistent with isotope values from diffusely degassing CO_2 in the Magadi and Natron basins that show a mixing relationship between air and mantle-derived CO_2 released from degassing magmas (Lee et al., 2016). Plots of $\delta^{13}C$-CO_2 and CO_2 concentrations of springs in the region also fit on a mixing line between air and magmatic CO_2 (Darling et al. 1995; Sano and Marty, 1995) (Fig. 10C).

TABLE 3. COMPOSITIONS OF SPRING SAMPLES FROM THE NATRON AND MAGADI BASINS

Location	ID	Lat (S°)	Long (E°)	*T* (°C)	pH	Lat (S°)	Long (E°)	CO_2	N_2	Ar	He	O_2	H_2	CH_4	CO	$\delta^{13}C\text{-}CO_2$	±
								(vol%)									
Magadi west	KN14-S01	1.85744	36.219	48.4	8.9	1.85788	36.21907	4.12	92.7	2.24	0.48	0.021	0.029	0.415	0.0078	–3.84	0.03
Magadi south	KN14-S06	1.99825	36.23131	44.6	9.9	2.00225	36.23146	8.42	88.42	1.68	0.61	0.43	0.018	0.423	<dl	–3.09	0.02
Magadi east	KN14-S11	1.85989	36.30636	35	10	1.85569	36.30675	3.63	87.85	1.41	0.01	7.095	n.d.	0.006	<dl	–3.22	0.03
Natron west	TZ14-S01	2.37314	35.90581	50.7	10.3	2.37314	35.90581	0.9	94.5	2.38	1.21	0.003	0.031	0.969	<dl	–3.25	0.01
Natron east	TZ14-S06	2.59283	36.01597	36.8	9.2	2.59325	36.01589	13.01	74.75	1.38	0.11	10.741	n.d.	n.d.	<dl	–5.68	0.03

Note: Sample locations are shown in text Figure 10. Gas volumes below the detection limit are reported as "<dl". *T*—temperature.

DISCUSSION

Data presented in this study are critical for investigating the development of rift basin architecture during continental rifting in the EAR, particularly the magmatic-tectonic processes that influence faulting in the first 10 m.y. of rift development (Figs. 2A, 2B). Results from this study provide insights into how and when strain migrates to the rift center prior to the development of magmatic segments, like those observed today in the Main Ethiopian Rift (Keranen et al., 2004; Fig. 2C). The evolution of fault systems in early-stage basins is discussed here by comparing the 7 Ma Magadi and 3 Ma Natron basins. Specific topics of interest are: (1) the volcanic-tectonic history of the Natron-Magadi region; (2) the importance of flexure of the border fault hanging wall for intra-rift faulting; (3) the amount of strain accommodated between border faults and intra-rift faults in each basin; (4) the evolving fault strain and basin morphology during early-stage rift development; and (5) the processes assisting the evolution of fault systems (e.g., kinematic, magmatic, hydrothermal).

Fault Evolution during Early-Stage Continental Rifting

Tectonic-Magmatic History of the Magadi and Natron Basins

Data presented in this study in context with previous work reveal that rift activity in the Natron and Magadi basins is characterized by persistent faulting and punctuated phases of volcanic activity (Baker and Mitchell, 1976; Crossley, 1979; Le Gall et al., 2008; Guth, 2015) (see Fig. 7; Supplemental Fig. S1 [footnote 2]). The earliest stages of rifting in the Natron-Magadi region were characterized by faulting and volcanism along the Nguruman escarpment of the Magadi basin. Faulting initiated on the rift border ca. 7 Ma, prior to the eruption of Lengitoto trachyte lavas (6.9–5.0 Ma) along the western rift edge (Crossley, 1979). Volcanism began on the eastern border of Magadi ca. 6.7 Ma with the eruption of Ol Eyaseti volcanics (Baker et al., 1971; Baker and Mitchell, 1976). The next major phase of volcanism involved eruption of Kirikiti lavas along the western side of the basin and the rift center from 5.1 to 2.5 Ma (Baker et al., 1971; Crossley, 1979). During this period, volcanism in the Natron region initiated with the development of Mosinik volcano at 4.05 Ma (Table 1), followed by faulting along the now-extinct Oldonyo Ogol border fault escarpment ca. 3 Ma (Foster et al., 1997; Le Gall et al., 2008; Stollhofen and Stanistreet, 2012). The Ngong-Turoka fault, which bounds the eastern side of Magadi basin, was active from 3.3 to 2.3 Ma (Baker and Mitchell, 1976), as were the Lenderut (2.7–2.5 Ma), Olorgesaile (2.7–2.2 Ma), and Ngong (2.6–2.5 Ma) composite volcanoes and related volcanics (Baker et al., 1971; Fairhead et al., 1972, 1977; Baker and Mitchell, 1976). Since 2 Ma, the Magadi and Natron basins have been subject to widespread, basin-filling lava eruptions, including the Limiru trachytes (2.05 Ma) and Singaraini basalts (1.96 Ma), with additional volcanism from Oldonyo Sambu (possibly 3.5 Ma to 1.8 Ma) and Shompole volcanoes [1.96 Ma–present(?)] (Fairhead et al., 1972; Isaacs and Curtis, 1974; Le Gall et al., 2008; Table 1). The final phase of tectonic-magmatic activity in the region was marked by a shift in border faulting in Natron from the Oldonyo Ogol escarpment to the Natron border fault between 1.2 and 1.0 Ma (Foster et al., 1997). Changes in the location of border faulting in Natron were both accompanied and preceded by voluminous axial volcanism in the rift center (combined minimum volume = 1263 km^3; Guth, 2015), with eruption of Gelai volcanics (1.23–0.95 Ma) and Magadi Trachyte lavas (1.4–0.95 Ma) (Baker and Mitchell, 1976; Table 1). This volcanic resurfacing event filled the entire rift valley floor, erasing earlier faulted topography (Baker and Mitchell, 1976). Since that time, both rift basins have been characterized by an extended phase (ca. 1 Ma to present) of rift-parallel, intra-rift faulting (Baker, 1958; Crossley, 1979; Le Gall et al., 2008; Fig. 7), whereas volcanism has been largely absent (Muirhead et al., 2015). Intra-rift faults dissecting rift valley–filling lavas provide important information on the upper crustal extensional strain accommodated within the rift center since these final phases of volcanic activity (Fig. 8).

Intra-Rift Faulting in the Natron and Magadi Basins: Regional Extension versus Hanging-Wall Flexure

During early-stage rifting in the Eastern rift, strain was primarily accommodated through slip along border faults (Hayward and Ebinger, 1996), which accumulated displacements of thousands of meters over the lifetime of rifting. Large-scale fault slip (e.g., >1000 m) along border faults and subsequent flexure of the downthrown hanging wall generate extensional stresses in half-graben basins (Vening Meinesz, 1950; McClay and Ellis, 1987; Lavier et al., 2000; Imber et al., 2003; Cowie et al., 2005) (Fig. 9) that are thought to activate

intra-rift faults in the border fault hanging wall (Ebinger, 2005) (Fig. 9). This style of faulting accommodates only localized bending strains, rather than regional extension (i.e., far-field extensional plate motions). The extensional strain measured within an intra-rift fault system (Fig. 8) represents strain accommodated by both hanging-wall flexure and regional extension. Therefore, hanging-wall flexural strains (Fig. 9) must be removed from the total intra-rift strain estimates to reveal the amount of regional extension accommodated via intra-rift faulting (Table 4).

Transects X-X′ and Y-Y′ in Figure 8 show the distribution of strain across intra-rift fault populations in the Magadi and Natron basins, as well as the cumulative time-averaged extension rate. Subtracting extension rates related to hanging-wall flexure (Fig. 9) from these estimates provides constraints on the amount of regional extension accommodated in the intra-rift fault systems (Table 4). Calculations from this study suggest that hanging-wall flexure in the Magadi basin has produced 0.13–0.18 mm yr^{-1} of extension. This hanging-wall flexure accounts for only a small fraction (<12%) of extension observed in this fault system (1.52–1.73 mm yr^{-1}). Based on these estimates, we infer that intra-rift faults in Magadi accommodate 1.34–1.60 mm yr^{-1} of regional extension. Hanging-wall flexure in the Natron basin, however, can explain a significant portion of observed strain in the intra-rift fault systems (0.34–0.45 mm yr^{-1}), accounting for between 38% and 96% of the 0.47–0.90 mm yr^{-1} time-averaged extension represented by intra-rift faults (Table 4). These results imply that intra-rift faults in the Natron basin accommodate 0.02–0.56 mm yr^{-1} of regional extension.

It is important to note that our results cannot resolve the proportion of extensional strain accommodated by dike intrusion, rather than normal faulting, at depth. Field, numerical, analog, geodetic, and geophysical studies illustrate a feedback between middle to upper crustal diking and normal faulting at the near surface, where static stress changes above the dike tip often initiate faulting and graben formation (e.g., Bjornsson et al., 1977; Brandsdóttir and Einarsson, 1979; Mastin and Pollard 1988; Rubin and Pollard, 1988; Chadwick and Embley, 1998; Buck et al., 2005, 2006; Behn et al., 2006; Keir et al., 2006; Wright et al., 2006, 2012; Rowland et al., 2007; Behn and Ito, 2008; Calais et al., 2008; Grandin et al., 2009; Ebinger et al., 2010; Belachew et al., 2013; Sigmundsson et al., 2015; Trippanera et al., 2015; Ruch et al., 2016). Based on these studies, extensional strain measured at the surface in the Natron and Magadi basins is expected to mirror that accommodated below the intra-rift fault system, regardless of what portion is accommodated through either dike intrusion or normal faulting in the upper crust.

Furthermore, length statistics in the Natron-Magadi fault population may have been affected by dike-fault interactions (i.e., Rowland et al., 2007). The low displacement-length coefficient (~6.0×10^{-3}) recorded in the Natron-Magadi region, as well as magmatic rifts elsewhere (e.g., Iceland, East Pacific Rise; Cowie et al., 1993; Angelier et al., 1997), suggest that these faults grow in length rapidly (Vetel et al., 2005) compared to faults in magma-poor extensional systems (e.g., displacement-length coefficients range 0.8–5.2×10^{-2} at Canyonlands and Volcanic Tablelands; Dawers et al., 1993; Cartwright et al., 1995; Dawers and Anders, 1995; Moore and Schultz, 1999). It is possible that these differences in displacement-length ratios reflect, in addition to varying mechanical strength of the host rock (Schultz et al., 2010), the effects of dike-imposed stresses along the length of the rift (i.e., Rubin and Pollard, 1988). In support of these assertions, the surface ruptures of dike-induced normal faults recorded in Afar are shown to have attained remarkable lengths (~60 km) when considering their largest earthquake magnitudes (moment magnitude, M_w 5.6; Rowland et al., 2007; Grandin et al., 2009; Ebinger et al., 2010).

Border Fault versus Intra-Rift Faulting

Fault system analyses presented in this study do not provide direct constraints on border fault extension rates. However, in early-stage rift basins the extension accommodated by fault systems (border faults and intra-rift faults) should equal the far-field extension rate. Therefore, by assuming that modeled plate motion vectors for the EAR (i.e., Saria et al., 2014) accurately reflect extension rates over the past few million years, and assuming that all upper crustal strain is accommodated along faults observed in the 50-km-wide basins, the maximum border fault extension rates can be estimated by subtract-

TABLE 4. SUMMARY OF STRAINS ACCOMMODATED BY INTRA-RIFT AND BORDER FAULT POPULATIONS IN THE MAGADI-NATRON REGION, BASED ON FAULT STRAIN AND BENDING STRAIN ANALYSES

	Basin age (Ma)	Regional extension rate (mm/yr)	Border fault throw (m)	Flexural strain (% extension)*	Flexural extension rate (mm/yr)†	Intra-rift extension rate (mm/yr)§	Regional extension accommodated via intra-rift faulting (mm/yr)**	Border fault extension rates (mm/yr)††
Natron	3 (1)	1.8 (3)	2200 (4)	0.8–1.1	0.34–0.45	0.47–0.90	0.02–0.56	1.24–1.78
Magadi	7 (2)	2 (3)	5000 (5)	1.8–2.4	0.13–0.18	1.52–1.73	1.34–1.60	0.40–0.66

Note: Sources of data are shown in parentheses: (1) Foster et al. (1997); (2) Crossley (1979) (3) Saria et al. (2014); (4) Ebinger et al. (1997); (5) Birt et al. (1997).
*Strains related to flexure of the border fault hanging wall from text Figure 9.
†Time-averaged extension rate estimated by dividing total extension related to flexure by the age of the border fault.
§Estimated from rift-normal transects shown in Figure 8.
**Estimated by subtracting the range of flexural extension rates from the range of extension rates for intra-rift faults.
††Estimated by subtracting the range of intra-rift extension rates (given in regional extension accommodated via intra-rift faulting) from the model regional extension rate.

ing the plate motion vectors by the calculated time-averaged extension in the intra-rift fault populations (Table 4; see Supplemental Materials, Section S3 [footnote 1]). Geodetic models (i.e., Saria et al., 2014) make the simplifying assumption that strain is confined to a rigid plate boundary (i.e., within the ~50-km-wide rift basin). With these limitations in mind, our results may also be tested and compared with time-averaged border fault extension rates inferred from basin depth estimates (see following).

Subtracting 1.34–1.60 mm yr^{-1} of regional extension measured across the Magadi intra-rift fault system in this study from the modeled 2.0 mm yr^{-1} extension rate for the basin, it is estimated here that the Nguruman border fault accommodates 0.40–0.66 mm yr^{-1} of extension. This is 20%–33% of the regional extension. Similarly, by subtracting the 0.02–0.56 mm yr^{-1} of regional extension measured across intra-rift faults of the Natron basin from the modeled 1.8 mm yr^{-1}, the Natron border fault is estimated to accommodate 1.24–1.78 mm yr^{-1} of extension, which is 69%–99% of the regional extension. Therefore, border fault activity is a far greater contributor to regional extension in the 3 Ma Natron basin than in the 7 Ma Magadi basin. This is consistent with field observations of recent activity along subsidiary segments of the Natron border fault (Figs. 3A, 3B).

Border Fault Slip Rates from Subsurface Throw

Border fault extension rate estimates presented in Table 4 may be further tested by comparing these values with estimated extension rates based on the age, throw, and assumed dip of the rift basin border faults (Table 5). Using a range of possible ages for the Natron border fault (1.2–1.0 Ma; Foster et al., 1997) and an assumed fault dip of 50°–60°, consistent with focal plane mechanisms in the region and normal faults in general (Foster et al., 1997; Lambert et al., 2014), the 2.2 km of throw accumulated on the Natron border fault corresponds to an extension rate of 1.06–1.85 mm yr^{-1}. This compares well to the 1.24–1.78 mm yr^{-1} from the fault strain analysis summarized in Tables 4 and 5. Similarly, a range of reasonable ages for the Nguruman fault (7.1–6.9 Ma; Crossley, 1979) and an assumed fault dip of 50°–60° corresponds to an extension rate of 0.41–0.61 mm yr^{-1}, which also compares favorably to the 0.4–0.66 mm yr^{-1} from the fault strain analysis (Tables 4 and 5). This simple approach provides comparable results, which lends confidence to the fault-strain analyses in this study (Fig. 11; Table 4).

Extension rates across the Natron border fault, however, do not match results from age dating and fault-throw analyses collected along border fault

TABLE 5. COMPARISON OF BORDER FAULT EXTENSION RATES AND SLIP RATES FROM ANALYSES OF BASIN DEPTHS AND AGES, TIME-AVERAGED EXTENSION RATES IN INTRA-RIFT FAULT SYSTEMS, AND FIELD DATA COLLECTED ON SUBSIDIARY BORDER FAULT SEGMENTS

Dip (°)	Basin depth (m)	Scarp height (m)	Throw (m)	Heave (m)	Minimum fault age (Ma)	Maximum fault age (Ma)	Minimum extension rate (mm yr^{-1})	Maximum extension rate (mm yr^{-1})	Minimum slip rate (mm yr^{-1})	Maximum slip rate (mm yr^{-1})
Natron border fault										
60	1600	600	2200	1270	1	1.2	1.06	1.27	2.12	2.54
					from fault-strain data*:		1.24	1.78	2.48	3.56
					From $^{40}Ar/^{39}Ar$ dates†:		0.05	0.08	0.09	0.16
55	1600	600	2200	1541	1	1.2	1.28	1.54	2.24	2.69
					from fault-strain data*:		1.24	1.78	2.16	3.1
					from $^{40}Ar/^{39}Ar$ dates†:		0.06	0.1	0.1	0.17
50	1600	6000	2200	1846	1	1.2	1.54	1.85	2.39	2.87
					from fault-strain data*:		1.24	1.78	1.93	2.77
					from $^{40}Ar/^{39}Ar$ dates†:		0.07	0.12	0.1	0.18
Nguruman border fault										
60	3600	1400	5000	2887	6.9	7.1	0.41	0.42	0.81	0.84
					from fault-strain data*:		0.4	0.66	0.8	1.32
					from $^{40}Ar/^{39}Ar$ dates†:		NA	NA	NA	NA
55	3600	1400	5000	3501	6.9	7.1	0.49	0.51	0.86	0.88
					from fault-strain data*:		0.4	0.66	0.7	1.15
					from $^{40}Ar/^{39}Ar$ dates†:		NA	NA	NA	NA
50	3600	1400	5000	4196	6.9	7.1	0.59	0.61	0.92	0.95
					from fault-strain data*:		0.4	0.66	0.62	1.03
					from $^{40}Ar/^{39}Ar$ dates†:		NA	NA	NA	NA

Note: Border fault ages from Foster et al. (1997) and Crossley (1979).
*Border fault extension rates based on data from Table 4.
†Slip rates on subsidiary border fault segments based on data from Table 1.

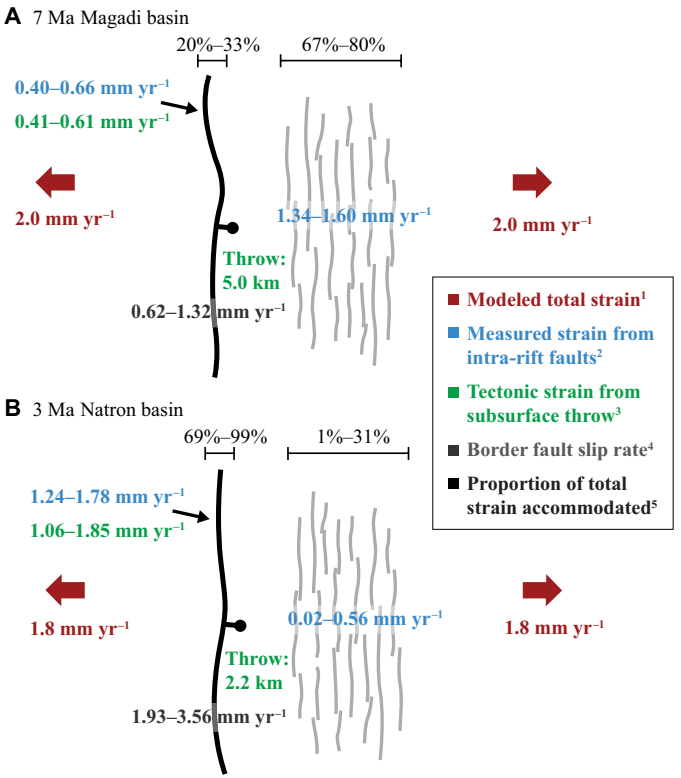

Figure 11. Summary of strain data from this study. (A) Distribution of fault strain in the 7 Ma Magadi basin. Black lines and gray lines represent border faults and intra-rift faults, respectively. Based on estimated extension rates, the greatest proportion of regional extension (i.e., modeled total strain) is accommodated in the intra-rift fault system (67%–80% of total strain). Analyses from this study give a mean border fault slip rate ranging from 0.62 to 1.32 mm yr^{-1}. (B) Distribution of fault strain in the 3 Ma Natron basin. Based on estimated extension rates, the greatest proportion of regional extension (i.e., modeled total strain) is accommodated along the border fault (69%–99% of total strain). Analyses from this study give a mean border fault slip rate ranging from 1.93 to 3.56 mm yr^{-1}. Numbers in superscripts in the key refer to data sources and relevant tables: 1—Saria et al. (2014); 2—refer also to Table 4; 3—Ebinger et al. (1997), Birt et al. (1997); 4—mean values from Table 5; 5—refer also to Table 4.

segments in the field (e.g., samples 2, 3, and 12 in Table 1; Table 5). The border fault segments analyzed in the field in this study are subsidiary structures of the main escarpment (Sherrod et al., 2013). Due to the border fault's overall size and the substantial basin-fill sediments concealing its vertical dimensions (Ebinger et al., 1997; Sherrod et al., 2013), analyses of extension rates along the primary fault escarpment can only be constrained from subsurface information or indirect techniques, such as the fault-strain analysis applied in this study.

Border fault extension rates shown in Table 5 correspond to a range of possible slip rates that are consistent with rates along major normal faults on Earth. Slip rates are well constrained for normal faults in extensional terrains such as the Apennines (Italy), Taupo Rift (New Zealand), and Basin and Range (United States). Field studies show that normal fault slip rates are typically ~0.1–4 mm yr^{-1} (Villamor and Berryman, 2001, 2006; Hetzel and Hampel, 2005; Kent et al., 2005; Hampel et al., 2007; Berryman et al., 2008; Blakeslee and Kattenhorn, 2013; Wilkinson et al., 2015), although they may be as high as tens of millimeters per year during periods of covolcanic slip associated with caldera-forming rhyolite volcanism in magmatic rifts (e.g., the Paeroa fault of the Taupo Rift, New Zealand; Rowland et al., 2010; Downs et al., 2014). Compared to normal faults elsewhere, the Natron border fault exhibits a relatively high slip rate, with estimates from this study ranging from 1.93 to 3.56 mm yr^{-1}. The slip rate of 0.62–1.32 mm yr^{-1} estimated for the Nguruman fault is typical of normal faults at many extensional settings.

By contrast, the highest slip rates on individual intra-rift faults (as much as 0.45 mm yr^{-1}) in both the Natron and Magadi basins are lower than the surrounding border faults (cf. Tables 1 and 5). These low slip rates are, however, consistent with a rift system where extensional strains are spread over a wide area and accommodated on many faults (e.g., >100).

Evolution of Fault-Related Strain and Structural Relief in the Natron-Magadi Region

We provide the first quantitative analysis of the spatial and temporal distribution of fault-related strain over the course of early-stage rift evolution in the Magadi and Natron basins (Fig. 11). These data illustrate how fault-related strain is distributed within rift basins after ~3 and 7 m.y. of rifting in the Eastern rift. Accounting for the various sources of uncertainty, there are clear differences in how strain is distributed between Natron and Magadi. Specifically, in the Natron basin, the majority (>69%) of regional extension is accommodated along the border fault, whereas in Magadi the greatest strain is primarily accommodated in the rift center in the intra-rift fault population (>67%). Furthermore, during early-stage rifting in the 3 Ma Natron basin, a significant amount of intra-rift faulting (38%–96%) is driven by hanging-wall flexure of the border fault. After 7 m.y. of rifting, however, flexure of the border fault hanging wall has less influence on the formation of intra-rift faults, accounting for only 8%–12% of the extensional strain (refer to Table 4). Intra-rift fault populations instead accommodate the majority of regional extension as border faults become less active, as illustrated by the Magadi rift basin.

Evolving fault system dynamics in continental rift basins are accompanied by changes in structural relief that affect water and sediment catchments (Scholz et al., 1990; Gawthorpe and Leeder, 2000; Ebinger and Scholz, 2012). For example, zones of maximum subsidence in half-graben basins in the Malawi and Tanganyika rifts of East Africa occur adjacent to border faults, where more than 4 km of synrift sediments have accumulated (Scholz et al., 1990). Similarly, border fault subsidence in the Natron and Magadi region has

clearly been a major control on the position of ephemeral lakes (Ebinger and Scholz, 2012). However, the transition to intra-rift faulting in the Magadi basin also appears to have affected the position of Lake Natron and the development of Lake Magadi (Crane, 1981) (Fig. 12). As shown in Figure 1C, the lowest relief in the Magadi basin occurs in the rift center, consistent with the focusing of strain into the intra-rift fault system. In the Natron basin, however, the lowest relief is observed adjacent to the border fault escarpment (Fig. 1D), where the greatest amount of strain is also accommodated. The occurrence of Pleistocene lake sediments from Lake Natron northward along the base of the Nguruman escarpment indicates that paleo–Lake Natron extended further north into the Magadi basin during the Pleistocene (Crossley, 1979). The transition to intra-rift faulting in the Magadi basin and subsequent reduction in border activity may explain the southward retreat of the northern shoreline of Lake Natron, as areas of structural relief evolved in response to changes in fault system dynamics (Fig. 12). However, during warmer and wetter climatic periods in the late Pleistocene, increasing water levels have also occasionally resulted in Lakes Natron and Magadi forming a single, contiguous lake (Roberts et al., 1993). Similar patterns in the distribution of lake systems in the Natron-Magadi region are observed in basins of different ages across south Kenya and north Tanzania (Fig. 13). For example, in the 1 Ma Manyara and 3 Ma Natron basins, lakes occur adjacent to border fault escarpments, whereas in more evolved basins in the Kenya Rift (15–7 Ma) lakes are situated along the rift axis. The positions of these lakes likely reflect the locus of upper crustal strain (rift border versus rift axis) within these basins (Ebinger and Scholz, 2012).

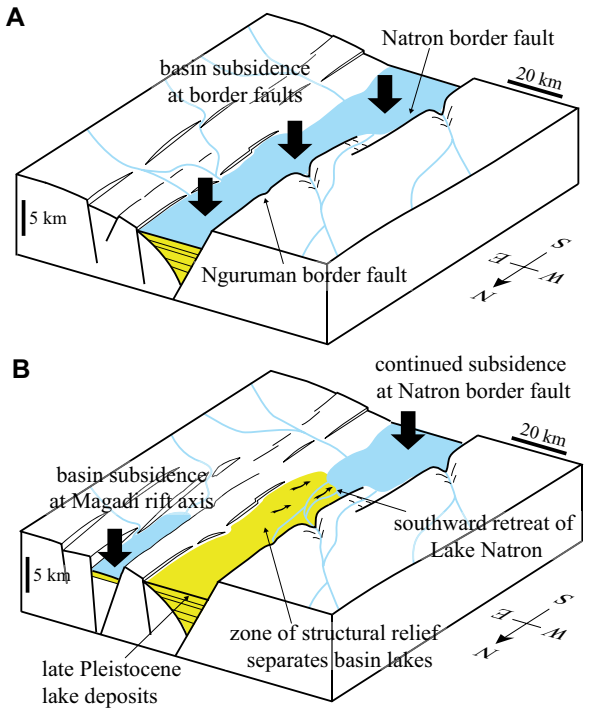

Figure 12. Simplified conceptual model of changing structural relief and water and sediment catchments resulting from fault system evolution in the Magadi-Natron region. Distribution of volcanism is not presented. (A) High activity on the border faults results in the formation of a contiguous lake in response to subsidence along the western side of the basins. (B) Over time, the locus of the strain, and greatest subsidence, in the Magadi basin migrates away from the Nguruman border fault and into the intra-rift fault population. Although the rate of subsidence along the Nguruman escarpment reduces, strain continues to be accommodated along the border fault in Natron, with continued subsidence along the western side of the basin. A zone of structural relief begins to develop at the base of the Nguruman escarpment in response to these evolving fault dynamics. The original border fault lake therefore retreats southward into Natron and a new lake develops in the subsiding center of the Magadi basin.

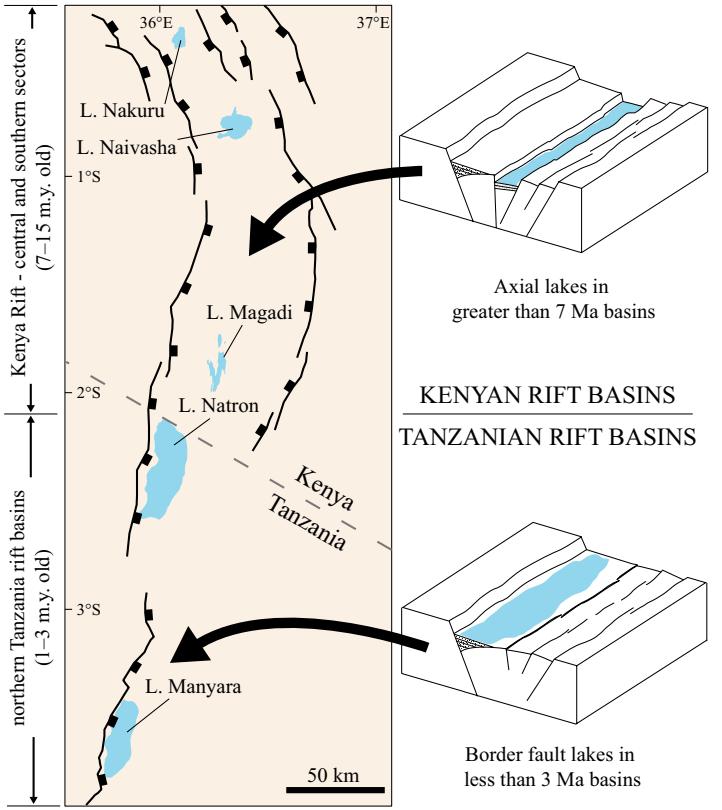

Figure 13. Distribution of basin lakes (L.—lake) in north Tanzania and the Kenya Rift. Major rift-bounding faults are from Smith (1994). Basin lakes in the 1–3 Ma Tanzanian basins (Manyara and Natron) occur adjacent to the border faults. Basin lakes in 7–15 Ma rift basins in the Kenya Rift occur along the rift axis.

Source of Spring Waters in the Natron and Magadi Basins

Diffuse soil CO_2 flux surveys and carbon isotope analyses from the Natron and Magadi basins reveal that rift-wide fault systems in the region act as pathways for the rise of mantle-derived CO_2 (Lee et al., 2016). This diffuse CO_2 is likely sourced from large magma bodies, which have been detected geophysically in the lower crust and upper mantle (Birt et al., 1997; Roecker et al., 2015; Lee et al., 2016). Is the chemical signature of springs in the Natron and Magadi basins also consistent with a magmatic source?

Spring samples from this study exhibit N_2/Ar ratios (15–67) within the range of, or slightly less than, air-saturated water (Fig. 10B). High He contents shown in Figure 10B, however, suggest additional inputs from either mantle or crustal sources. Similar N_2-He-Ar abundances have been observed previously in the EAR for springs in the Rungwe Province and fumaroles from Oldoinyo Lengai, which were interpreted to be sourced from magma bodies (Fischer et al., 2009; Barry et al., 2013; de Moor et al., 2013). A magmatic interpretation for the observed N_2-He-Ar abundances is also consistent with $\delta^{13}C$-CO_2 values in the Natron and Magadi springs (Fig. 10C), and isotope investigations of diffusely degassing CO_2 (Lee et al., 2016). In line with this assertion, helium isotope data from springs in Lake Magadi (reported in McNitt et al., 1989) are consistent with significant contributions (~25%–50%) of mantle-derived fluids. These geochemical data, combined with geophysical studies supporting the presence of lower crustal and upper mantle magma bodies in the region (Birt et al., 1997; Roecker et al., 2015), suggest a magmatic, rather than crustal, source for dissolved gas species in Natron and Magadi springs.

Controls on Fault System Evolution

Fault strain analyses in this study demonstrate that the Magadi and Natron basins are in a transitional stage of continental rift evolution; the locus of strain is actively transitioning from border faults to intra-rift fault populations (e.g., Figs. 2A, 2B). Previous studies in the Main Ethiopian Rift have attributed these transitions to the influence of magmatism, oblique rifting, and crustal inheritance (Chorowicz et al., 1994; Bonini et al., 1997; Kendall et al., 2005; Corti, 2008). We discuss here how each of these processes applies to the Natron and Magadi basins, as well as the role of magmatic fluids.

Crustal Inheritance

Chorowicz et al. (1994) attributed intra-rift faulting in the Main Ethiopian Rift in the late Pleistocene to the reactivation of preexisting Pan-African basement structures. This interpretation was challenged in later studies (e.g., Bonini et al., 1997; Corti, 2009) given the difficulties in explaining why optimally oriented structural fabrics would not be activated immediately during the initial stages of rifting. The influence of crustal inheritance in the Kenya Rift is illustrated by orientations of transfer structures between border faults, as well as the broad geometry of central Kenya Rift basins, which follow major northwest-southeast–striking shear zones mapped in Mozambique basement rocks (Smith and Mosley, 1993; Mosley, 1993; Smith, 1994; Katumwehe et al., 2016; Robertson et al., 2015). These observations support previous assertions that border faulting in the EAR often initiates on preexisting basement fabrics (McConnell, 1972; Daly et al., 1989; Foster et al., 1997; Katumwehe et al., 2015; Laó-Dávila et al., 2015). However, as basins evolve and favorably oriented faults develop orthogonal to the regional extension direction, the earlier formed, unfavorably oriented and/or located faults are eventually abandoned (Ebinger, 2005). Structural investigations in the Kenya Rift show a number of transverse, northwest-southeast–striking intra-rift faults, which probably initiated on preexisting basement fabrics (Le Turdu et al., 1999; Atmaoui and Hollnack, 2003; Kattenhorn et al., 2013). However, the majority of intra-rift faults in the Natron and Magadi basins, as well as intra-rift faults farther north in the Naivasha-Nakuru basin (Muirhead et al., 2015), trend orthogonal to the east-southeast–west-northwest regional extension direction (Fig. 7), and oblique to the northwest-southeast–striking basement structures. These observations suggest that, although some border fault segments and intra-rift faults (e.g., Kordjya fault of the Magadi basin; Le Turdu et al., 1999; Kattenhorn et al., 2013) may have initiated along inherited crustal fabrics (e.g., Smith and Mosley, 1993; Foster et al., 1997), the transition to an intra-rift dominated faulting regime in the study area cannot be attributed to the reactivation of basement weaknesses.

Oblique Rifting

Strain localization into intra-rift faults in the Main Ethiopian Rift has also been proposed to be the result of oblique extension along the border fault system (rift obliquity as great as 45°; Corti, 2008; Agostini et al., 2011b). These assertions are based on the timing and kinematics of faulting observed from analog experiments (Corti, 2008; Agostini et al., 2011b; Corti, 2012), which compare favorably with field and remote-sensing studies in the region (Corti, 2009; Agostini et al., 2011a). Rifting in the Natron and Magadi basins, however, has been inferred to occur primarily under orthogonal extension (Le Gall et al., 2008). Accordingly, intra-rift faults (008° mean trend) and border faults (006° mean trend) trend approximately normal to the 090°–110° extension direction inferred from analyses of fault plane solutions, volcanic vent alignments, neotectonic joints, and GPS plate motion vectors (Ibs-von Seht et al., 2001; Atmaoui and Hollnack, 2003; Brazier et al., 2005; Stamps et al., 2008; Saria et al., 2014). Focal mechanisms for earthquakes in the central parts of the Natron basin (Lambert et al., 2014) show dip-slip motions along north-northeast–trending normal faults. It is therefore unlikely that the evolution to intra-rift faulting in the study area has been assisted by oblique-style rifting along the border system.

Role of Magma

The development of intra-rift fault systems in the Natron and Magadi region occurred with accompanying magma intrusion (Baer et al., 2008; Calais et al., 2008; Biggs et al., 2009; Ebinger et al., 2013) and magmatic volatile release in the rift basins (Lee et al., 2016). An axial gravity anomaly has been traced along the Kenya Rift into the Magadi basin (Baker and Wohlenberg, 1971; Mechie et al., 1997; Ibs-von Seht et al., 2001), and interpreted as lower crustal intrusions. Ibs-von Seht et al. (2001) attributed high seismic velocities in the center of the Magadi basin to a zone of cooled middle to upper crustal dikes, and Birt et al. (1997) observed a low seismic velocity zone in the upper mantle that they interpreted as partial melt below the central rift axis. The presence of magma along the rift center is consistent with asthenospheric upwelling and enhanced melt production below the zone of maximum lithospheric extension in the center of the rift (Ebinger and Casey, 2001; Ebinger, 2005; Rooney, 2010). Furthermore, asthenospheric melts are likely guided (upward) along steep gradients in the lithosphere-asthenosphere boundary produced by thinning and flexing of the lithosphere, resulting in magma migration at depth from the rift margins into the rift center (Rooney et al., 2011, 2014; Keir et al., 2015). Geological, geophysical, and numerical modeling studies suggest that during early-stage rifting, when faulting is concentrated along rift margins, magmatism may also be focused along the margins of the rift (e.g., Bastow et al., 2005, 2008; Corti, 2009; Maccaferri et al., 2014). The rise of magmatic fluids along the western side of the 3 Ma Natron basin, from the border fault outward ~20 km toward the rift center, supports these previous assertions. In all, data from this study and previous work support the notion that fault-controlled strain plays a key role in controlling along-axis upper mantle segmentation and aiding melt focusing at depth (Bastow et al., 2005, 2008). Magma and related volatiles ascending from melt zones at depth can also be guided along the border fault and into the rift center along intra-rift faults (Casey et al., 2006; Le Corvec et al., 2013), some of which formed from flexure in the border fault hanging wall.

Magma rising into the center of these rift basins is likely to help localize deformation in intra-rift fault populations and drive the transition from border fault to intra-rift fault-dominated strain accommodation (Ebinger and Casey, 2001; Keir et al., 2006; Beutel et al., 2010). For example, dikes emplaced at middle to upper crustal levels enhance extensional stresses in the area above the dike tip (Rubin and Pollard, 1988). These static stress changes can initiate faulting in the shallow crust, as has been demonstrated during dike rifting events in Iceland and Ethiopia (Bjornsson et al., 1977; Rowland et al., 2007; Belachew et al., 2013; Wright et al., 2012; Sigmundsson et al., 2015; Trippanera et al., 2015). Similarly, a diking event in south Natron in 2007 was accompanied by slip along several intra-rift faults, based on seismicity, focal mechanisms, InSAR (interferometric synthetic aperture radar) displacements, and measured surface ruptures (Baer et al., 2008; Calais et al., 2008; Biggs et al., 2009; Wauthier, 2011). However, this event was confined to a volcanic field at the southern end of the Natron basin, and may not represent a rift-wide process of upper crustal diking from the center of the Natron basin northward along the length of Magadi (Muirhead et al., 2015). Despite the presence of underlying magma at the rift center (Birt et al., 1997), there is no evidence (i.e., volcanic cones, lava flows) of significant surface-breaching dike intrusions since the eruption of Magadi Trachyte lavas (Muirhead et al., 2015), suggesting dike arrest at predominantly lower to middle crustal depths, with upper crustal extensional strain (i.e., upper few kilometers) accommodated almost entirely by normal faulting.

Numerical modeling studies show that cooling magma intrusions transfer heat to the surrounding country rock, causing thermally driven variations in crustal rheology (Daniels et al., 2014). Dike intrusions can therefore locally weaken lithosphere and assist in crustal thinning and strain localization in the basin center (Bialas et al., 2010; Daniels et al., 2014). Extensional stresses are also shown numerically to localize around cooled axial intrusions emplaced within continental crust (Beutel et al. 2010), thereby focusing extensional strain into the rift center even during episodes of low magma flux. In the Magadi basin in particular, geophysical and geochemical observations (e.g., Baker and Wohlenberg, 1971; Birt et al., 1997; Mechie et al., 1997; Ibs-von Seht et al., 2001; Lee et al., 2016) suggest that the transition to intra-rift faulting shown in this study (Fig. 11) has been accompanied by axial magma emplacement in the lower crust and upper mantle. These observations provide support for the potential role of magmatism in assisting the transition to focused intra-rift faulting in the study region.

Role of Magmatic Fluids

An important factor controlling lithospheric weakening and the localization of rifting of cratonic lithosphere is the presence of CO_2-rich fluids (Geissler et al., 2005; Lindenfeld et al., 2012; Albaric et al., 2014). In continental rift settings exhibiting high fluid flow (e.g., Taupo Volcanic Zone, New Zealand), the magnitude of extensional tectonic stresses required for normal faulting decreases locally in areas exhibiting high pore-fluid pressures (Reyners et al., 2007; Rowland and Simmons, 2012). Similarly, lower crustal earthquakes observed in the EAR may require anomalously high pore-fluid pressures at depth (Seno and Saito, 1994; Lindenfeld et al., 2012), with some of these fluids likely exsolved from lower crustal magma intrusions (Keir et al., 2009; Lee et al., 2016). The rheology of lithosphere, particularly within fault zones, will vary cyclically depending on the presence or absence of fluids (Yardley et al., 2010). Deeply derived magmatic fluids (e.g., CO_2, H_2O) are redistributed en masse during earthquake slip events (Sibson, 2000; Brodsky et al., 2003; Shelly et al., 2015). Depending on oxygen fugacity, the presence of these magmatic fluids (i.e., CO_2 and H_2O) may enhance intracrystalline deformation in quartz and other crystalline minerals (Chen et al., 2006; Chernak et al., 2009; Holyoke and Kronenberg, 2013). During periods of seismic quiescence, fluids present in fault zones are gradually consumed during hydration reactions to produce weaker, fine-grained, hydrous minerals (Moore and Rymer, 2007; Yardley et al., 2010).

Geochemical data from spring systems throughout the Natron and Magadi basins (Fig. 10) and recently published seismicity and diffuse soil CO_2 data support the release of volatiles into the rift from lower crustal and/or upper mantle magma bodies (Lee et al., 2016). The high output of magmatic gases (>1 Mt yr^{-1} of magmatic CO_2; Lee et al., 2016) along rift-wide fault networks in the Magadi-Natron region suggests a significant supply of deeply circulating fluids that may be able to weaken faults and assist in strain localization. In line with these assertions, the locations of hot springs in the Magadi-Natron region coincide with areas of high strain (Figs. 8 and 10; Table 2). For example, time-averaged extension rates in the Magadi basin are highest within faults dissecting the Magadi Trachyte lava group (0.93 ± 0.28 mm yr^{-1}) in the center of the rift. Within this area of high strain (unit 3 in Table 2), hot springs manifest at the base of intra-rift fault scarps (Fig. 3E), whereas no springs were observed along the Nguruman border fault escarpment. In the Natron basin, however, hydrothermal systems are present along the western border fault of the rift and ~20 km outward into the border fault hanging wall. In contrast to Magadi, the border fault accommodates significantly more regional extension (1.24–1.78 mm yr^{-1}) than intra-rift faults (0.0.2–0.56 mm yr^{-1}). Therefore, we assert that magmatic fluids in the Natron basin likely ascend along the border fault, and then possibly outward into nearby faults forming in the flexing border fault hanging wall (Fig. 14). As flexure imposes compressional stresses in the lower half of an the elastic plate, and extensional stresses in the upper half, fluid migration along subvertical extensional structures (e.g., normal faults and dilational joints) within the hanging wall is expected to be enhanced in the upper ~10 km of the crust in Natron. The close associations between areas of high strain and volatile release suggest that magmatic volatiles may also play an active role in weakening lithosphere and assisting the transition to focused intra-rift faulting in the study region.

Conceptual Model: Evolving Fault-Fluid Systems in the Natron and Magadi Basins

By comparing the 3 Ma Natron and 7 Ma Magadi basins we provide a revised conceptual model for evolving fault and magmatic volatile systems during early-stage rifting. Results from the Natron basin show that, within the first 3 m.y. of rifting, border faults accommodate the majority of strain (>69%) related to regional extension. In Natron specifically, the depth of syn-rift basin fill suggests that the border fault system accrued ~2200 m of throw during this period, which caused significant flexure of the hanging wall in the ~50-km-wide half-graben basin. Horizontal extensional strain related to this flexure drove the formation of intra-rift faults, which acted to accommodate regional extension as well as localized stresses in the flexing hanging wall. Evidence for diking in south Natron (i.e., Calais et al., 2008; Biggs et al., 2013; Muirhead et al., 2015), lower crustal seismicity (Roecker et al., 2015; Lee et al., 2016) and rift-wide release of magmatic volatiles at the surface (Lee et al., 2016; Fig. 10) support the development of intra-rift fault systems coevally with the emplacement of crustal magmas. Fluids released from magmas interact with these fault systems (Figs. 10 and 14), and may explain the presence of lower to mid-crustal earthquake swarms documented in

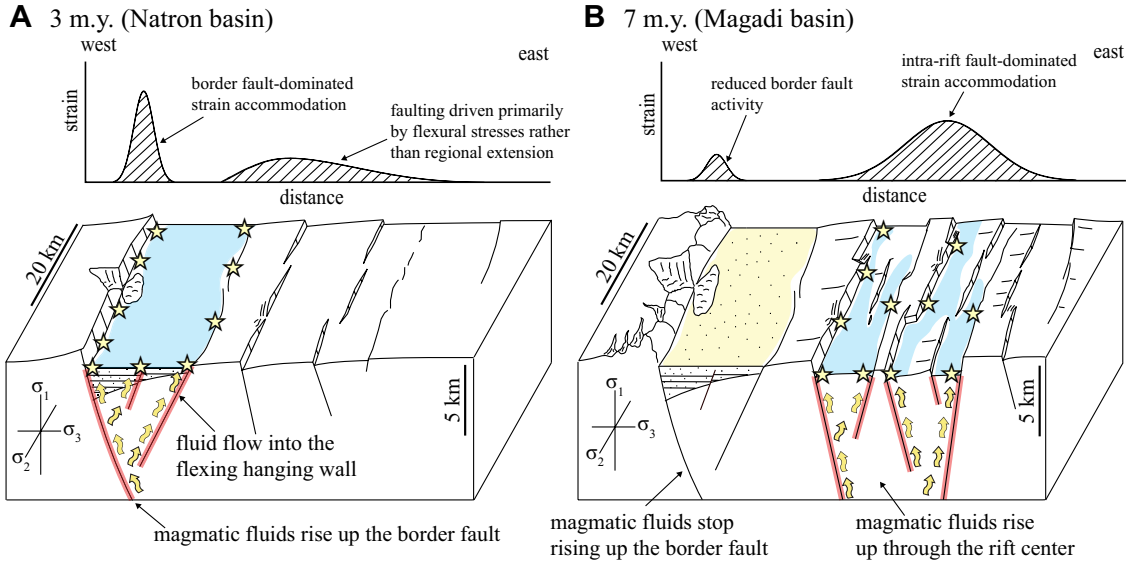

Figure 14. Conceptual model of evolving fault-related strain and magmatic fluid systems during early-stage rifting (the first 7 m.y.) in the Natron and Magadi basins. (A) Rift configuration 3 m.y. after rift initiation in the Natron basin. Strain is primarily accommodated along the border fault. Minor faulting occurs on intra-rift faults in the rift center from stresses generated by flexure of the border fault hanging wall. These intra-rift faults accommodate only a small proportion of regional extension. Magmatic fluids ascend the crust (yellow arrows) along the border fault system and then outward into nearby intra-rift faults in the flexing hanging wall (red lines). These fluids are observed at the surface as hot springs (yellow stars) that feed water into an ephemeral lake (light blue). (B) Rift configuration 7 m.y. after rift initiation in the Magadi basin. At this stage of rifting, the locus of strain has migrated from the border fault to the intra-rift fault population. The border fault escarpment becomes progressively more degraded. Magmatic fluids ascend the crust in areas of high strain in the center of the rift, and no longer rise up along the relatively inactive border fault. Paleolake deposits on the rift border (light yellow) on the western side of the basin reflect the earlier locus of strain and hydrothermal fluid release. Based on previous studies in the study area, magma bodies sourcing the fluids are likely situated at upper mantle and/or lower crustal depths (Birt et al., 1997; Mechie et al., 1997; Lee et al., 2016). Note that if extension is accommodated primarily via diking at middle to lower crustal levels, then extensional strain at these depths may be focused in a narrower zone than that represented by intra-rift faults in the near surface (Rubin and Pollard, 1988; Ebinger et al., 2010).

these basins (Seno and Saito, 1994; Lee et al., 2016). The focusing of magma toward the rift center and concomitant release of magmatic fluids into the flexing hanging wall provide a previously unrecognized mechanism that may help to weaken crust and assist the transition to intra-rift dominated strain accommodation.

Findings from the Magadi basin show that, by 7 m.y., regional extension was primarily accommodated in the intra-rift fault population. By this stage of rifting, the border fault became relatively less active (accommodating 0.40–0.66 mm yr^{-1} of extension, compared to 1.24–1.78 mm yr^{-1} in Natron), and hanging-wall flexure played only a minor role in driving intra-rift faulting. The transition to intra-rift faulting was accompanied by widespread magma emplacement below the rift axis (Baker and Wohlenberg, 1971; Birt et al., 1997; Ibs-von Seht et al., 2001; Lee et al., 2016). Furthermore, the migration of strain away from the border fault into the rift center is followed by a similar migration in the locations of magmatic volatile release. These observations highlight a strong association between strain localization and the release of magmatic fluids in the rift.

Our results provide important insights into the processes governing strain localization into the rift center that may also apply to other parts of the Eastern rift. Competing hypotheses for the development of intra-rift faults in the Main Ethiopian Rift (Fig. 1B) focus on the influence of oblique rifting versus the role magmatism (see Corti, 2009, and references therein; Fig. 2). The Natron and Magadi basins are currently in this transitional phase, and our results support the role of not only magmatism, but also magmatic volatiles in establishing intra-rift fault systems and focusing strain in the rift center. Once this fault system is developed, crustal thinning within the rift center may enhance magma production from decompression melting (Ebinger, 2005; Corti, 2008; Rooney, 2010) and assist in the development of magmatic segments like those present in the Main Ethiopian Rift (Ebinger et al., 2001; Keranen et al., 2004; Maguire et al., 2006; Fig. 2). Magmatic volatile release may have therefore been a key process for weakening lithosphere to localize strain in the rift center prior to the establishment of magmatic segments in Ethiopia.

CONCLUSIONS

This study is the first to investigate the evolving distribution of upper crustal deformation in the 3 Ma Natron and 7 Ma Magadi basins from quantitative fault-strain analyses. These data are examined alongside spring geochemistry and new $^{40}Ar/^{39}Ar$ ages of rift volcanics to elucidate the timing of volcanic and tectonic activity. Results demonstrate for the first time a clear link between zones of high upper crustal strain and magmatic fluid release within early-stage rift basins (younger than 10 m.y.) in the East African Rift.

New $^{40}Ar/^{39}Ar$ ages provide revised constraints on the timing of activity in the Natron basin from Mosonik (as old as 4.05 Ma), Gelai (1.23–0.95 Ma), and Oldonyo Sambu volcanoes (as young as 1.97 Ma). Results also suggest that the Singaraini basalts in the Magadi basin were emplaced by 1.96 Ma. Intra-rift faults measured and dated in the field in the Natron basin exhibit minimum slip rates that range from 0.06 to 0.09 mm yr^{-1}, whereas analyzed (subsidiary) border fault segments range from 0.09 to 0.16 mm yr^{-1}. Time-averaged minimum slip rates from intra-rift faults measured in the field in Magadi range from 0.01 to 0.13 mm yr^{-1}, but likely reach as high as 0.45 mm yr^{-1} on the largest faults. Basin-wide strain analyses give estimated slip rates of 1.93–3.56 mm yr^{-1} for the Natron border fault and 0.62–1.32 mm yr^{-1} for the Nguruman border fault, which are in good agreement with estimates based on rift basin depths and border fault ages.

Results from the Natron basin in this study show that, within the first 3 m.y. of rifting, border faults accommodate the majority of strain (>69%) related to regional extension. Flexure of the border fault hanging wall may have been an important driver of the initial formation of intra-rift faults, which ultimately accommodated both regional extension as well as localized stresses in the flexing plate. Within the 7 Ma Magadi basin, regional extension is primarily accommodated in the intra-rift fault population (67%–80%), revealing a transition from border fault- to intra-rift fault–dominated strain accommodation sometime between 3 and 7 m.y. after rift initiation. The transition to intra-rift faulting in the Magadi basin also affected the position of Lake Natron and the development of Lake Magadi, where a reduction in activity along the Nguruman border fault resulted in the southward retreat of the northern shoreline of Lake Natron.

The localization of strain into intra-rift faults in the Magadi basin did not require the reactivation of preexisting structures (Chorowicz, et al., 1994) or oblique-style rifting (Corti, 2008), as has been asserted previously for the Main Ethiopian Rift. Instead, the transition to intra-rift faulting in Magadi has been accompanied by recent magmatism and magmatic volatile release in the rift center. Areas of high strain in each basin also coincide with the presence of hydrothermal spring systems, and geochemical analyses of dissolved gas species support a magmatic source for these fluids. These observations highlight a strong association between strain localization and the introduction of magmatic fluids into the rift, likely sourced from magma bodies in the upper mantle and lower crust. The ascent of magmatic volatiles within rift basins may therefore help to weaken lithosphere and localize strain in the rift center prior to the establishment of magmatic segments.

ACKNOWLEDGMENTS

This study was supported by National Science Foundation grants EAR-1113677 (to Kattenhorn) and EAR-1113066 (to Fischer). Additional support to Muirhead was provided by Fulbright New Zealand and the Ministry of Science and Innovation. We thank the Tanzania Commission for Science and Technology (COSTECH) and the Kenyan National Council for Science and Technology for granting research permits, and Majura Songo and Norbert Opiyo-Akech for assistance. Aerial photographs were provided by the Polar Geospatial Center, University of Minnesota (St. Paul). We are grateful to Remigius Gama, Matt Blakeslee, Benson Onguso, Nicole Thomas, and Melania Maqway for assistance in the field. We thank Cindy Ebinger in particular for valuable discussions on continental rifting, and Eric Mittelstaedt, Catherine Cooper, John Watkinson, Dennis Geist, Alexandria Guth, Christelle Wauthier, Julie Rowland, Pilar Villamor, Matt Pendleton, Darin Schwartz, and Alexa Van Eaton for helpful discussions and comments. We also thank two anonymous reviewers, who provided constructive and insightful comments that improved the manuscript.

REFERENCES CITED

Acocella, V., Korme, T., and Salvini, F., 2003, Formation of normal faults along the axial zone of the Ethiopian Rift: Journal of Structural Geology, v. 25, p. 503–513, doi:10.1016/S0191-8141(02)00047-0.

Acocella, V., Abebe, B., Korme, T., and Barberi, F., 2008, Structure of Tendaho Graben and Manda Hararo Rift: Implications for the evolution of the southern Red Sea propagator in Central Afar: Tectonics, v. 27, TC4016, doi:10.1029/2007TC002236.

Agostini, A., Corti, G., Zeoli, A., and Mulugeta, G., 2009, Evolution, pattern, and partitioning of deformation during oblique continental rifting: Inferences from lithospheric-scale centrifuge models: Geochemistry, Geophysics, Geosystems, v. 10, Q11015, doi:10.1029/2009GC002676.

Agostini, A., Bonini, M., Corti, G., Sani, F., and Manetti, P., 2011a, Distribution of Quaternary deformation in the central Main Ethiopian Rift, East Africa: Tectonics, v. 30, TC4010, doi:10.1029/2010TC002833.

Agostini, A., Bonini, M., Corti, G., Sani, F., and Mazzarini, F., 2011b, Fault architecture in the Main Ethiopian Rift and comparison with experimental models: Implications for rift evolution and Nubia-Somalia kinematics: Earth and Planetary Science Letters, v. 301, p. 479–492, doi:10.1016/j.epsl.2010.11.024.

Albaric, J., Deverchere, J., Petit, C., Perrot, J., and Le Gall, B., 2009, Crustal rheology and depth distribution of earthquakes: Insights from the central and southern East African Rift System: Tectonophysics, v. 468, p. 28–41, doi:10.1016/j.tecto.2008.05.021.

Albaric, J., Deverchere, J., Perrot, J., Jakovlev, A., and Deschamps, A., 2014, Deep crustal earthquakes in North Tanzania, East Africa: Interplay between tectonic and magmatic processes in an incipient rift: Geochemistry, Geophysics, Geosystems, v. 15, p. 374–394, doi:10.1002/2013GC005027.

Angelier, J., Bergerat, F., Dauteuil, O., and Villemin, T., 1997, Effective tension-shear relationships in extensional fissure swarms, axial rift zone of northeastern Iceland: Journal of Structural Geology, v. 19, p. 673–685, doi:10.1016/S0191-8141(96)00106-X.

Atmaoui, N., and Hollnack, D., 2003, Neotectonics and extension direction of the southern Kenya Rift, Lake Magadi area: Tectonophysics, v. 364, p. 71–83, doi:10.1016/S0040-1951(03)00051-9.

Baer, G., Hamiel, Y., Shamir, G., and Nof, R., 2008, Evolution of a magma-driven earthquake swarm and triggering of the nearby Oldoinyo Lengai eruption, as resolved by InSAR, ground observations and elastic modeling, East African Rift, 2007: Earth and Planetary Science Letters, v. 272, p. 339–352, doi:10.1016/j.epsl.2008.04.052.

Baker, B.H., 1958, Geology of the Magadi Area: Geological Survey of Kenya Report 42, 81 p.

Baker, B.H., 1963, Geology of the Area of South of Magadi: Geological Survey of Kenya Report 61, 27 p.

Baker, B.H., 1986, Tectonics and volcanism of the southern Kenya Rift Valley and its influence on rift sedimentation, *in* Frostick, L.E., et al., eds., Sedimentation in the African Rifts: Geological Society of London Special Publication 25, p. 45–57, doi:10.1144/GSL.SP.1986.025.01.05.

Baker, B.H., and Mitchell, J.G., 1976, Volcanic stratigraphy and geochronology of the Kedong-Olorgesaile area and the evolution of the south Kenya rift valley: Journal of the Geological Society [London], v. 132, p. 467–484, doi:10.1144/gsjgs.132.5.0467.

Baker, B.H., and Wohlenberg, J., 1971, Structure and evolution of Kenya Rift Valley: Nature, v. 229, p. 538–542, doi:10.1038/229538a0.

Baker, B.H., Williams, L.A., Miller, J.A., and Fitch, F.J., 1971, Sequence and geochronology of Kenya Rift volcanics: Tectonophysics, v. 11, p. 191–215, doi:10.1016/0040-1951(71)90030-8.

Baker, B.H., Goles, G.G., Leeman, W.P., and Lindstrom, M.M., 1977, Geochemistry and petrogenesis of a basalt-benmoreite-trachyte suite from the southern part of the Gregory Rift, Kenya: Contributions to Mineralogy and Petrology, v. 64, p. 303–332, doi:10.1007/BF00371759.

Baker, B.H., Mitchell, J.G., and Williams, L.A.J., 1988, Stratigraphy, geochronology and volcano-tectonic evolution of the Kedong-Naivasha-Kinangop region, Gregory Rift Valley, Kenya: Journal of the Geological Society [London], v. 145, p. 107–116, doi:10.1144/gsjgs.145.1.0107.

Barry, P.H., Hilton, D.R., Fischer, T.P., de Moor, J.M., Mangasini, F., and Ramirez, C., 2013, Helium and carbon isotope systematics of cold "mazuku" CO_2 vents and hydrothermal gases and fluids from Rungwe Volcanic Province, southern Tanzania: Chemical Geology, v. 339, p. 141–156, doi:10.1016/j.chemgeo.2012.07.003.

Bastow, I.D., Stuart, G.W., Kendall, J.M., and Ebinger, C.J., 2005, Upper-mantle seismic structure in a region of incipient continental breakup: northern Ethiopian rift: Geophysical Journal International, v. 162, p. 479–493, doi:10.1111/j.1365-246X.2005.02666.x.

Bastow, I.D., Nyblade, A.A., Stuart, G.W., Rooney, T.O., and Benoit, M.H., 2008, Upper mantle seismic structure beneath the Ethiopian hot spot: Rifting at the edge of the African low-velocity anomaly: Geochemistry, Geophysics, Geosystems, v. 9, Q12022, doi:10.1029/2008GC002107.

Bastow, I.D., Pilidou, S., Kendall, J.M., and Stuart, G.W., 2010, Melt-induced seismic anisotropy and magma assisted rifting in Ethiopia: Evidence from surface waves: Geochemistry, Geophysics, Geosystems, v. 11, QOAB05, doi:10.1029/2010GC003036.

Behn, M.D., and Ito, G., 2008, Magmatic and tectonic extension at mid-ocean ridges: 1. Controls on fault characteristics: Geochemistry, Geophysics, Geosystems, v. 9, Q08O10, doi:10.1029/2008GC001965.

Behn, M.D., Buck, W.R., and Sacks, I.S., 2006, Topographic controls on dike injection in volcanic rift zones: Earth and Planetary Science Letters, v. 246, p. 188–196, doi:10.1016/j.epsl.2006.04.005.

Behr, H.J., and Rohricht, C., 2000, Record of seismotectonic events in siliceous cyanobacterial sediments (Magadi cherts), Lake Magadi, Kenya: International Journal of Earth Sciences, v. 89, p. 268–283, doi:10.1007/s005319900070.

Belachew, M., Ebinger, C., and Cote, D., 2013, Source mechanisms of dike-induced earthquakes in the Dabbahu-Manda Hararo rift segment in Afar, Ethiopia: Implications for faulting above dikes: Geophysical Journal International, v. 192, p. 907–917, doi:10.1093/gji/ggs076.

Berryman, K., Villamor, P., Nairn, I., van Dissen, R., Begg, J., and Lee, J., 2008, Late Pleistocene surface rupture history of the Paeroa fault, Taupo Rift, New Zealand: New Zealand Journal of Geology and Geophysics, v. 51, p. 135–158, doi:10.1080/00288300809509855.

Beutel, E., van Wijk, J., Ebinger, C., Keir, D., and Agostini, A., 2010, Formation and stability of magmatic segments in the Main Ethiopian and Afar rifts: Earth and Planetary Science Letters, v. 293, p. 225–235, doi:10.1016/j.epsl.2010.02.006.

Bialas, R.W., Buck, W.R., and Qin, R., 2010, How much magma is required to rift a continent?: Earth and Planetary Science Letters, v. 292, p. 68–78, doi:10.1016/j.epsl.2010.01.021.

Biggs, J., Amelung, F., Gourmelen, N., Dixon, T.H., and Kim, S.W., 2009, InSAR observations of 2007 Tanzania rifting episode reveal mixed fault and dyke extension in an immature continental rift: Geophysical Journal International, v. 179, p. 549–558, doi:10.1111/j.1365-246X.2009.04262.x.

Biggs, J., Chivers, M., and Hutchinson, M.C., 2013, Surface deformation and stress interactions during the 2007–2010 sequence of earthquake, dyke intrusion and eruption in northern Tanzania: Geophysical Journal International, v. 195, p. 16–26.

Billings, S.E., and Kattenhorn, S.A., 2005, The great thickness debate: Ice shell thickness models for Europa and comparisons with estimates based on flexure at ridges: Icarus, v. 177, p. 397–412, doi:10.1016/j.icarus.2005.03.013.

Bird, P., Liu, Z., and Rucker, W.K., 2008, Stresses that drive the plates from below: Definitions, computational path, model optimization, and error analysis: Journal of Geophysical Research, v. 113, B11406, doi:10.1029/2007JB005460.

Birt, C.S., Maguire, P.K.H., Khan, M.A., Thybo, H., Keller, G.R., and Patel, J., 1997, The influence of pre-existing structures on the evolution of the southern Kenya Rift Valley—Evidence from seismic and gravity studies: Tectonophysics, v. 278, p. 211–242, doi:10.1016/S0040-1951(97)00105-4.

Bjornsson, A., Saemundsson, K., Einarsson, P., Tryggvason, E., and Gronvold, K., 1977, Current rifting episode in north Iceland: Nature, v. 266, p. 318–323, doi:10.1038/266318a0.

Blakeslee, M.W., and Kattenhorn, S.A., 2013, Revised earthquake hazard of the Hat Creek fault, northern California: A case example of a normal fault dissecting variable-age basaltic lavas: Geosphere, v. 9, p. 1397–1409, doi:10.1130/GES00910.1.

Boccaletti, M., Bonini, M., Mazzuoli, R., Abebe, B., Piccardi, L., and Tortorici, L., 1998, Quaternary oblique extensional tectonics in the Ethiopian Rift (Horn of Africa): Tectonophysics, v. 287, p. 97–116, doi:10.1016/S0040-1951(98)80063-2.

Bohnenstiehl, D.R.R., and Kleinrock, M.C., 1999, Faulting and fault scaling on the median valley floor of the trans-Atlantic geotraverse (TAG) segment, similar to 26 degrees N on the Mid-Atlantic Ridge: Journal of Geophysical Research, v. 104, p. 29,351–29,364, doi:10.1029/1999JB900256.

Bohnenstiehl, D.R., and Kleinrock, M.C., 2000, Evidence for spreading-race dependence in the displacement-length ratios of abyssal hill faults at mid-ocean ridges: Geology, v. 28, p. 395–398, doi:10.1130/0091-7613(2000)28<395:EFSDIT>2.0.CO;2.

Bonini, M., Souriot, T., Boccaletti, M., and Brun, J.P., 1997, Successive orthogonal and oblique extension episodes in a rift zone: Laboratory experiments with application to the Ethiopian Rift: Tectonics, v. 16, p. 347–362, doi:10.1029/96TC03935.

Bonnet, E., Bour, O., Odling, N.E., Davy, P., Main, I., Cowie, P., and Berkowitz, B., 2001, Scaling of fracture systems in geological media: Reviews of Geophysics, v. 39, p. 347–383, doi:10.1029/1999RG000074.

Bott, M.H.P., 1996, Flexure associated with planar faulting: Geophysical Journal International, v. 126, p. F21–F24, doi:10.1111/j.1365-246X.1996.tb04692.x.

Brandsdóttir, B., and Einarsson, P., 1979, Seismic activity associated with the September 1977 deflation of the Krafla central volcano in northeastern Iceland: Journal of Volcanology and Geothermal Research, v. 6, p. 197–212, doi:10.1016/0377-0273(79)90001-5.

Brazier, R.A., Nyblade, A.A., and Florentin, J., 2005, Focal mechanisms and the stress regime in NE and SW Tanzania, East Africa: Geophysical Research Letters, v. 32, L14315, doi:10.1029/2005GL023156.

Brodsky, E.E., Roeloffs, E., Woodcock, D., Gall, I., and Manga, M., 2003, A mechanism for sustained groundwater pressure changes induced by distant earthquakes: Journal of Geophysical Research, v. 108, 2390, doi:10.1029/2002JB002321.

Buck, W.R., 2004, Consequences of asthenospheric variability on continental rifting, *in* Karner, G.D., et al., eds., Rheology and Deformation of the Lithosphere at Continental Margins: MARGINS Theoretical and Experimental Earth Science Series: New York, Columbia University Press, p. 1–30.

Buck, W.R., Lavier, L.L., and Poliakov, A.N.B., 2005, Modes of faulting at mid-ocean ridges: Nature, v. 434, p. 719–723, doi:10.1038/nature03358.

Buck, W.R., Einarsson, P., and Brandsdottir, B., 2006, Tectonic stress and magma chamber size as controls on dike propagation: Constraints from the 1975–1984 Krafla rifting episode: Journal of Geophysical Research, v. 111, B12404, doi:10.1029/2005jb003879.

Burnard, P., Graham, D., and Turner, G., 1997, Vesicle-specific noble gas analyses of "popping rock": Implications for primordial noble gases in earth: Science, v. 276, p. 568–571, doi:10.1126/science.276.5312.568.

Calais, E., et al., 2008, Strain accommodation by slow slip and dyking in a youthful continental rift, East Africa: Nature, v. 456, p. 783–787, doi:10.1038/nature07478.

Campbell, I.H., 2005, Large igneous provinces and the mantle plume hypothesis: Elements, v. 1, p. 265–269, doi:10.2113/gselements.1.5.265.

Carbotte, S.M., and MacDonald, K.C., 1994, Comparison of seafloor tectonic fabric at intermediate, fast, and super fast spreading ridges: Influence of spreading rate, plate motions, and ridge segmentation of fault patterns: Journal of Geophysical Research, v. 99, p. 13,609–13,631, doi:10.1029/93JB02971.

Cartwright, J.A., Trudgill, B.D., and Mansfield, C.S., 1995, Fault growth by segment linkage—An explanation for scatter in maximum displacement and trace length data from the Canyonlands grabens of SE Utah: Journal of Structural Geology, v. 17, p. 1319–1326, doi:10.1016/0191-8141(95)00033-A.

Casey, M., Ebinger, C., Keir, D., Gloaguen, R., and Mohamed, F., 2006, Strain accommodation in transitional rifts: Extension by magma intrusion and faulting in Ethiopian rift magmatic segments, *in* Yirgu, G., et al., eds., Afar Volcanic Province Within the East African Rift System: Geological Society of London Special Publication 259, p. 143–163, doi:10.1144/GSL.SP.2006.259.01.13.

Chadwick, W.W., and Embley, R.W., 1998, Graben formation associated with recent dike intrusions and volcanic eruptions on the mid-ocean ridge: Journal of Geophysical Research, v. 103, p. 9807–9825, doi:10.1029/97JB02485.

Chen, S., Hiraga, T., and Kohlstedt, D.L., 2006, Water weakening of clinopyroxene in the dislocation creep regime: Journal of Geophysical Research, v. 111, B08203, doi:10.1029/2005jb003885.

Chernak, L.J., Hirth, G., Selverstone, J., and Tullis, J., 2009, Effect of aqueous and carbonic fluids on the dislocation creep strength of quartz: Journal of Geophysical Research, v. 114, B04201, doi:10.1029/2008jb005884.

Chorowicz, J., Collet, B., Bonavia, F.F., and Korme, T., 1994, Northwest to north-northwest extension direction in the Ethiopian Rift deduced from the orientation of extension structures and fault-slip analysis: Geological Society of America Bulletin, v. 106, p. 1560–1570, doi:10.1130/0016-7606(1994)105<1560:NTNNED>2.3.CO;2.

Clifton, A.E, and Schlische, R.W., 2001, Nucleation, growth, and linkage of faults in oblique rift zones: Results from experimental clay models and implications for maximum fault size: Geology, v. 29, p. 455–458, doi:10.1130/0091-7613(2001)029<0455:NGALOF>2.0.CO;2.

Clifton, A.E., Schlische, R.W., Withjack, M.O., and Ackermann, R.V., 2000, Influence of rift obliquity on fault-population systematics: Results of experimental clay models: Journal of Structural Geology, v. 22, p. 1491–1509, doi:10.1016/S0191-8141(00)00043-2.

Coblentz, D.D., and Sandiford, M., 1994, Tectonic stresses in the African plate: Constraints on the ambient lithospheric stress state: Geology, v. 22, p. 831–834, doi:10.1130/0091-7613(1994)022<0831:TSITAP>2.3.CO;2.

Cornwell, D.G., Mackenzie, G.D., England, R.W., Maguire, P.K.H., Asfaw, L.M., and Oluma, B., 2006, Northern Main Ethiopian Rift crustal structure from new high-precision gravity data, *in* Yirgu, G., et al., eds., The Afar Volcanic Province Within the East African Rift System: Geological Society of London Special Publication 259, p. 307–321, doi:10.1144/GSL.SP.2006.259.01.23.

Corti, G., 2008, Control of rift obliquity on the evolution and segmentation of the main Ethiopian rift: Nature Geoscience, v. 1, p. 258–262, doi:10.1038/ngeo160.

Corti, G., 2009, Continental rift evolution: From rift initiation to incipient break-up in the Main Ethiopian Rift, East Africa: Earth-Science Reviews, v. 96, p. 1–53, doi:10.1016/j.earscirev.2009.06.005.

Corti, G., 2012, Evolution and characteristics of continental rifting: Analog modeling-inspired view and comparison with examples from the East African Rift System: Tectonophysics, v. 522, p. 1–33, doi:10.1016/j.tecto.2011.06.010.

Corti, G., Bonini, M., Conticelli, S., Innocenti, F., Manetti, P., and Sokoutis, D., 2003, Analogue modelling of continental extension: A review focused on the relations between the patterns of deformation and the presence of magma: Earth-Science Reviews, v. 63, p. 169–247, doi:10.1016/S0012-8252(03)00035-7.

Corti, G., Sani, F., Philippon, M., Sokoutis, D., Willingshofer, E., and Molin, P., 2013, Quaternary volcano-tectonic activity in the Soddo region, western margin of the southern Main Ethiopian Rift: Tectonics, v. 32, p. 861–879, doi:10.1002/tect.20052.

Corti, G., Agostini, A., Keir, D., Van Wijk, J., Bastow, I.D., and Ranalli, G., 2015, Magma-induced axial subsidence during final-stage rifting: Implications for the development of seaward-dipping reflectors: Geosphere, v. 11, p. 563–571, doi:10.1130/GES01076.1.

Courtillot, V., Jaupart, C., Manighetti, I., Tapponnier, P., and Besse, J., 1999, On causal links between flood basalts and continental breakup: Earth and Planetary Science Letters, v. 166, p. 177–195, doi:10.1016/S0012-821X(98)00282-9.

Cowie, P.A., and Scholz, C.H., 1992, Physical explanation for the displacement-length relationship of faults using a post-yield fracture mechanics model: Journal of Structural Geology, v. 14, p. 1133–1148, doi:10.1016/0191-8141(92)90065-5.

Cowie, P.A., Scholz, C.H., Edwards, M., and Malinverno, A., 1993, Fault strain and seismic coupling on mid-ocean ridges: Journal of Geophysical Research, v. 98, p. 17,911–17,920, doi:10.1029/93JB01567.

Cowie, P.A., Malinverno, A., Ryan, W.B.F., and Edwards, M.H., 1994, Quantitative fault studies on the East Pacific Rise: A comparison of sonar imaging techniques: Journal of Geophysical Research, v. 99, p. 15,205–15,218, doi:10.1029/94JB00041.

Cowie, P.A., Underhill, J.R., Behn, M.D., Lin, J., and Gill, C.E., 2005, Spatio-temporal evolution of strain accumulation derived from multi-scale observations of Late Jurassic rifting in the northern North Sea: A critical test of models for lithospheric extension: Earth and Planetary Science Letters, v. 234, p. 401–419, doi:10.1016/j.epsl.2005.01.039.

Crane, K., 1981, Thermal variations in the Gregory Rift of southern Kenya: Tectonophysics, v. 74, p. 239–262, doi:10.1016/0040-1951(81)90192-X.

Crossley, R., 1979, The Cenozoic stratigraphy and structure of the western part of the Rift Valley in southern Kenya: Journal of the Geological Society [London], v. 136, p. 393–405, doi:10.1144/gsjgs.136.4.0393.

Daly, M.C., Chorowicz, J., and Fairhead, J.D., 1989, Rift basin evolution in Africa: The influence of steep basement shear zones, *in* Cooper, M.A., and Williams, G.D., eds., Inversion Tectonics: Geological Society of London Special Publication 44, p. 309–334, doi:10.1144/GSL.SP.1989.044.01.17.

Daly, E., Keir, D., Ebinger, C.J., Stuart, G.W., Bastow, I.D., and Ayele, A., 2008, Crustal tomographic imaging of a transitional continental rift: The Ethiopian rift: Geophysical Journal International, v. 172, p. 1033–1048, doi:10.1111/j.1365-246X.2007.03682.x.

Daniels, K.A., Bastow, I.D., Keir, D., Sparks, R.S.J., and Menand, T., 2014, Thermal models of dyke intrusion during development of continent-ocean transition: Earth and Planetary Science Letters, v. 385, p. 145–153, doi:10.1016/j.epsl.2013.09.018.

Darling, W.G., Griesshaber, E., Andrews, J.N., Armannsson, H., and Onions, R.K., 1995, The origin of hydrothermal and other gases in the Kenya Rift valley: Geochimica et Cosmochimica Acta, v. 59, p. 2501–2512, doi:10.1016/0016-7037(95)00145-X.

Dawers, N.H., and Anders, M.H., 1995, Displacement-length scaling and fault linkage: Journal of Structural Geology, v. 17, p. 607–614, doi:10.1016/0191-8141(94)00091-D.

Dawers, N.H., Anders, M.H., and Scholz, C.H., 1993, Growths of normal faults—Displacement-length scaling: Geology, v. 21, p. 1107–1110, doi:10.1130/0091-7613(1993)021<1107:GONFDL>2.3.CO;2.

Dawson, J.B., 1992, Neogene tectonics and volcanicity in the north Tanzania sector of the Gregory Rift Valley—Contrasts with the Kenya sector: Tectonophysics, v. 204, p. 81–92, doi:10.1016/0040-1951(92)90271-7.

de Moor, J.M., Fischer, T.P., Sharp, Z.D., Hilton, D.R., Barry, P.H., Mangasini, F., and Ramirez, C., 2013, Gas chemistry and nitrogen isotope compositions of cold mantle gases from Rungwe Volcanic Province, southern Tanzania: Chemical Geology, v. 339, p. 30–42, doi:10.1016/j.chemgeo.2012.08.004.

Downs, D.T., Rowland, J.V., Wilson, C.J.N., Rosenberg, M.D., Leonard, G.S., and Calvert, A.T., 2014, Evolution of the intra-arc Taupo-Reporoa Basin within the Taupo Volcanic Zone of New Zealand: Geosphere, v. 10, p. 185–206, doi:10.1130/GES00965.1.

Ebinger, C.J., 2005, Continental break-up: The East African perspective: Astronomy & Geophysics, v. 46, 2390, doi:10.1111/j.1468-4004.2005.46216.x.

Ebinger, C.J., and Casey, M., 2001, Continental breakup in magmatic provinces: An Ethiopian example: Geology, v. 29, p. 527–530, doi:10.1130/0091-7613(2001)029<0527:CBIMPA>2.0.CO;2.

Ebinger, C.J., and Scholz, C.A., 2012, Continental rift basins: The East African perspective, *in* Busby, C., and Azor, A., eds., Tectonics of Sedimentary Basins: Recent Advances: Chichester, UK, John Wiley & Sons, p. 185–208, doi:10.1002/9781444347166.ch9.

Ebinger, C.J., Djomani, Y.P., Mbede, E., Foster, A., and Dawson, J.B., 1997, Rifting Archaean lithosphere: The Eyasi-Manyara-Natron rifts, East Africa: Journal of the Geological Society [London], v. 154, p. 947–960, doi:10.1144/gsjgs.154.6.0947.

Ebinger, C.J., Yemane, T., Harding, D.J., Tesfaye, S., Kelley, S., and Rex, D.C., 2000, Rift deflection, migration, and propagation: Linkage of the Ethiopian and Eastern rifts, Africa: Geological Society of America Bulletin, v. 112, p. 163–176, doi:10.1130/0016-7606(2000)112<163:RDMAPL>2.0.CO;2.

Ebinger, C., Ayele, A., Keir, D., Rowland, J., Yirgu, G., Wright, T., Belachew, M., and Hamling, I., 2010, Length and timescales of rift faulting and magma intrusion: The Afar rifting cycle from 2005 to present: Annual Review of Earth and Planetary Sciences, v. 38, p. 439–466, doi:10.1146/annurev-earth-040809-152333.

Ebinger, C.J., van Wijk, J., and Keir, D., 2013, The time scales of continental rifting: Implications for global processes, *in* Bickford, M.E., ed., The Web of Geological Sciences: Advances, Impacts, and Interactions: Geological Society of America Special Paper 500, p. 371–396, doi:10.1130/2013.2500(11).

Eugster, H.P., 1970, Chemistry and origin of the brines of Lake Magadi, Kenya, *in* Morgan, B.A., ed., Fiftieth Anniversary Symposia: Mineralogy and Petrology of the Upper Mantle Sulfides; Mineralogy and Geochemistry of Non-Marine Evaporites: Mineralogical Society of America Special Paper 3, p. 213–235.

Fairhead, J.D., Mitchell, J.G., and Williams, L.A.J., 1972, New K/Ar determinations on rift volcanics of S. Kenya and their bearing on age of rift faulting: Nature Physical Science, v. 238, p. 66–69, doi:10.1038/physci238066a0.

Fischer, T.P., Burnard, P., Marty, B., Hilton, D.R., Furi, E., Palhol, F., Sharp, Z.D., and Mangasini, F., 2009, Upper-mantle volatile chemistry at Oldoinyo Lengai volcano and the origin of carbonatites: Nature, v. 459, p. 77–80, doi:10.1038/nature07977.

Forslund, T., and Gudmundsson, A., 1992, Structure of Tertiary and Pleistocene normal faults in Iceland: Tectonics, v. 11, p. 57–68, doi:10.1029/91TC01536.

Foster, A., Ebinger, C., Mbede, E., and Rex, D., 1997, Tectonic development of the northern Tanzanian sector of the east African rift system: Journal of the Geological Society [London], v. 154, p. 689–700, doi:10.1144/gsjgs.154.4.0689.

Gawthorpe, R.L., and Leeder, M.R., 2000, Tectono-sedimentary evolution of active extensional basins: Basin Research, v. 12, p. 195–218, doi:10.1046/j.1365-2117.2000.00121.x.

Geissler, W.H., Kampf, H., Kind, R., Brauer, K., Klinge, K., Plenefisch, T., Horalek, J., Zednik, J., and Nehybka, V., 2005, Seismic structure and location of a CO_2 source in the upper mantle of the western Eger (Ohre) Rift, central Europe: Tectonics, v. 24, TC5001, doi:10.1029/2004TC001672.

Gibson, I.L., 1969, Structure and volcanic geology of an axial portion of the Main Ethiopian Rift: Tectonophysics, v. 8, p. 561–565, doi:10.1016/0040-1951(69)90054-7.

Gillespie, P.A., Walsh, J.J., and Watterson, J., 1992, Limitations of dimension and displacement data from single faults and the consequences for data analysis and interpretation: Journal of Structural Geology, v. 14, p. 1157–1172, doi:10.1016/0191-8141(92)90067-7.

Grandin, R., et al., 2009, 2005 Manda Hararo-Dabbahu rifting event, Afar (Ethiopia): Constraints provided by geodetic data: Journal of Geophysical Research, v. 114, B08404, doi:10.1029/2008jb005843.

Gudmundsson, A., 1992, Formation and growth of normal faults at the divergent plate boundary in Iceland: Terra Nova, v. 4, p. 464–471, doi:10.1111/j.1365-3121.1992.tb00582.x.

Gudmundsson, A., and Bäckström, K., 1991, Structure and development of the Sveinagja graben, northeast Iceland: Tectonophysics, v. 200, p. 111–125, doi:10.1016/0040-1951(91)90009-H.

Gupta, A., and Scholz, C.H., 2000, Brittle strain regime transition in the Afar depression: Implications for fault growth and seafloor spreading: Geology, v. 28, p. 1087–1090, doi:10.1130/0091-7613(2000)28<1087:BSRTIT>2.0.CO;2.

Guth, A.L., 2015, Volcanic volumes associated with the Kenya Rift: Recognition and correlation of preservation biases, *in* Wright, T.J., et al., eds., Magmatic Rifting and Active Volcanism: Geological Society of London Special Publication 420, p. 43–67, doi:10.1144/sp420.3.

Halldórsson, S.A., Hilton, D.R., Scarsi, P., Abebe, T., and Hopp, J., 2014, A common mantle plume source beneath the entire East African Rift System revealed by coupled helium-neon systematics: Geophysical Research Letters, v. 41, p. 2304–2311, doi:10.1002/2014GL059424.

Hampel, A., Hetzel, R., and Densmore, A.L., 2007, Postglacial slip-rate increase on the Teton normal fault, northern Basin and Range Province, caused by melting of the Yellowstone ice cap and deglaciation of the Teton Range?: Geology, v. 35, p. 1107–1110, doi:10.1130/G24093A.1.

Hayward, N.J., and Ebinger, C.J., 1996, Variations in the along-axis segmentation of the Afar Rift system: Tectonics, v. 15, p. 244–257, doi:10.1029/95TC02292.

Hetzel, R., and Hampel, A., 2005, Slip rate variations on normal faults during glacial-interglacial changes in surface loads: Nature, v. 435, p. 81–84, doi:10.1038/nature03562.

Holyoke, C.W., and Kronenberg, A.K., 2013, Reversible water weakening of quartz: Earth and Planetary Science Letters, v. 374, p. 185–190, doi:10.1016/j.epsl.2013.05.039.

Ibs-von Seht, M., Blumenstein, S., Wagner, R., Hollnack, D., and Wohlenberg, J., 2001, Seismicity, seismotectonics and crustal structure of the southern Kenya Rift—New data from the Lake Magadi area: Geophysical Journal International, v. 146, p. 439–453, doi:10.1046/j.0956-540x.2001.01464.x.

Imber, J., Childs, C., Nell, P.A.R., Walsh, J.J., Hodgetts, D., and Flint, S., 2003, Hanging wall fault kinematics and footwall collapse in listric growth fault systems: Journal of Structural Geology, v. 25, p. 197–208, doi:10.1016/S0191-8141(02)00034-2.

Isaacs, G.L., and Curtis, G.H., 1974, Age of early Acheulian industries from Peninj Group, Tanzania: Nature, v. 249, p. 624–627, doi:10.1038/249624a0.

Jagniecki, E.A., Lowenstein, T.K., Jenkins, D.M., and Demicco, R.V., 2015, Eocene atmospheric CO_2 from the nahcolite proxy: Geology, v. 43, p. 1075–1078, doi:10.1130/g36886.1.

Jones, B.F., Eugster, H.P., and Rettig, S.L., 1977, Hydrochemistry of Lake Magadi basin, Kenya: Geochimica et Cosmochimica Acta, v. 41, p. 53–72, doi:10.1016/0016-7037(77)90186-7.

Kattenhorn, S.A., and Pollard, D.D., 2001, Integrating 3-D seismic data, field analogs, and mechanical models in the analysis of segmented normal faults in the Wytch Farm oil field, southern England, United Kingdom: American Association of Petroleum Geologists Bulletin, v. 85, p. 1183–1210.

Kattenhorn, S.A., Muirhead, J.D., Dindi, E., Fischer, T.P., Lee, H., and Ebinger, C.J., 2013, Contribution of transverse structures, magma, and crustal fluids to continental rift evolution: The East African Rift in southern Kenya: American Geophysical Union, Fall Meeting 2013, abs. T12B-02.

Katumwehe, A.B., Abdelsalam, M.G., and Atekwana, E.A., 2015, The role of pre-existing Precambrian structures in rift evolution: The Albertine and Rhino grabens, Uganda: Tectonophysics, v. 646, p. 117–129, doi:10.1016/j.tecto.2015.01.022.

Katumwehe, A.B., Abdelsalam, M.G., Atekwana, E.A., and Laó-Dávila, D.A., 2016, Extent, kinematics and tectonic origin of the Precambrian Aswa Shear Zone in eastern Africa: Gondwana Research, v. 34, p. 241–253, doi:10.1016/j.gr.2015.03.007.

Keir, D., Kendall, J.M., Ebinger, C.J., and Stuart, G.W., 2005, Variations in late syn-rift melt alignment inferred from shear-wave splitting in crustal earthquakes beneath the Ethiopian rift: Geophysical Research Letters, v. 32, L23308, doi:10.1029/2005GL024150.

Keir, D., Ebinger, C.J., Stuart, G.W., Daly, E., and Ayele, A., 2006, Strain accommodation by magmatism and faulting as rifting proceeds to breakup: Seismicity of the northern Ethiopian rift: Journal of Geophysical Research, v. 111, B05314, doi:10.1029/2005jb003748.

Keir, D., Bastow, I.D., Whaler, K.A., Daly, E., Cornwell, D.G., and Hautot, S., 2009, Lower crustal earthquakes near the Ethiopian rift induced by magmatic processes: Geochemistry, Geophysics, Geosystems, v. 10, Q0Ab02, doi:10.1029/2009gc002382.

Keir, D., Belachew, M., Ebinger, C.J., Kendall, J.M., Hammond, J.O.S., Stuart, G.W., Ayele, A., and Rowland, J.V., 2011, Mapping the evolving strain field during continental breakup from crustal anisotropy in the Afar Depression: Nature Communications, v. 2, p. 285, doi:10.1038/ncomms1287.

Keir, D., Bastow, I.D., Corti, G., Mazzarini, F., and Rooney, T.O., 2015, The origin of along-rift variations in faulting and magmatism in the Ethiopian Rift: Tectonics, v. 34, p. 464–477, doi:10.1002/2014TC003698.

Kendall, J.M., Stuart, G.W., Ebinger, C.J., Bastow, I.D., and Keir, D., 2005, Magma-assisted rifting in Ethiopia: Nature, v. 433, p. 146–148, doi:10.1038/nature03161.

Kent, G.M., et al., 2005, 60 k.y. record of extension across the western boundary of the Basin and Range province: Estimate of slip rates from offset shoreline terraces and a catastrophic slide beneath Lake Tahoe: Geology, v. 33, p. 365–368, doi:10.1130/G21230.1.

Keranen, K., Klemper, S.L., and Gloaguen, R., and EAGLE Working Group, 2004, Three-dimensional seismic imaging of a protoridge axis in the Main Ethiopian rift: Geology, v. 32, p. 949–952, doi:10.1130/G20737.1.

Kervyn, M., Ernst, G.G.J., Harris, A.J.L., Belton, F., Mbede, E., and Jacobs, P., 2008, Thermal remote sensing of the low-intensity carbonatite volcanism of Oldoinyo Lengai, Tanzania: International Journal of Remote Sensing, v. 29, p. 6467–6499, doi:10.1080/01431160802167105.

Kostrov, V.V., 1974, Seismic moment and energy of earthquakes, and seismic flow rocks: Izvestiya, Academy of Sciences, USSR, Physics of the Solid Earth, no. 1, p. 23–44.

Lambert, C., Muirhead, J.D., Ebinger, C.J., Tiberi, C., Roecker, S., Ferdinand-Wambura, R., Kianji, G., and Mulibo, G., 2014, Lower crustal seismicity, volatiles, and evolving strain fields during the initial stages of cratonic rifting: American Geophysical Union, Fall Meeting 2014, abs. T53B-4678.

Laó-Dávila, D.A., Al-Salmi, H.S., Abdelsalam, M.G., and Atekwana, E.A., 2015, Hierarchical segmentation of the Malawi Rift: The influence of inherited lithospheric heterogeneity and kinematics in the evolution of continental rifts: Tectonics, v. 34, p. 2399–2417, doi:10.1002/2015TC003953.

Lavier, L.L., Buck, W.R., and Poliakov, A.N.B., 2000, Factors controlling normal fault offset in an ideal brittle layer: Journal of Geophysical Research, v. 105, p. 23,431–23,442, doi:10.1029/2000JB900108.

Le Corvec, N., Menand, T., and Lindsay, J., 2013, Interaction of ascending magma with pre-existing crustal fractures in monogenetic basaltic volcanism: An experimental approach: Journal of Geophysical Research, v. 118, p. 968–984, doi:10.1002/jgrb.50142.

Lee, H., Muirhead, J.D., Fischer, T.P., Ebinger, C.J., Kattenhorn, S.A., Sharp, Z.D., and Kianji, G., 2016, Massive and prolonged deep carbon emissions associated with continental rifting: Nature Geoscience, v. 9, p. 145–149, doi:10.1038/ngeo2622.

Le Gall, B., Tiercelin, J.J., Richert, J.P., Gente, P., Sturchio, N.C., Stead, D., and Le Turdu, C., 2000, A morphotectonic study of an extensional fault zone in a magma-rich rift: The Baringo Trachyte fault system, central Kenya Rift: Tectonophysics, v. 320, p. 87–106, doi:10.1016/S0040-1951(00)00069-X.

Le Gall, B., Nonnotte, P., Rolet, J., Benoit, M., Guillou, H., Mousseau-Nonnotte, M., Albaric, J., and Deverchere, J., 2008, Rift propagation at craton margin. Distribution of faulting and volcanism in the North Tanzanian Divergence (East Africa) during Neogene times: Tectonophysics, v. 448, p. 1–19, doi:10.1016/j.tecto.2007.11.005.

Le Turdu, C., Richert, J.P., Xavier, J.-P., Renaut, R.W., Tiercelin, J.-J., Rolet, J., Lezzar, K.E., and Coussement, C., 1999, Influence of preexisting oblique discontinuities on the geometry and evolution of extensional fault patterns: Evidence from the Kenya Rift using SPOT imagery, *in* Morley, C.K., ed., Geoscience of Rift Systems—Evolution of East Africa: American Association of Petroleum Geologists Studies in Geology 44, p. 173–191.

Lindenfeld, M., Rumpker, G., Link, K., Koehn, D., and Batte, A., 2012, Fluid-triggered earthquake swarms in the Rwenzori region, East African Rift—Evidence for rift initiation: Tectonophysics, v. 566, p. 95–104, doi:10.1016/j.tecto.2012.07.010.

Maccaferri, F., Rivalta, E., Keir, D., and Acocella, V., 2014, Off-rift volcanism in rift zones determined by crustal unloading: Nature Geoscience, v. 7, p. 297–300, doi:10.1038/ngeo2110.

Mackenzie, G.D., Thybo, H., and Maguire, P.K.H., 2005, Crustal velocity structure across the Main Ethiopian Rift: results from two-dimensional wide-angle seismic modelling: Geophysical Journal International, v. 162, p. 994–1006, doi:10.1111/j.1365-246X.2005.02710.x.

Maguire, P.K.H., et al., 2006, Crustal structure of the northern Main Ethiopian Rift from the EAGLE controlled-source survey; a snapshot of incipient lithospheric break-up, *in* Yirgu, G., et al., eds., Afar Volcanic Province Within the East African Rift System: Geological Society of London Special Publication 259, p. 269–292, doi:10.1144/GSL.SP.2006.259.01.21.

Mana, S., Furman, T., Turrin, B.D., Feigenson, M.D., and Swisher, C.C., 2015, Magmatic activity across the East African North Tanzanian Divergence Zone: Journal of the Geological Society [London], v. 172, p. 368–389, doi:10.1144/jgs2014-072.

Manighetti, I., King, G.C.P., Gaudemer, Y., Scholz, C.H., and Doubre, C., 2001, Slip accumulation and lateral propagation of active normal faults in Afar: Journal of Geophysical Research, v. 106, p. 13,667–13,696, doi:10.1029/2000JB900471.

Marrett, R., and Allmendinger, R.W., 1991, Estimates of strain due to brittle faulting: Sampling of fault populations: Journal of Structural Geology, v. 13, p. 735–738, doi:10.1016/0191-8141(91)90034-G.

Marty, B., and Zimmermann, L., 1999, Volatiles (He, C, N, Ar) in mid-ocean ridge basalts: Assessment of shallow-level fractionation and characterization of source composition: Geochimica et Cosmochimica Acta, v. 63, p. 3619–3633, doi:10.1016/S0016-7037(99)00169-6.

Mastin, L.G., and Pollard, D.D., 1988, Surface deformation and shallow dike intrusion processes at Inyo Craters, Long valley, California: Journal of Geophysical Research, v. 93, p. 13,221–13,235, doi:10.1029/JB093iB11p13221.

Mazzarini, F., Le Corvec, N., Isola, I., and Favalli, M., 2016, Volcanic field elongation, vent distribution and tectonic evolution of a continental rift: The Main Ethiopian Rift example: Geosphere, v. 12, p. 706–720, doi:10.1130/GES01193.1.

McCartney, T., and Scholz, C.A., 2016, A 1.3 million year record of synchronous faulting in the hangingwall and border fault of a half-graben in the Malawi (Nyasa) Rift: Journal of Structural Geology, v. 91, p. 114–129, doi:10.1016/j.jsg.2016.08.012.

McClay, K.R., and Ellis, P.G., 1987, Geometries of extensional fault systems developed in model experiments: Geology, v. 15, p. 341–344, doi:10.1130/0091-7613(1987)15<341:GOEFSD>2.0.CO;2.

McConnell, R.B., 1972, Geological development of the rift system of eastern Africa: Geological Society of America Bulletin, v. 83, p. 2549–2572, doi:10.1130/0016-7606(1972)83[2549:GDOTRS]2.0.CO;2.

McKenzie, D., and Bickle, M.J., 1988, The volume and composition of melt generated by extension of the lithosphere: Journal of Petrology, v. 29, p. 625–679, doi:10.1093/petrology/29.3.625.

McNitt, J.R., Klein, C.W., and Koenig, J.B., 1989, Probable Subsurface Temperature at Lake Magadi, Kenya, as Indicated by Hot Spring Geochemistry and the Potential for Development of Geothermal Electric Power: U.S. Department of Energy Report DOE/ID/12850–T1, 29 p.

Mechie, J., Keller, G.R., Prodehl, C., Khan, M.A., and Gaciri, S.J., 1997, A model for the structure, composition and evolution of the Kenya rift: Tectonophysics, v. 278, p. 95–119, doi:10.1016/S0040-1951(97)00097-8.

Mohr, P., 1967, Major volcanotectonic lineament in the Ethiopian rift system: Nature, v. 213, p. 664–665, doi:10.1038/213664a0.

Monnin, C., and Schott, J., 1984, Determination of the solubility products of sodium carbonate minerals and an application to trona deposition in Lake Magadi (Kenya): Geochimica et Cosmochimica Acta, v. 48, p. 571–581, doi:10.1016/0016-7037(84)90285-0.

Moore, D.E., and Rymer, M.J., 2007, Talc-bearing serpentinite and the creeping section of the San Andreas fault: Nature, v. 448, p. 795–797, doi:10.1038/nature06064.

Moore, J.M., and Schultz, R.A., 1999, Processes of faulting in jointed rocks of Canyonlands National Park, Utah: Geological Society of America Bulletin, v. 111, p. 808–822, doi:10.1130/0016-7606(1999)111<0808:POFIJR>2.3.CO;2.

Morley, C.K., 1999, Patterns of displacement along large normal faults: Implications for basin evolution and fault propagation, based on examples from east Africa: American Association of Petroleum Geologists Bulletin, v. 83, p. 613–634.

Mosley, P.N., 1993, Geological evolution of the late Proterozoic Mozambique Belt of Kenya: Tectonophysics, v. 221, p. 223–250, doi:10.1016/0040-1951(93)90334-G.

Muirhead, J.D., 2016, Tectonic-magmatic controls on volcanism, rifting, and volatile release [Ph.D. thesis]: Moscow, University of Idaho, 369 p.

Muirhead, J.D., Kattenhorn, S.A., and Le Corvec, N., 2015, Varying styles of magmatic strain accommodation in the East African Rift: Geochemistry, Geophysics, Geosystems, v. 16, p. 2775–2795, doi:10.1002/2015GC005918.

Nahm, A.L., and Schultz, R.A., 2011, Magnitude of global contraction on Mars from analysis of surface faults: Implications for martian thermal history: Icarus, v. 211, p. 389–400, doi:10.1016/j.icarus.2010.11.003.

Neukirchen, F., Finkenbein, T., and Keller, J., 2010, The Lava sequence of the East African Rift escarpment in the Oldoinyo Lengai–Lake Natron sector, Tanzania: Journal of African Earth Sciences, v. 58, p. 734–751, doi:10.1016/j.jafrearsci.2010.06.002.

Nicol, A., Watterson, J., Walsh, J.J., and Childs, C., 1996, The shapes, major axis orientations and displacement patterns of fault surfaces: Journal of Structural Geology, v. 18, p. 235–248, doi: 10.1016/S0191-8141(96)80047-2.

Parks, M.M., Caliro, S., Chiodini, G., Pyle, D.M., Mather, T.A., Berlo, K., Edmonds, M., Biggs, J., Nomikou, P., and Raptakis, C., 2013, Distinguishing contributions to diffuse CO_2 emissions in volcanic areas from magmatic degassing and thermal decarbonation using soil gas Rn-222-delta C-13 systematics: Application to Santorini volcano, Greece: Earth and Planetary Science Letters, v. 377, p. 180–190, doi:10.1016/j.epsl.2013.06.046.

Peacock, D.C.P., 2002, Propagation, interaction and linkage in normal fault systems: Earth-Science Reviews, v. 58, p. 121–142, doi:10.1016/S0012-8252(01)00085-X.

Peacock, D.C.P., and Sanderson, D.J., 1991, Displacements, segment linkage and relay ramps in normal fault zones: Journal of Structural Geology, v. 13, p. 721–733, doi:10.1016/0191-8141(91)90033-F.

Pik, R., Marty, B., and Hilton, D.R., 2006, How many mantle plumes in Africa? The geochemical point of view: Chemical Geology, v. 226, p. 100–114, doi:10.1016/j.chemgeo.2005.09.016.

Pollard, D.D., and Fletcher, R.C., 2005, Fundamentals of Structural Geology: Cambridge, UK, Cambridge University Press, 496 p.

Reyners, M., Eberhart-Phillips, D., and Stuart, G., 2007, The role of fluids in lower-crustal earthquakes near continental rifts: Nature, v. 446, p. 1075–1078, doi:10.1038/nature05743.

Roberts, N., Taieb, M., Barker, P., Damnati, B., Icole, M., and Williamson, D., 1993, Timing of the Younger Dryas event in East Africa from lake level changes: Nature, v. 366, p. 146–148, doi: 10.1038/366146a0.

Robertson, E.A.M., Biggs, J., Cashman, K.V., Floyd, M.A., and Vye-Brown, C., 2015, Influence of regional tectonics and pre-existing structures on the formation of elliptical calderas in the Kenyan Rift, *in* Wright, T.J., et al., eds., Magmatic Rifting and Active Volcanism: Geological Society of London Special Publication 420, p. 43–67, doi:10.1144/sp420.12.

Rodríguez, E., Morris, C.S., Belz, J.E., Chapin, E.C., Martin, J.M., Daffer, W., and Hensley, S., 2005, An assessment of the SRTM topographic products: Jet Propulsion Laboratory Technical Report D-31639, 125 p.

Roecker, S.W., et al., 2015, Images of the East Africa Rift System from the joint inversion of body waves, surface waves, and gravity: investigating the role of magma in early-stage continental rifting: American Geophysical Union, Fall Meeting 2013, abs. T51G-3013.

Rooney, T.O., 2010, Geochemical evidence of lithospheric thinning in the southern Main Ethiopian Rift: Lithos, v. 117, p. 33–48, doi:10.1016/j.lithos.2010.02.002.

Rooney, T.O., Furman, T., Yirgu, G., and Ayalew, D., 2005, Structure of the Ethiopian lithosphere: Xenolith evidence in the Main Ethiopian Rift: Geochimica et Cosmochimica Acta, v. 69, p. 3889–3910, doi:10.1016/j.gca.2005.03.043.

Rooney, T.O., Bastow, I.D., and Keir, D., 2011, Insights into extensional processes during magma assisted rifting: Evidence from aligned scoria cones: Journal of Volcanology and Geothermal Research, v. 201, p. 83–96, doi:10.1016/j.jvolgeores.2010.07.019.

Rooney, T.O., Herzberg, C., and Bastow, I.D., 2012, Elevated mantle temperature beneath East Africa: Geology, v. 40, p. 27–30, doi:10.1130/G32382.1.

Rooney, T.O., Bastow, I.D., Keir, D., Mazzarini, F., Movsesian, E., Grosfils, E.B., Zimbelman, J.R., Ramsey, M.S., Ayalew, D., and Yirgu, G., 2014, The protracted development of focused magmatic intrusion during continental rifting: Tectonics, v. 33, p. 875–897, doi:10.1002/2013TC003514, doi:10.1002/2013tc003514.

Rosendahl, B.R., 1987, Architecture of continental rifts with special reference to East Africa: Annual Review of Earth and Planetary Sciences, v. 15, p. 445–503, doi:10.1146/annurev.ea.15.050187.002305.

Rowland, J.V., and Simmons, S.F., 2012, Hydrologic, magmatic, and tectonic controls on hydrothermal flow, Taupo Volcanic Zone, New Zealand: Implications for the formation of epithermal vein deposits: Economic Geology and the Bulletin of the Society of Economic Geologists, v. 107, p. 427–457, doi:10.2113/econgeo.107.3.427.

Rowland, J.V., Baker, E., Ebinger, C.J., Keir, D., Kidane, T., Biggs, J., Hayward, N., and Wright, T.J., 2007, Fault growth at a nascent slow-spreading ridge: 2005 Dabbahu rifting episode, Afar: Geophysical Journal International, v. 171, p. 1226–1246, doi:10.1111/j.1365-246X.2007.03584.x.

Rowland, J.V., Wilson, C.J.N., and Gravley, D.M., 2010, Spatial and temporal variations in magma-assisted rifting, Taupo Volcanic Zone, New Zealand: Journal of Volcanology and Geothermal Research, v. 190, p. 89–108, doi:10.1016/j.jvolgeores.2009.05.004.

Rubin, A.M., and Pollard, D.D., 1988, Dike-induced faulting in rift zones of Iceland and Afar: Geology, v. 16, p. 413–417, doi:10.1130/0091-7613(1988)016<0413:DIFIRZ>2.3.CO;2.

Ruch, J., Wang, T., Xu, W., Hensch, M., and Jónsson, S., 2016, Oblique rift opening revealed by reoccurring magma injection in central Iceland: Nature Communications, v. 7, 12352, doi:10.1038/ncomms12352.

Sano, Y., and Marty, B., 1995, Origin of carbon in fumarolic gas from island arcs: Chemical Geology, v. 119, p. 265–274, doi:10.1016/0009-2541(94)00097-R.

Saria, E., Calais, E., Stamps, D.S., Delvaux, D., and Hartnady, C.J.H., 2014, Present-day kinematics of the East African Rift: Journal of Geophysical Research, v. 119, p. 3584–3600, doi:10.1002/2013JB010901.

Schlische, R.W., Young, S.S., Ackermann, R.V., and Gupta, A., 1996, Geometry and scaling relations of a population of very small rift-related normal faults: Geology, v. 24, p. 683–686, doi: 10.1130/0091-7613(1996)024<0683:GASROA>2.3.CO;2.

Scholz, C.A., Rosendahl, B.R., and Scott, D.L., 1990, Development of coarse-grained facies in lacustrine rift basins: Examples from East Africa: Geology, v. 18, p. 140–144, doi:10.1130/0091-7613(1990)018<0140:DOCGFI>2.3.CO;2.

Scholz, C.H., and Cowie, P.A., 1990, Determination of total strain from faulting using slip measurements: Nature, v. 346, p. 837–839, doi:10.1038/346837a0.

Schultz, R.A., Okubo, C.H., and Wilkins, S.J., 2006, Displacement-length scaling relations for faults on the terrestrial planets: Journal of Structural Geology, v. 28, p. 2182–2193, doi:10.1016/j.jsg.2006.03.034.

Schultz, R.A., Soliva, R., Okubu, C.H., and Mege, D., 2010, Fault populations, *in* Watters, R., and Schultz, R.A., eds., Planetary Tectonics: New York, Cambridge University Press, p. 457–510.

Seno, T., and Saito, A., 1994, Recent East African earthquakes in the lower crust: Earth and Planetary Science Letters, v. 121, p. 125–136, doi:10.1016/0012-821X(94)90036-1.

Shelly, D.R., Taira, T., Prejean, S.G., Hill, D.P., and Dreger, D.S., 2015, Fluid-faulting interactions: Fracture-mesh and fault-valve behavior in the February 2014 Mammoth Mountain, California earthquake swarm: Geophysical Research Letters, v. 42, p. 5803–5812, doi:10.1002/2015GL064325.

Sherrod, D.R., Magigita, M.M., and Kwelwa, S., 2013, Geologic Map of Oldonyo Lengai (Oldoinyo Lengai) and Surroundings, Arusha Region, United Republic of Tanzania: U.S. Geological Survey Open-File Report 2013-1306, scale 1:50,000, 50 p.

Sibson, R.H., 2000, Fluid involvement in normal faulting: Journal of Geodynamics, v. 29, p. 469–499, doi:10.1016/S0264-3707(99)00042-3.

Sigmundsson, F., et al., 2015, Segmented lateral dyke growth in a rifting event at Bardarbunga volcanic system, Iceland: Nature, v. 517, p. 191–195, doi:10.1038/nature14111.

Smith, M., 1994, Stratigraphic and structural constraints on mechanisms of active rifting in the Gregory Rift, Kenya: Tectonophysics, v. 236, p. 3–22, doi:10.1016/0040-1951(94)90166-X.

Smith, M., and Mosley, P., 1993, Crustal heterogeneity and basement influence on the development of the Kenya Rift, East Africa: Tectonics, v. 12, p. 591–606, doi:10.1029/92TC01710.

Soliva, R., and Schultz, R.A., 2008, Distributed and localized faulting in extensional settings: Insight from the North Ethiopian Rift-Afar transition area: Tectonics, v. 27, TC2003, doi:10.1029/2007TC002148.

Stamps, D.S., Calais, E., Saria, E., Hartnady, C., Nocquet, J.M., Ebinger, C.J., and Fernandes, R.M., 2008, A kinematic model for the East African rift: Geophysical Research Letters, v. 35, L05304, doi:10.1029/2007GL032781.

Stamps, D.S., Flesch, L.M., Calais, E., and Ghosh, A., 2014, Current kinematics and dynamics of Africa and the East African Rift System: Journal of Geophysical Research, v. 119, p. 5161–5186, doi:10.1002/2013JB010717.

Stamps, D.S., Iaffaldano, G., and Calais, E., 2015, Role of mantle flow in Nubia-Somalia plate divergence: Geophysical Research Letters, v. 42, p. 290–296, doi:10.1002/2014GL062515.

Stein, R.S., and Barrientos, S.E., 1985, Planar high-angle faulting in the Basin and Range: Geodetic analysis of the 1983 Borah Peak, Idaho, earthquake: Journal of Geophysical Research, v. 90, p. 1355–1366, doi:10.1029/JB090iB13p11355.

Stein, R.S., King, G.C.P., and Rundle, J.B., 1988, The growth of geological structures by repeated earthquakes 2. Field examples of continental dip-slip faults: Journal of Geophysical Research, v. 93, p. 13,319–13,331, doi:10.1029/JB093iB11p13319.

Stein, R.S., Briole, P., Ruegg, J.C., Tapponnier, P., and Gasse, F., 1991, Contemporary, Holocene, and Quaternary deformation of the Asal Rift, Djibouti: Implications for the mechanics of slow spreading ridges: Journal of Geophysical Research, v. 96, p. 21,789–21,806, doi:10.1029/91JB02118.

Stollhofen, H., and Stanistreet, I.G., 2012, Plio-Pleistocene synsedimentary fault compartments, foundation for the eastern Olduvai Basin paleoenvironmental mosaic, Tanzania: Journal of Human Evolution, v. 63, p. 309–327, doi:10.1016/j.jhevol.2011.10.002.

Trippanera, D., Ruch, J., Acocella, V., and Rivalta, E., 2015, Experiments of dike-induced deformation: Insights on the long-term evolution of divergent plate boundaries: Journal of Geophysical Research, v. 120, p. 6913–6942, doi:10.1002/2014JB011850.

Turcotte, D., and Schubert, G., 1982, Geodynamics: Applications of Continuum Physics to Geological Problems: New York, John Wiley & Sons, 450 p.

Vening Meinesz, F., 1950, Les grabens africains, resultat de compression ou de tension dans la croute terrestre?: Institut Royal Colonial Belge Bulletin des Séances, v. 21, p. 539–552.

Vetel, W., Le Gall, B., and Walsh, J.J., 2005, Geometry and growth of an inner rift fault pattern: The Kino Sogo Fault Belt, Turkana Rift (North Kenya): Journal of Structural Geology, v. 27, p. 2204–2222, doi:10.1016/j.jsg.2005.07.003.

Villamor, P., and Berryman, K., 2001, A late Quaternary extension rate in the Taupo Volcanic Zone, New Zealand, derived from fault slip data: New Zealand Journal of Geology and Geophysics, v. 44, p. 243–269, doi:10.1080/00288306.2001.9514937.

Villamor, P., and Berryman, K.R., 2006, Evolution of the southern termination of the Taupo Rift, New Zealand: New Zealand Journal of Geology and Geophysics, v. 49, p. 23–37, doi:10.1080/00288306.2006.9515145.

Walsh, J.J., and Watterson, J., 1988, Analysis of the relationship between displacements and dimensions of faults: Journal of Structural Geology, v. 10, p. 239–247, doi:10.1016/0191-8141(88)90057-0.

Walsh, J.J., and Watterson, J., 1991, Geometric and kinematic coherence and scale effects in normal fault systems, *in* Roberts, A.M., et al., eds., The Geometry of Normal Faults: Geological Society of London Special Publication 56, p. 193–203, doi:10.1144/GSL.SP.1991.056.01.13.

Walsh, J.J., Bailey, W.R., Childs, C., Nicol, A., and Bonson, C.G., 2003, Formation of segmented normal faults: A 3-D perspective: Journal of Structural Geology, v. 25, p. 1251–1262, doi:10.1016/S0191-8141(02)00161-X.

Wauthier, C., 2011, InSAR Applied to the Study of Active Volcanic and Seismic Areas in Africa [Ph.D. thesis]: Belgium, University of Liege, 209 p.

White, R.S., and McKenzie, D.P., 1989, Magmatism at rift zones: the generation of volcanic continental margins and flood basalts: Journal of Geophysical Research, v. 94, p. 7685–7729, doi:10.1029/JB094iB06p07685.

Wilkinson, M., et al., 2015, Slip distributions on active normal faults measured from LiDAR and field mapping of geomorphic offsets: an example from L'Aquila, Italy, and implications for modelling seismic moment release: Geomorphology, v. 237, p. 130–141, doi:10.1016/j.geomorph.2014.04.026.

Willemse, E.J.M., Pollard, D.D., and Aydin, A., 1996, Three-dimensional analyses of slip distributions on normal fault arrays with consequences for fault scaling: Journal of Structural Geology, v. 18, p. 295–309, doi:10.1016/S0191-8141(96)80051-4.

Wolfenden, E., Ebinger, C., Yirgu, G., Deino, A., and Ayalew, D., 2004, Evolution of the northern Main Ethiopian rift: Birth of a triple junction: Earth and Planetary Science Letters, v. 224, p. 213–228, doi:10.1016/j.epsl.2004.04.022.

Wright, T.J., Ebinger, C.J., Biggs, J., Ayele, A., Yirgu, G., Keir, D., and Stork, D., 2006, Magma-maintained rift segmentation at continental rupture in the 2005 Afar dyking episode: Nature, v. 442, p. 291–294, doi:10.1038/nature04978.

Wright, T.J., et al., 2012, Geophysical constraints on the dynamics of spreading centres from rifting episodes on land: Nature Geoscience, v. 5, p. 242–250, doi:10.1038/ngeo1428.

Yardley, B.W.D., Harlov, D.E., and Heinrich, W., 2010, Rates of retrograde metamorphism and their implications for crustal rheology: Geofluids, v. 10, p. 234–240, doi:10.1111/j.1468-8123.2010.00286.x.